TD 98-025

HGQS01 Test Summary Report

J. DiMarco, S. Feher, D. Orris, J.P. Ozelis, P. Schlabach, G. Sabbi,
M. Tartaglia, J.C. Tompkins
(FNAL)

June 4, 1998

Contents

List of Figures

List of Tables

Chapter 1

General Overview

1.1 Test Summary Report Outline

This report presents preliminary results of HGQS01 testing at the FNAL Vertical Magnet Test Facility. HGQS01 is the first 70 mm-aperture, short R&D model LHC quadrupole built at FNAL.

After a brief description of magnet features and assembly, the cold testing overview is presented in chapter 1.

Chapter 2 is devoted to quench performance tests. An overview of quench history is first given, followed by presentation of ramp rate and temperature dependence studies. Particular attention is paid to quench start locations. Relevant test conditions and results are given in summary tables.

Heater studies are presented in Capter 3. Heater induced quenches were performed at several different excitation currents and heater voltages at 1.9K. The time delay in quench initiation under these various conditions is presented as a function of the normalized current. We also determined the minimum voltage required to quench the magnet at different excitation currents.

Chapter 4 summarizes strain gauge (SG) runs performed throughout the first test cycle. Included here are summary sheets of all SG runs, and representative plots of coil stress and end force vs. I^2 (where I is the magnet excitation current) to the highest attainable current at each test temperature. Also included are tables summarizing SG readings at 0 A magnet excitation current (warm, before and after cool down), and plots of stress and end forces

vs. time (summarizing SG history for the entire first test cycle).

Magnetic measurements results are given in chapter 5. Tables summarizing a_n, b_n harmonic coefficients from room temperature, 4.5K, and 1.9K measurements are presented. Also included are representative plots of harmonics for warm and cold axial scans, and plots of time dependence and current loop measurements.

Chapter 6 presents the results of splice resistance measurements. RRR study is summarized in Chapter 7 and "snapshot" events were described in Chapter 8.

1.2 Magnet Features

HGQS01 is the first short model (177 cm magnetic length) "High Gradient Quadrupole" (HGQ) built and tested at FNAL as part of Fermilab's High Gradient Quadrupole R&D program. The primary goal for building this magnet was to make a magnet which will meet the requirements for the LHC insertion region low-β quadrupoles.

1.3 Magnet assembly

The magnet design is described in the "HGQ Design Report" and the assembly procedure is described in the HGQ traveler. A detailed description of the construction, including all failures, anomalies and the deviations of HGQS01 from the baseline design relevant to magnet testing, have been reported by R. Bossert.

During the assembly of the magnet several shorts had to be repaired. These shorts were in the end region of the coils. To minimize the possibility of creating additional shorts, the end bullets were not tightened down to the design values after these repairs.

1.4 Test Overview

HGQS01 was tested according to the runplan attached as an Appendix to this note. The magnet was placed into the VMTF dewar and room temperature magnetic measurements were performed on Jan. 30. HGQS01 was first

cooled down on February 2, 1998 and cold testing began on February 5. The first test cycle ended February 18 with subsequent warm up to room temperature. The second test cycle started on March 10^{th} after cool down to 4.5K and ended on March 24^{th} Between the two tests the magnet went through several changes:

- The end bullets were tightened down to 6000 lb.
- Shell gauges were added to the skin of the magnet.
- The iron shim configuration was changed.

1.4.1 Test Cycle 1

Initial cooldown was to 4.5K without restriction on the differences between any of the temperature sensors located in the VMTF dewar. To obtain data for RRR measurements, 5 Amps current was applied to the magnet, and the magnet voltage monitored during cool down. This data was being recorded with the VMTF slow scan (pentek-scribe) data acquisition system (see appendix), but a software bug caused this information to be lost.

At 4.5K, magnetic measurements up to currents of 6kA were performed first, followed by strain gauge runs. The first spontaneous quench of the magnet occurred at 8808A. Three additional quenches were made at the same 16A/sec ramp rate before proceeding with ramps to quench at 200A/sec and 300A/sec. Next the magnet was cooled to 1.9K and strain gauge runs performed. At 9672A the DQD detected a voltage rise and the magnet protection system initiated the relevant protection sequence. Examination of the instrumentation signals showed no apparent resistive growth in the coils, so we concluded that it was not a quench. Three more of these "trip events" occurred and were studied before the voltage thresholds of the quench detection modules (both DQD and AQD) were raised to avoid them. This allowed us to ramp the magnet to the first 1.9K quench which occurred at 10364A - quite low relative to the HGQS01 cable short sample limit. The magnet was quenched five additional times and then, given the slow training, we decided to do no more than four additional spontaneous quenches (two of which were to be done at high ramp rates).

Since we wanted to understand the nature of the trip events, we implemented a special way of capturing these events without initiating the quench

protection logic. The new scan (Snapshot scan) was able to trigger on low DQD threshold values and store eight coil signals. We also implemented a fast strain gauge run to be able to monitor strain gauges during ramping. These tools were used before and during the magnetic measurements which followed quench testing.

After magnetic measurements heater studies were made at 1.9K. The magnet was quenched 20 times with various magnet excitation currents and protection heater voltages.

We closed our first test cycle with quench current temperature dependence studies. The magnet was quenched at 8 different temperatures ranging from 1.8K to 4.5K.

1.4.2 Test Cycle 2

The second test cycle began with warm magnetic measurements. The magnet was cooled down to 4.5K and strain gauge runs were performed. The first quench of TC 2 occured at 9421 A. One additional quench was made at the same 16 A/sec ramp rate, and the magnet was cooled to 1.9 K. Strain gauge runs were performed, and the first quench at 1.9K occurred at 10653A. The magnet was quenched 11 additional times. Since the last two quench currents were lower then I_{qmax} we stopped the training. Next we performed magnetic measurements. During high current magnetic measurements the magnet quenched at 11300A, so we had to reduce the I_{max} for magnetic measurements to 11000A. Following magnetic measurements were six additional heater studies performed with various magnet excitation currents but with fixed protection heater voltage (400V).

We closed the second test cycle with quench current temperature dependence studies. The magnet was quenched at 7 different temperatures ranging from 1.8K to 4.5K.

During magnet warm up we performed 4 wire resistance measurements to obtain data for RRR studies.

Chapter 2

Quench behavior

This chapter summarizes the quench behavior of the magnet. Instrumentation settings for the HGQS01 test are summarized in Table 3.1 and Table 2.2; a detailed description of the instrumentation and its configuration is presented elsewhere.

Quench data acquisition was performed using the VMTF (pentek) readout system with binary quench data stored on a UNIX workstation. The location of the files are on MTF UNIX cluster:

/jbcd/HGQS01_19980130_19980301/quench/ and

/jbcd/HGQS01_19980302_19980331/quench/.

The names of the quench files are summarized in Table 2.5 and 2.6. The data were analyzed using the quenchXmgr utility. HGQS01 had 96 voltage taps, primarily instrumenting the pole turns and wedges on the four inner and outer coil quadrants and inner/outer coil splice regions.

2.1 Quench history

2.1.1 Test Cycle I

HGQS01 was tested according to the run plan attached as an Appendix to this note. The quench history is summarized in Table 2.3 and Table 2.4 and in Figure 2.1. Quench testing began at 4.5K at a ramp rate of 16A/s. The first spontaneous quench current was at 8808A, and the three additional quenches at 16A/s successively increased in quench current; the fourth quench reached

9342A. Since the predicted short sample limit of the superconducting cable used in this magnet is 10340kA, the quench current obtained is about 15% below that expected. All four quenches were in the end region (see Table 2.3). The magnet was then ramped to quench at ramp rates of 300A/s and 150A/s (quench numbers 5 and 6).

Testing at 4.5K was followed by cooldown and spontaneous quench testing at 1.9K. At the higher currents attainable at 1.9K, however, the quench detection circuits (QDC's) were tripping on non-quench events (the reproducible voltage rises which caused these trips will be described later). In order to proceed, it was necessary to increase the thresholds of QDC#2 (Whole coil -Idot) and QDC#3 (Bucked Half-Half coils) by a factor of two.

The magnet was quenched 8 times (quench numbers 7-14) at 1.9K with an overall, though monotonic, increase in current at quench of $\sim$ 100A -300A. The ramp rate for these quenches was 16A/sec to $\sim$ 9000A then 2A/sec above 9000A (this was done for consistency, as the first quench was taken at 2A/s when trying to avoid the trip events). As with 4.3K, the current at quench at 1.9K ceased to increase significantly even though it was several hundred Amps below the predicted short sample limit of 13900A. Next, ramps to quench at 1.9K were performed at ramp rates of 300A/s, 200A/s, 150A/s, (quench numbers 15-17). During magnetic measurements and heater studies additional (heater-induced) magnet quenches were performed at various excitation currents.

At the end of the first test cycle, 9 additional quenches were taken at temperatures ranging from 1.8K to 4.5K to study quench current dependence on temperature. In these studies, the magnet was ramped to quench at 16A/sec.

2.1.2 Test Cycle II

The magnet underwent thermal cycle to 300K and was cooled back down to 4.5K. The magnet was quenched twice at this temperature. The 27^{th} spontaneous quench current (first quench of the second test cycle) was at 9421 A. Since, the 28^{th} quench current (9755A) was also far below the short sample limit, we cooled the magnet to 1.9K. At 1.9K the magnet was quenched 15 times (quench number 29 - 43). The 29^{th} (first 1.9K quench of the second test cycle) was at 10653 A, which is about 23% below the short sample limit of the cable. To train the magnet we performed an additional 11 quenches. All

of these quenches had 16 A/sec ramp rate and increased QDC thresholds (see previous subsection). Since the 39^{th} and 40^{th} quench currents were significally lower than that of the 38^{th}, we stopped spontaneous quench testing. During magnetic measurements, however, the magnet quenched two additional times at relatively low current values.

Finally, 7 additional quenches were taken at temperatures ranging from 1.8K to 4.5K as a quench current temperature dependence study. In these studies the magnet was ramped to quench at 16A/sec.

2.2 Quench training

The training curve of HGQS01 is shown in Fig 2.2. The magnet quench current both at 4.5K and 1.9K would seem to be mechanically or otherwise limited since all of the quenches but one (which we were not able to identify since it occurred in the region of the coil which was not instrumented with voltage taps) were located near the end regions of the magnet, and very shallow training curves were observed. Indeed, strain gauge measurements (see below) showed that the preload of the end section under current excitation is relatively low and the load between the lead and return end of the magnet is uneven. In both test cycles, the last quench current at 4.45K after temperature dependence studies was close to the short sample limit. It seems that the additional magnet training at 1.9K helped to train the magnet for 4.5K.

Between test cycle I and test cycle II the magnet end preload was increased so it was expected that the magnet would not "remember" its previous training. Indeed, in test cycle II, the magnet quench current at 4.5K was much lower than the last quench current at 4.45K in test cycle I. At 1.9K the 29^{th} quench was slightly higher that that of the first test cycle but it was still much lower than the short sample limit value. The magnet quench current during training increased non-monotically. Between the 29^{th} and 30^{th} quenches, the quench current increased by 772A, however, between quenches #34 and #35 the quench current decreased by 58 A. The quench current of the 39^{th} quench suddenly dropped 345 A relative to that of the 38^{TH} quench and the 40^{th} quench current decreased an additional 43 A. Most of the quenches were in the end region. It seems the magnet is mechanically limited. Consistent with this conclusion are the additional quenches with even lower quench currents during magnetic measurements (#41 and #42).

2.3 Temperature dependence of quench current

Quench current dependence on temperature is plotted in Fig. ??. HGQS01 did not train to the short sample limit of the superconducting cable at 1.9K, so it was expected not to follow the predicted temperature dependence curve. We observed that the quench current in test cycle I is higher around the lambda point but that otherwise it shows flat temperature dependence up to 3.75K. This effect is perhaps caused by the increased cooling afforded by superfluid He which has higher thermoconductivity and specific heat around the lambda point. At 4.13K the magnet quench current was much lower than one would expect based on quench currents at other temperatures. This odd quench current is not inconsistent with a mechanically limited magnet. Furthermore, in test cycle II we observed irratic quench current temperature dependence. However, it is interesting to point out that the quench current at 4.42 K was at the short sample limit in both test cycles.

2.4 Quench locations and quench propagation velocity

The 96 voltage taps that instrumented HGQS01 allowed for localization and determination of quench propagation velocity for most quenches. The quench propagation velocity was determined using a "time of flight" technique. The basic idea of this technique is to determine the time needed for the quench to propagate between voltage taps separated by a known distance. The start time of a quench in a voltage tap segment was determined by tracing back the voltage rise in the segment to the last point 2σ below the noise. The difference between this start time and the start time of the adjacent segment was used to determine the velocity. In some cases, the change in slope of the segment where the quench was initiated was used to indicate that the quench had moved to an adjacent segment rather than using the start time of the adjacent segment itself.

The resulting quench velocity can then be used to determine the location of the quench in the segment. The accuracy of these measurements is on the order of a couple of inches. Fig 2.4 shows the schematic view of the magnet

and the location of the voltage taps on the magnet. Figure 2.5 shows voltage tap signals during a sample spontaneous quench (quench number 21). The locations of each spontaneous quench and their quench propagation velocities are summarized in Table 2.3-Table 2.7. Quench propagation velocity as a function of the normalized current (I/I_c) is plotted in Fig 2.6. From Fig 2.6 one observes that the quenches in the end region are slower than those in straight sections.

Most of the spontaneous quenches occurred in the end regions close to voltage taps. It was important to verify whether the quenches were right at the voltage taps or just close by. For each quench we determined the noise level of the signal and estimated how much error it contributes in finding the start time of the quench. In Table 2.3 we listed the time difference between the two adjacent voltage segments for quenches starting near a voltage tap. Also listed is the estimated value of the time difference. These start time differences and uncertainties are fractions of a millisecond and it is difficult to make conclusions. Some particular quenches, however, would seem clearly not to start directly at a voltage tap (e.g. #19).

2.5 Quench current ramp rate dependence studies

HGQS01 quench current as a function of ramp rate is shown in Fig 2.7. Since the magnet was not trained, there was no reason to do low ramp rate quenches. 4.5K ramp rate quenches occurred at the ramp splice region and at the same location in the magnet. 1.9K quenches were close to the end region. Fig 2.8 shows the ramp rate dependence as a function of the normalized current.

Table 2.1: Instrumentation settings - spontaneous quenches

Dump Resistor	Resistance	$60m\Omega$
	Time Delay	$25msec$
Power Supply	Time Constant	$0.5sec$
HFU	Capacitance	$14.4mF$
	Time Delay	$0 - 20msec$
	Voltage	$250V@4.3K$
		$300V@1.9K$
Data Logger	Sampling frequency	$7.4kHz$
	Pre-quench window	50%
Current read back	Hollec	

Table 2.2: QDC settings

AQDC name	Threshold settings	Threshold values
Whole coil	1.0	10 V
Whole coil - Idot	0.09	0.9 V
Bucked Half coils	0.06	0.24 V
SC Leads	0.72	0.03 V
Cu Leads	0.74	0.03 V
Ground	1.26	0.1 V

Table 2.3: Quench history. Test cycle I

Quench num	T [K]	dI/dt [A/s]	I_q [A]	Quench location
1	4.504	16	8776	Q3O15d_Q3O15b st.sec. next to Vtap 15d .0008 sec +-.0012
2	4.500	16	9107	Q1IOrs_Q1I16a Le.end next to Vtap 16a .0004 sec +-.0003
3	4.515	16	9265	Q4I14d_Q4I14c Re.end
4	4.523	16	9310	Q3O15c_Q3O15d Re.end
5	4.556	149	8187	Q1I14b_Q1IOrs Ramp splice
6	4.563	295	6586	Q1I14b_Q1IOrs Ramp splice
7	1.864	2	10327	Q4O15d_Q4O15c Re.end next to Vtap 15d .0003 sec +-.0006
8	1.874	2	10568	Q3O15c_Q3O15d Re.end next to Vtap 15c .0002 sec +-.0008
9	1.872	2	10773	Q2O15c_Q2O15a st.sec next to Vtap 15a .0005 sec +-.0003 Q4O15c_Q4O15a st.sec from Vtap 15a .0013 sec +-.0012
10	1.867	2	11001	Q1O3Is_Q1O15b unknown; Re.end quenched as well (15c-15d)
11	1.877	2	11226	Q3O16b_Q3O15a Le.end next to Vtap 15a .0004 sec +-.0005
12	1.875	2	11281	Q2O15d_Q2O15c Re.end next to Vtap 15c .0003 sec +-.0003
13	1.884	1	11447	Q1O15c_Q1O15d St.sec next to Vtap 15d .001 sec +-.0008
14	1.857	3	11562	Q4O15a_Q4O16b Le.end next to Vtap 15a .0003 sec +-.0004
15	1.872	150	11752	Q1IOrs_Q1I16a Vtap 16a +-.0002 sec
16	1.874	198	11707	Q3O15c_Q3O15d Re.end
17	1.890	297	10965	Q1I14b_Q1IOrs Le.end next to Vtap 14a .0009 sec
18	1.753	16	11192	Q2O15d_Q2O15c Re.end closer to 15c
19	1.935	16	11656	Q1O16b_Q1O15a Le.end next to Vtap 15a .0005 sec +-.0005
20	2.094	16	11898	Q4I14d_Q4I14c Re.end closer to 14d
21	2.217	16	11866	Q4O15b_Q4O15d st.sec closer to 15b
22	2.747	16	11372	Q4I11b_Q4I11d st.sec
23	3.266	16	11237	Q4I2Os_Q4O15b Re.end closer to 15c
24	3.751	16	11208	Q4O15d_Q4O15c Re.end closer to 15d
25	4.133	16	10306	Q1O3Is_Q1O15b Re.end closer to 15d
26	4.457	15	10477	Q4I11c_Q4I11a st.sec closer to 11a

Table 2.4: Quench history. Test cycle II

Quench num	T [K]	dI/dt [A/s]	I_q [A]	Quench location
27	4.5	16	9421	Q3O15b_Q3O4O Mult. turn
28	4.5	16	9755	Q3O16b_Q3O15a Le.end next to Vtap 16b
29	1.9	16	10653	Q3O15d_Q3O15b Re.end next to Vtap 15d
30	1.9	16	11425	Q3O15c_Q3O15d Re.end next to Vtap 15c
31	1.9	16	11718	Q1O15d_Q1O15b st.sec middle
32	1.9	16	11777	Q4I11d_Q4I11c Re.end
33	1.9	16	11809	Q2O15d_Q2O15c Re.end next to Vtap 15c
34	1.9	16	12254	Q1O15c_Q1O15d Re.end next to Vtap 15c
35	1.9	16	12196	Q4I2O_Q4O15b Multi. turn
				Q2O15c_Q2O15d Re.end middle
36	1.9	16	12245	Q4O15c_Q1O15a Le.end next to Vtap 15a
37	1.9	16	12384	Q3O16c_Q3O16d Re.end next to Vtap 16d
38	1.9	16	12543	Q2O15c_Q2O15a Re.end next to Vtap 15c
39	1.9	16	12198	Q4I2O_Q4O15b Multi. turn
				Q2O16c_Q2O16d Re.end middle
40	1.9	16	12155	Q4I2O_Q4O15b Multi. turn
				Q2O15c_Q2O15d Re.end middle
				Q2O16c_Q2O16d Re.end middle
41	1.9	16	11386	Q4I2O_Q4O15b Multi. turn
42	1.9	16	11199	Q2O15c_Q2O15d Re.end
43	1.9	16	12551	Q4I11d_Q4I11c Re.end
44	2.15	16	11465	Q3O15c_Q3O15d Re.end next to Vtap 15d
45	2.5	16	11392	Q4I2O_Q4O15b Multi. turn
46	2.9	16	11608	Q4I2O_Q4O15b Multi. turn
47	3.7	16	10530	Q2O15d_Q2O15c Re.end
48	4.2	16	9713	Q2O15d_Q2O15c Re.end
49	4.42	16	10674	Q1O16d_Q1O16b st.sec

Table 2.5: Quench files; test cycle I

Quench num	File name
1	hgqs01.Quench.980206191022.266
2	hgqs01.Quench.980206200008.901
3	hgqs01.Quench.980206203452.027
4	hgqs01.Quench.980206210845.355
5	hgqs01.Quench.980207100628.095
6	hgqs01.Quench.980207104206.429
7	hgqs01.Quench.980209194750.419
8	hgqs01.Quench.980209202844.761
9	hgqs01.Quench.980209214020.309
10	hgqs01.Quench.980209222243.972
11	hgqs01.Quench.980209230659.641
12	hgqs01.Quench.980209235547.919
13	hgqs01.Quench.980211161637.567
14	hgqs01.Quench.980211173725.424
15	hgqs01.Quench.980211185229.883
16	hgqs01.Quench.980211200439.993
17	hgqs01.Quench.980211204437.265
18	hgqs01.Quench.980217120655.987
19	hgqs01.Quench.980217130946.098
20	hgqs01.Quench.980217134619.230
21	hgqs01.Quench.980217143216.588
22	hgqs01.Quench.980217161318.105
23	hgqs01.Quench.980217173350.080
24	hgqs01.Quench.980217181038.576
25	hgqs01.Quench.980217185255.233
26	hgqs01.Quench.980217214912.299

Table 2.6: Quench files, test cycle II

Quench num	File name
27	hgqs01.Quench.980314150328.159
28	hgqs01.Quench.980314155338.281
29	hgqs01.Quench.980319141741.161
30	hgqs01.Quench.980319172623.281
31	hgqs01.Quench.980319190457.432
32	hgqs01.Quench.980319204509.246
33	hgqs01.Quench.980319215612.857
34	hgqs01.Quench.980320153718.258
35	hgqs01.Quench.980320170911.812
36	hgqs01.Quench.980320181523.750
37	hgqs01.Quench.980320192657.008
38	hgqs01.Quench.980320203527.483
39	hgqs01.Quench.980320213905.909
40	hgqs01.Quench.980321100330.598
41	hgqs01.Quench.980321111813.636
42	hgqs01.Quench.980323165937.641
43	hgqs01.Quench.980324131458.008
44	hgqs01.Quench.980324152704.008
45	hgqs01.Quench.980324161832.250
46	hgqs01.Quench.980324173120.567
47	hgqs01.Quench.980324184446.990
48	hgqs01.Quench.980324200722.220

Table 2.7: Quench propagation velocities

Quench number	Coil	15c-15d m/sec	15a-15c m/sec	15b-15d m/sec	15a-16b m/sec	16c-16d m/sec	16a-16c m/sec	16b-16d m/sec
1	Q3	33.9	98.2					
2	Q1					66.0		
4	Q3		104.3	101.4	53.3			
7	Q4	13.4						
8	Q3	19.7	46.0					
9	Q2 Q4		51.1 52.6		15.0			
11	Q3	34.6	61.2					68.6
12	Q2	17.0	52.0					
13	Q1	18.0						
14	Q4	43.3	66.0		19.7	33.9		85.7
15	Q1					38.3	69.7	
19	Q1	36.8	71.3			37.1		92.9
21	Q4	61.8		93.9				
23	Q2		133.8	125.3		33.9		
24	Q4		142.7	128.2		32.2		

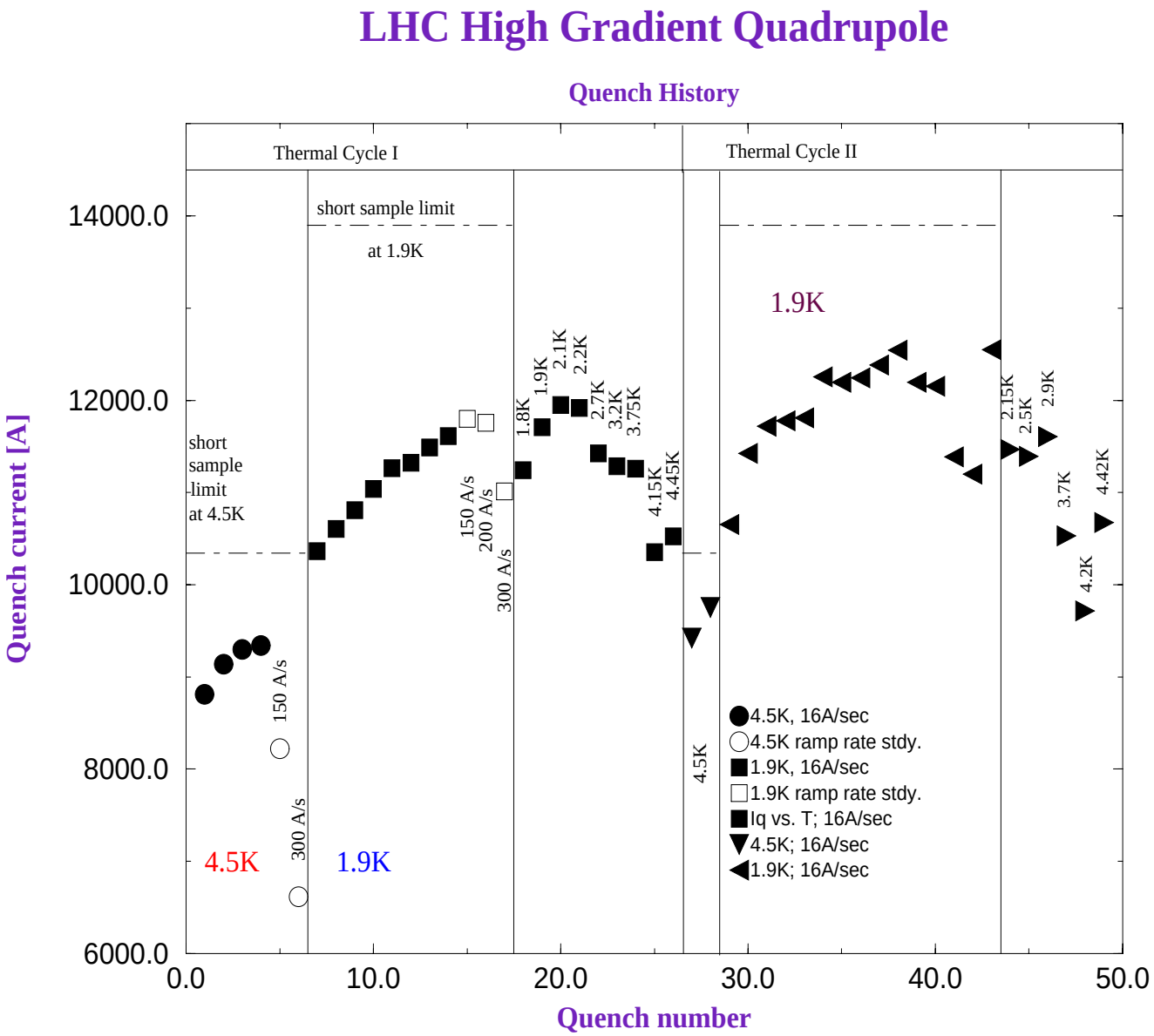

Figure 2.1: Quench history (qhist.eps)

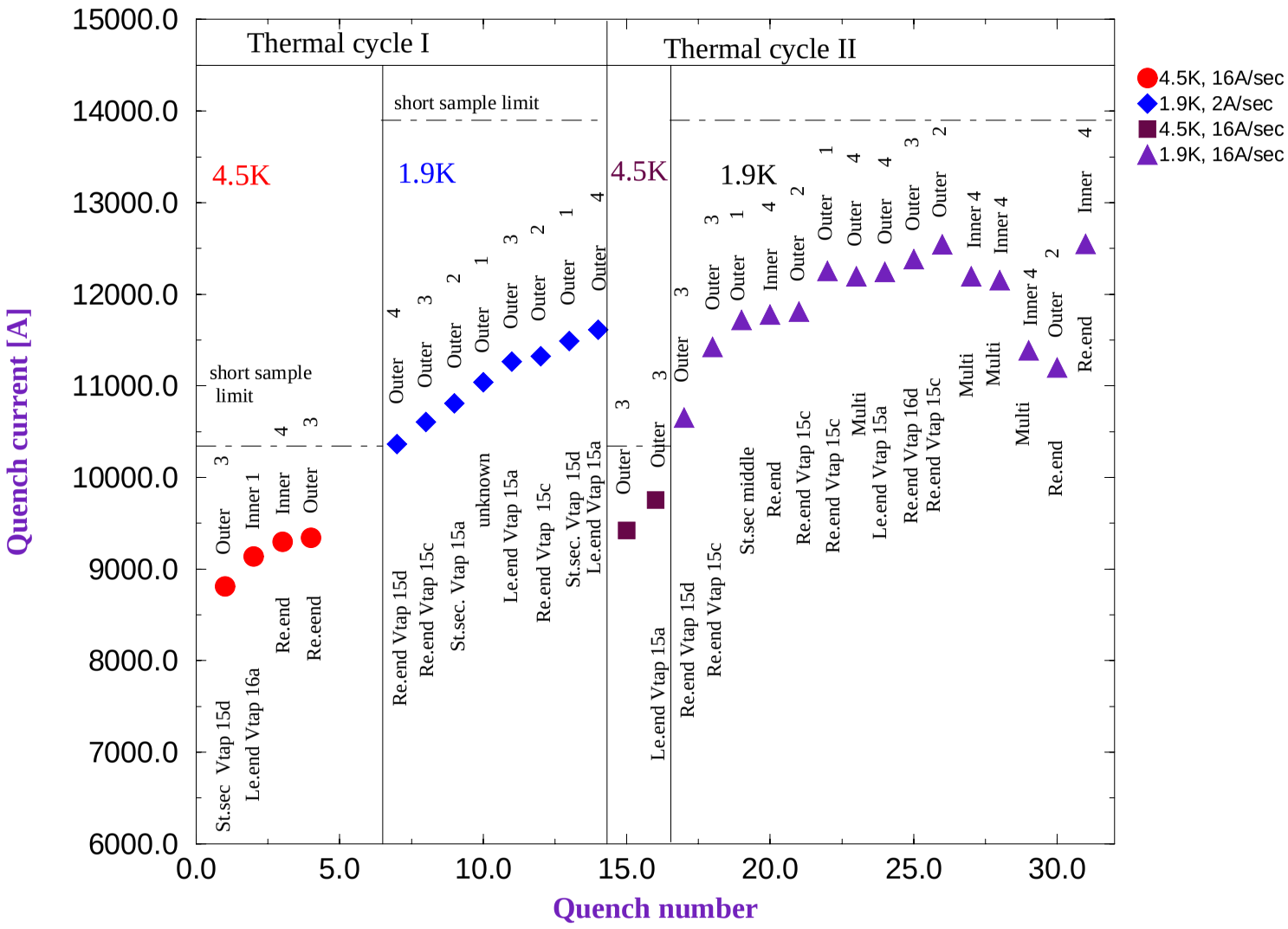

Figure 2.2: Training quenches (qtrain.eps)

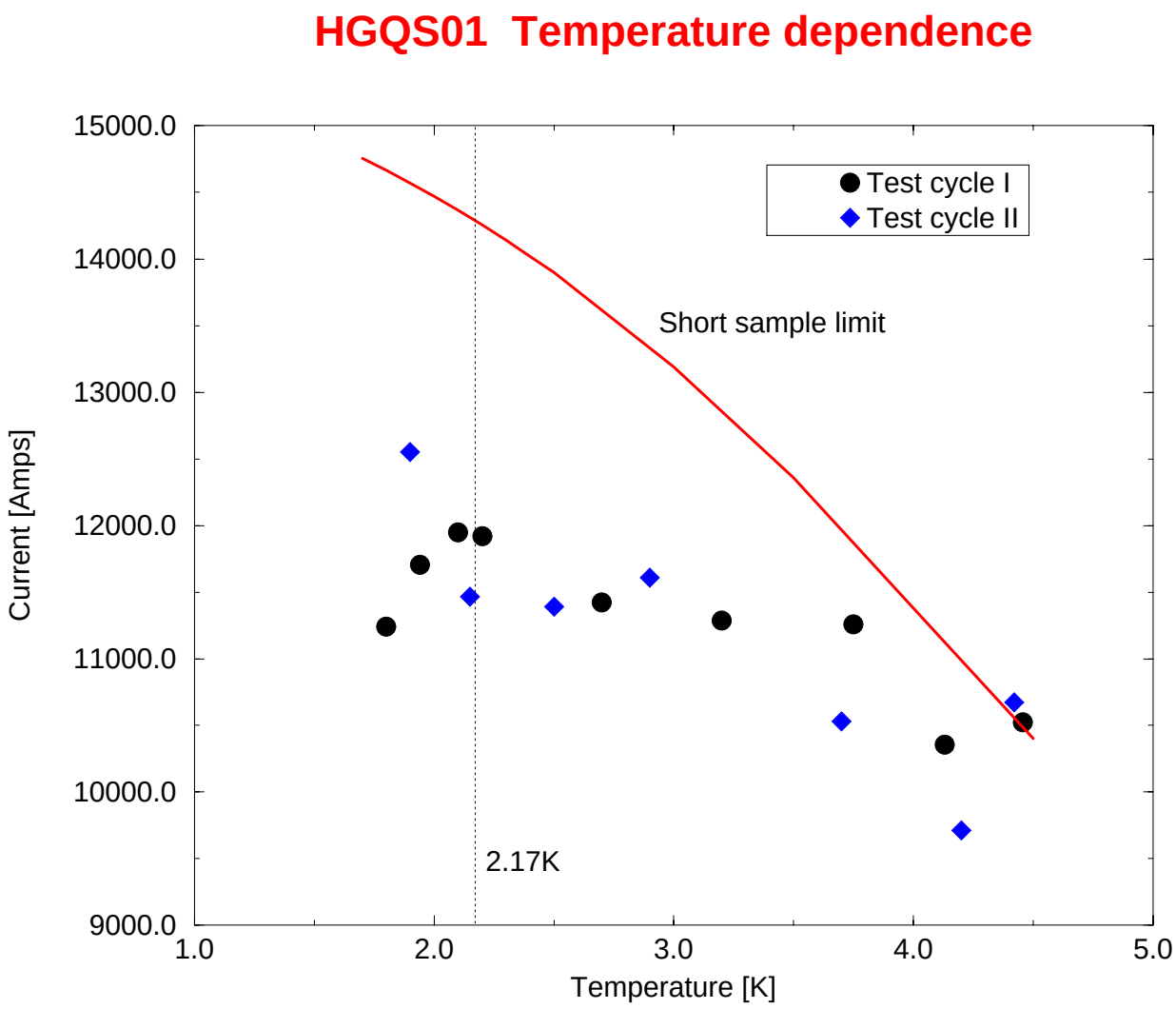

Figure 2.3: Quench current temperature dependence (qtemp.eps)

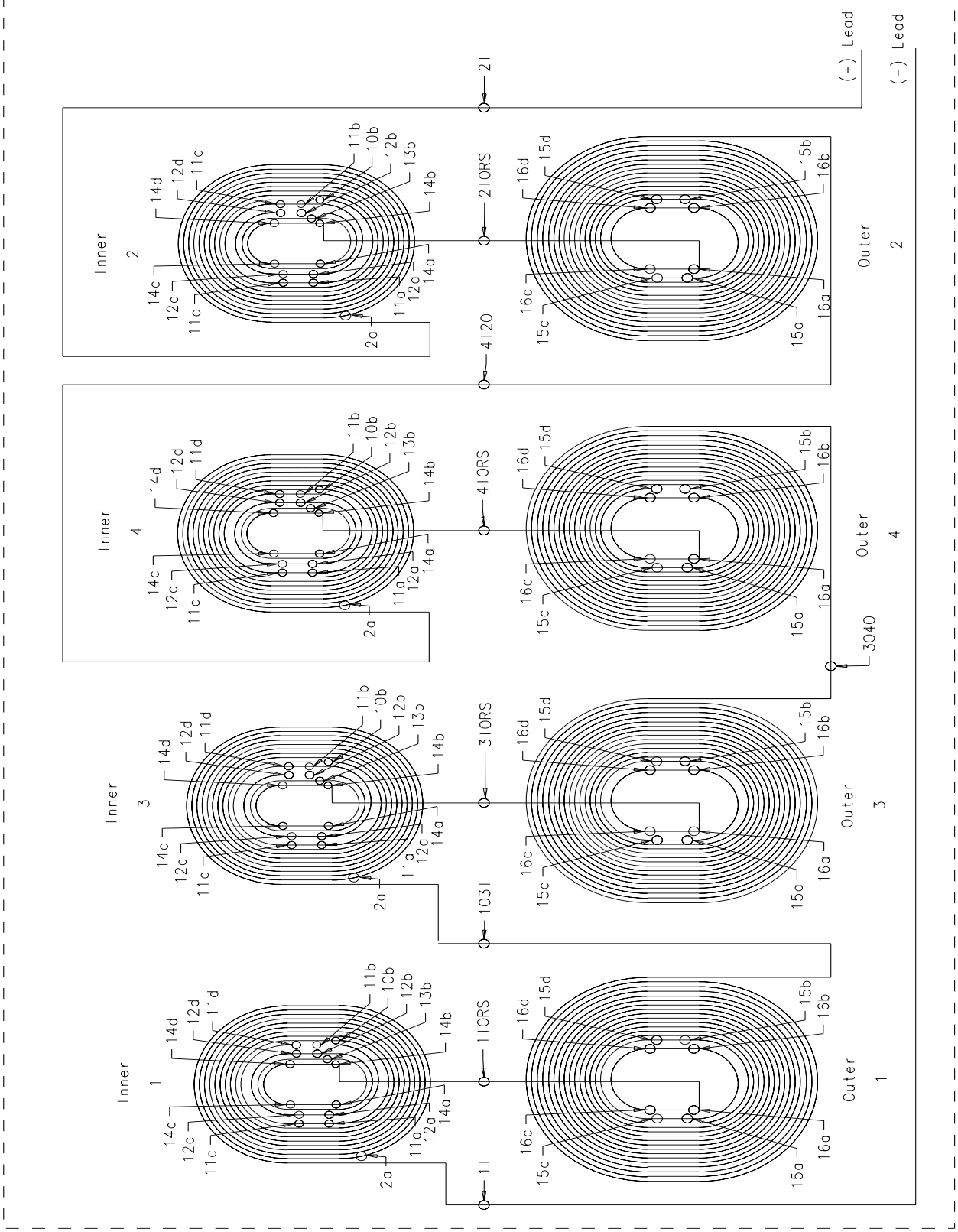

Figure 2.4: Layout of the coils and location of the voltage taps. (hgq_coil.ps)

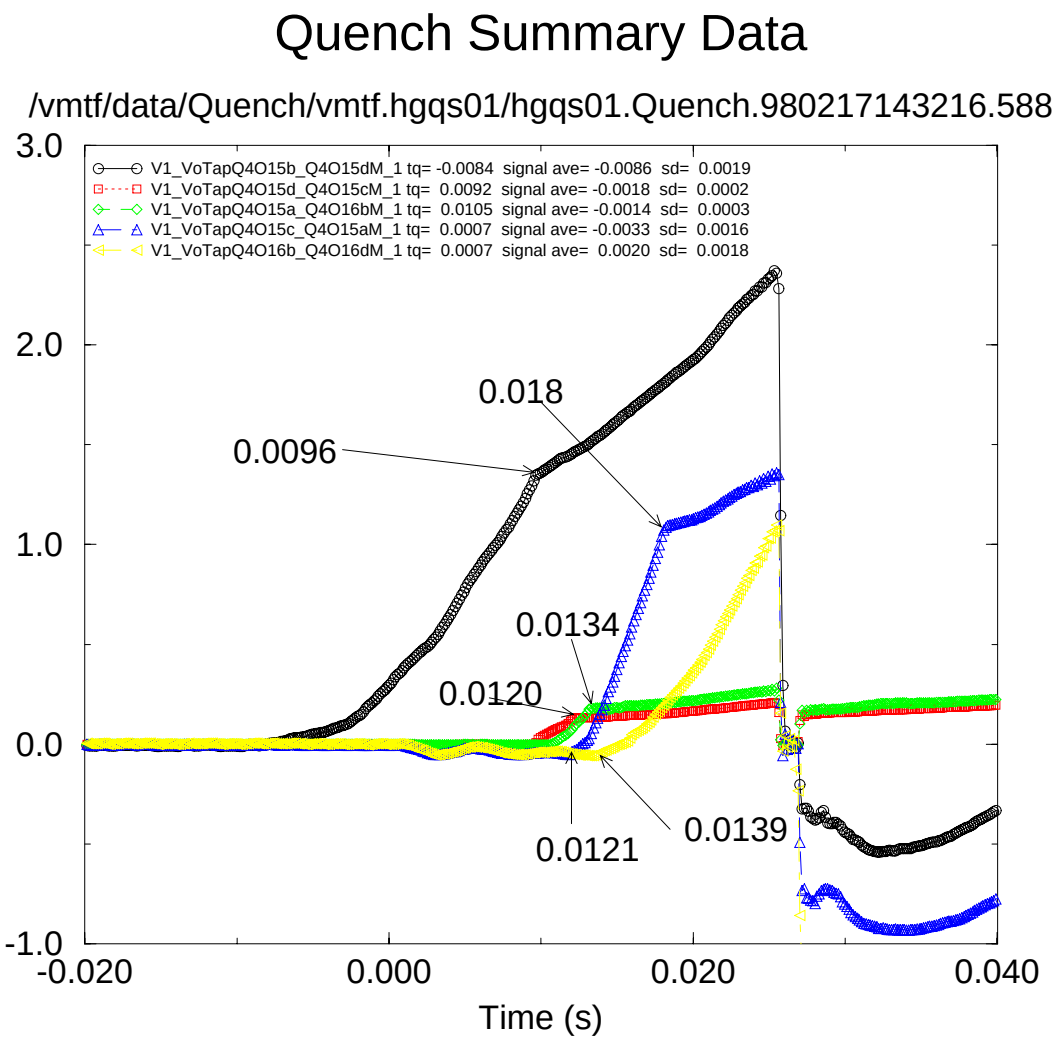

Figure 2.5: Voltage rise (*voltage_rise.eps*)

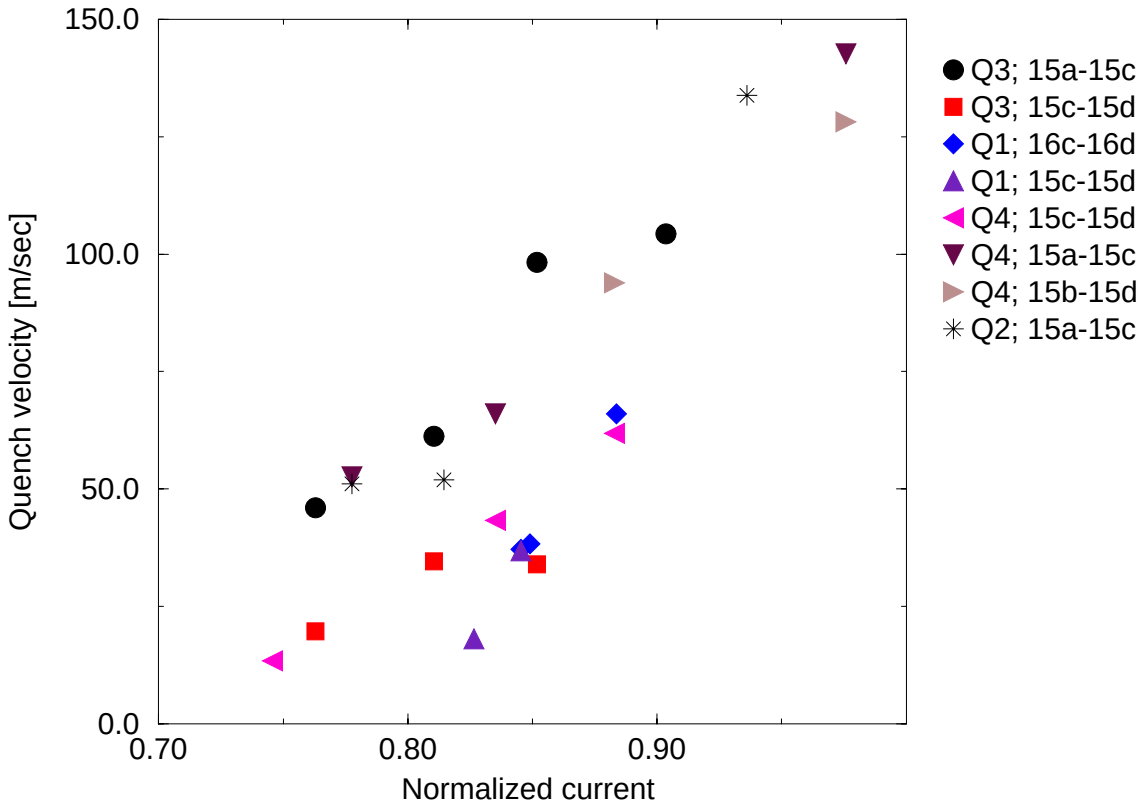

Figure 2.6: Quench propagation velocity as a function of I/I_c (qvel.eps)

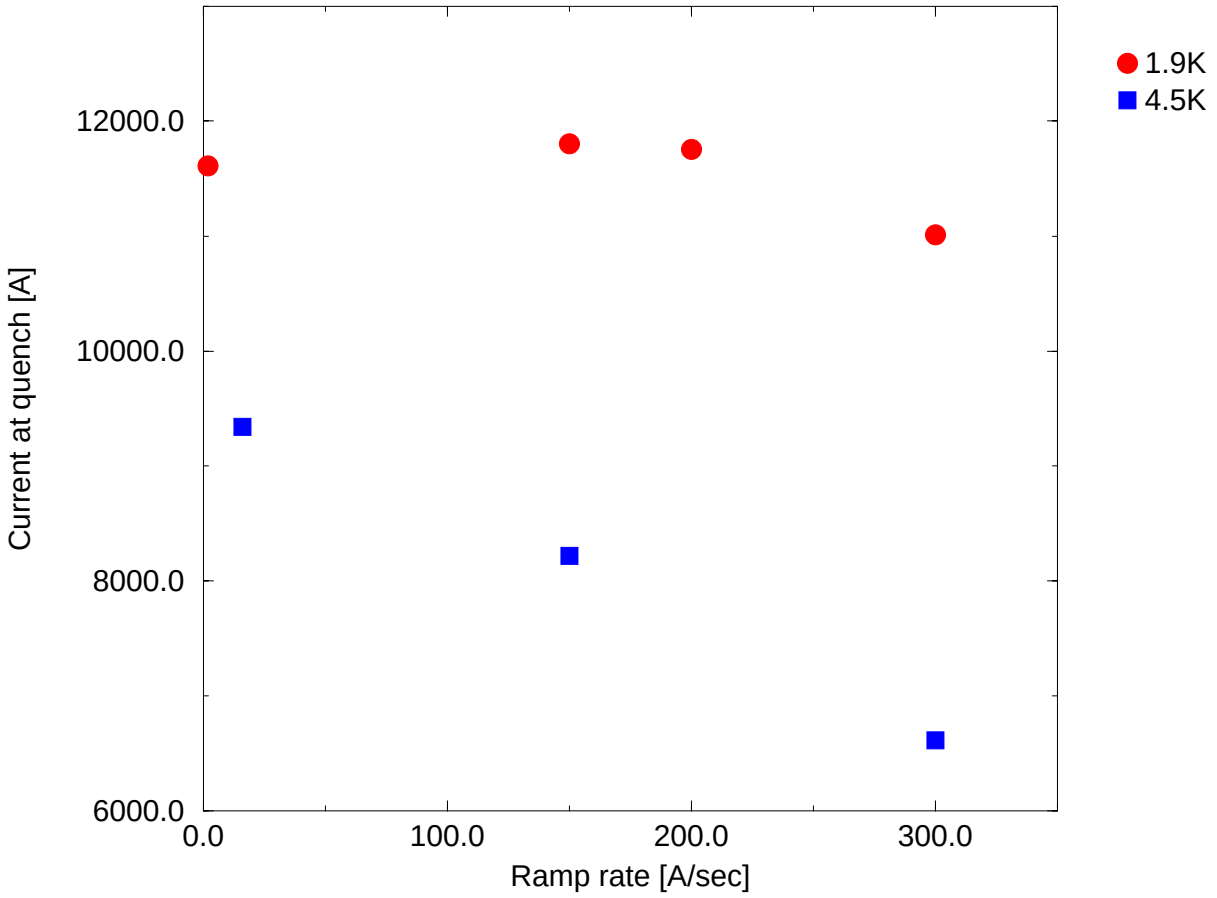

Figure 2.7: Quench current ramp rate dependence (qramp.eps)

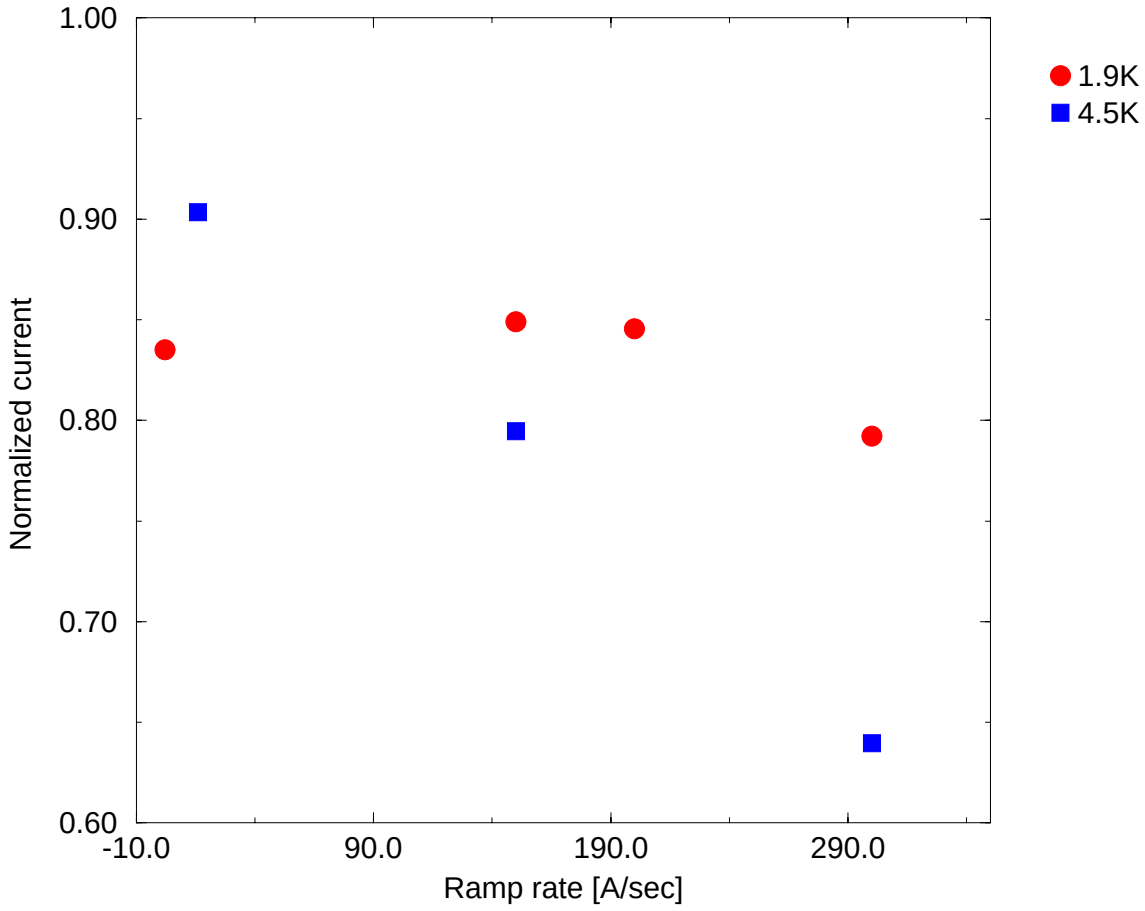

Figure 2.8: Normalized quench current ramp rate dependence (*norm_qramp.eps*)

Chapter 3

Quench protection heater study

This chapter presents the results of the quench protection heater studies.

3.1 Quench protection heaters

The heaters are 25μm thick, 15.88 mm wide, stainless steel strips and are located radially between the inner and outer coil, in the middle of four layers of 125 μm Kapton sheets. One heater covers approximately 10 turns (turn #2-#11) of two midplane-adjacent outer and inner coils. This is accomplished by running the heater longitudinally along the body of the magnet and making the appropriate connection (soldering a wire) between two strips in the magnet return end region. Four heaters were installed in HGQS01. However, since two heaters oriented 180 degrees apart provide coverage for one side of each of the four coils, it was sufficient to use only one pair of heaters at any given time. The resistance of the heater for coils 1 and 2 was 4.95 Ω, that for 2 and 3 was 4.97 Ω, that for 3 and 4 was 4.95 Ω and that for 4 and 1 was 4.93 Ω. The system resistance (including cabling from the Strip Heater Firing Unit (SHFU) to the magnet) was 5.4 Ω , which means that $\sim$ 92 % of the SHFU voltage was deposited directly to the heaters. Note that in all studies, the voltage reading of the SHFU is used as the voltage applied to the heater.

3.2 Heater induced quenches

In the heater studies, the minimum energy required to initiate a quench as well as the time delay, t_{fn} (the time from protection heater current initiation to the presence of a detectable quench voltage in the outer coils), were measured as a function of various heater, heater power supply, and magnet parameters. The minimum voltage to induce a quench (V_{min}) was determined by firing the SHFU at a voltage low enough not to initiate a quench and then gradually increasing the SHFU voltage and re-firing until the magnet did quench. Since the last voltage set on the SHFU that first initiated a quench was taken as V_{min} and the voltage increments were 10 volts, the uncertainty of the determination of the minimum voltage is $\sim$ 10V. Fig 3.1 shows an example of the t_{fn} determination. Both the start time of the quench and the firing time of the heater were determined by quenchXmgr, the same program used to find the quench initiation time for spontaneous quenches. Since some of the quench signals were noisy and the program sometimes was unable to find the correct start time, the quenches were each checked and if necessary corrected for these ambiguities.

The results are summarized in Figures 3.2 to 3.6 . The I_c used in the plots (for current normalization) corresponds to the expected short sample limit of the superconducting cable: 10340A @ 4.5K and 13900A @ 1.9K.

3.2.1 Minimum quench voltage

Fig 3.2 shows the minimum SHFU voltage required to quench the magnet as a function of the normalized magnet current I/I_c at quench (where I is the magnet current at quench and I_c is the expected short sample limit of the superconducting cable). As expected, the deposited energy increases as the applied current decreases and one is further from the critical surface. Furthermore, one can conclude that by setting the SHFU voltage to 300V, the heaters can always initiate a quench in the outer coils for $I/I_c > 0.2$.

3.2.2 Time delay t_{fn}

Figures 3.3- 3.5 show t_{fn} as a function of the SHFU voltage at four different currents. Each of the plots represents the same data but uses a different signal to get the quench initiation time: Fig 3.3 uses the digital quench

detection signal, Fig 3.4 the analog quench detection signal, and Fig 3.5 the 8^{th} coil signal. Note that for the 8^{th} coil quench initiation times of Fig 3.5, a fixed resistance of $33\mu\Omega$ was used as a threshold to indicate the start of a quench. As one can see, at the lower heater energies (close to V_{min}), the t_{fn} increases rapidly while at higher energies t_{fn} levels off. At sufficiently large SHFU voltage, t_{fn} does not change significantly with changes in SHFU voltage.

Fig 3.7 plots the 8^{th} coil signals of a heater induced quench ($SHFU = 400V, I/I_c = 0.84$) as a function of time. It shows a definite spread of the start time of the quenches among the different 8^{th} coils. The spread is on the order of 30 msec, with the outer coils were quenching first, then the inner coils.

Table 3.1: Instrumentation settings - heater induced quenches

Dump Resistor	Resistance	$60m\Omega$
	Time Delay	$25msec$
Power Supply	Time Constant	$0.5sec$
HFU	Capacitance	$14.4mF$
	Voltage	$90 - 400V@1.9K$
Data Logger	Sampling frequency	$7.4kHz$
	Pre-quench window	50%
Current read back	Hollec	

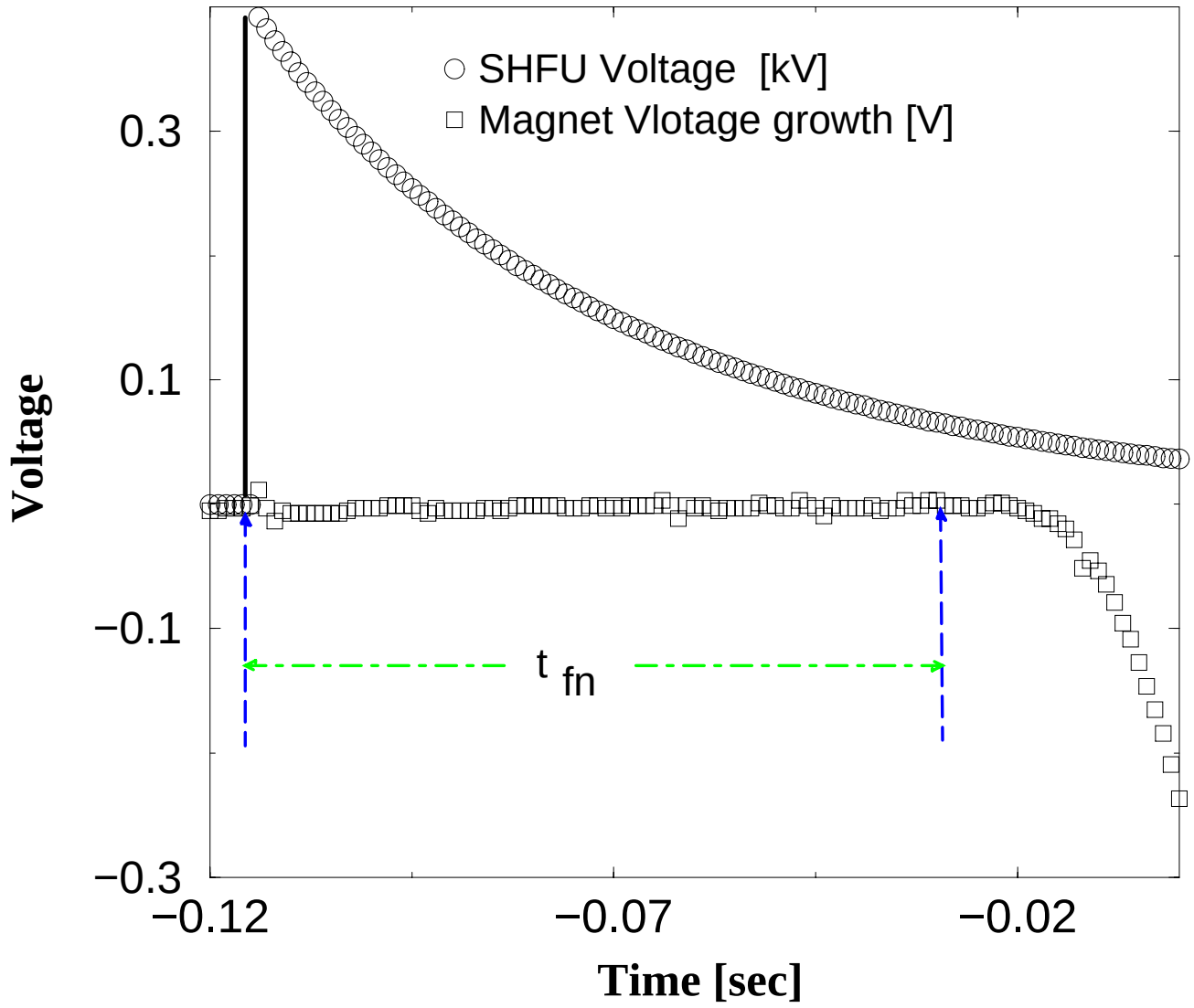

Figure 3.1: Description of t_{fn} (heat_examp.eps)

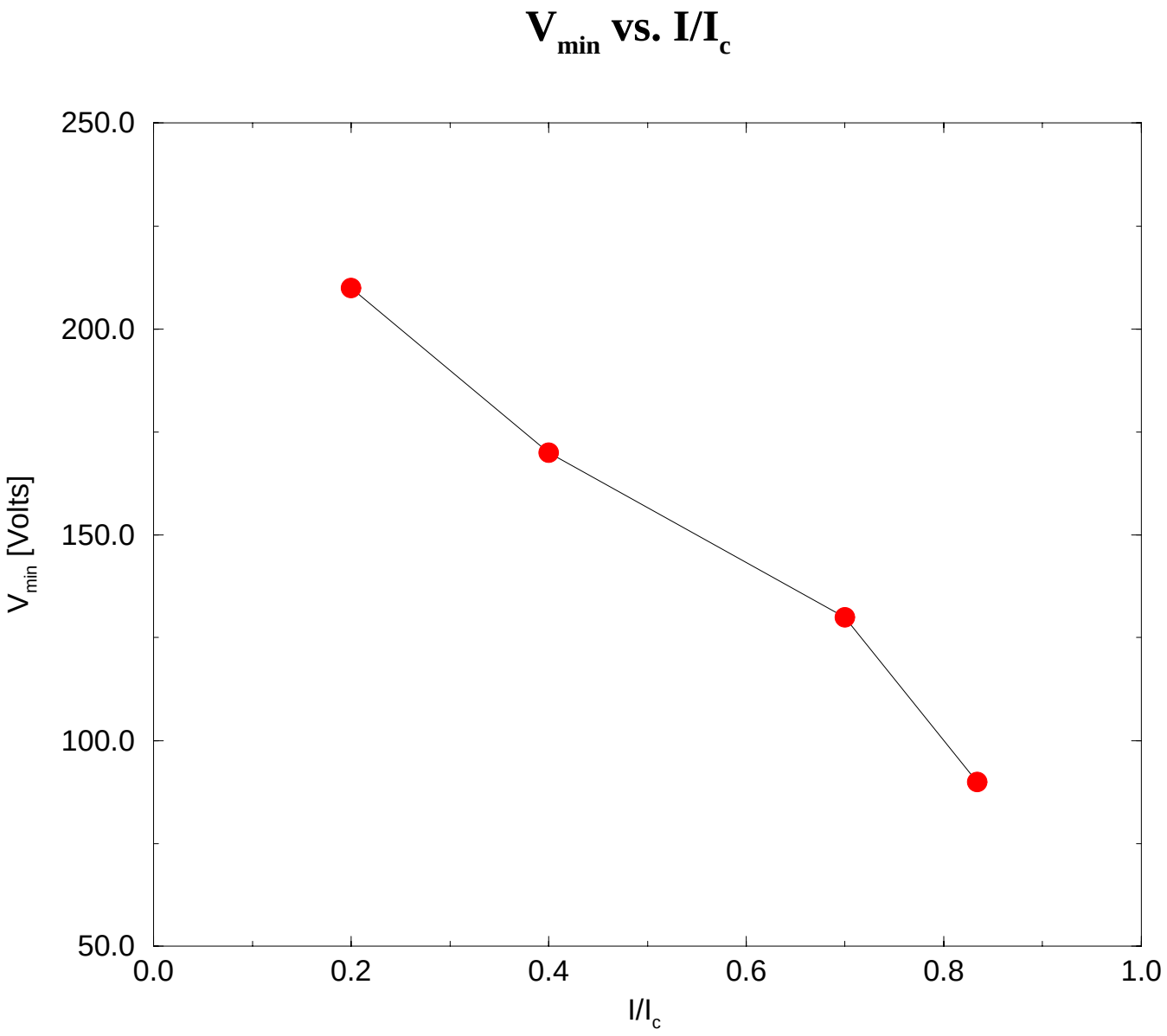

Figure 3.2: Heater induced quenches. Minimum heater voltage is plotted to quench the magnet vs. normalized current at quench (vmin.eps)

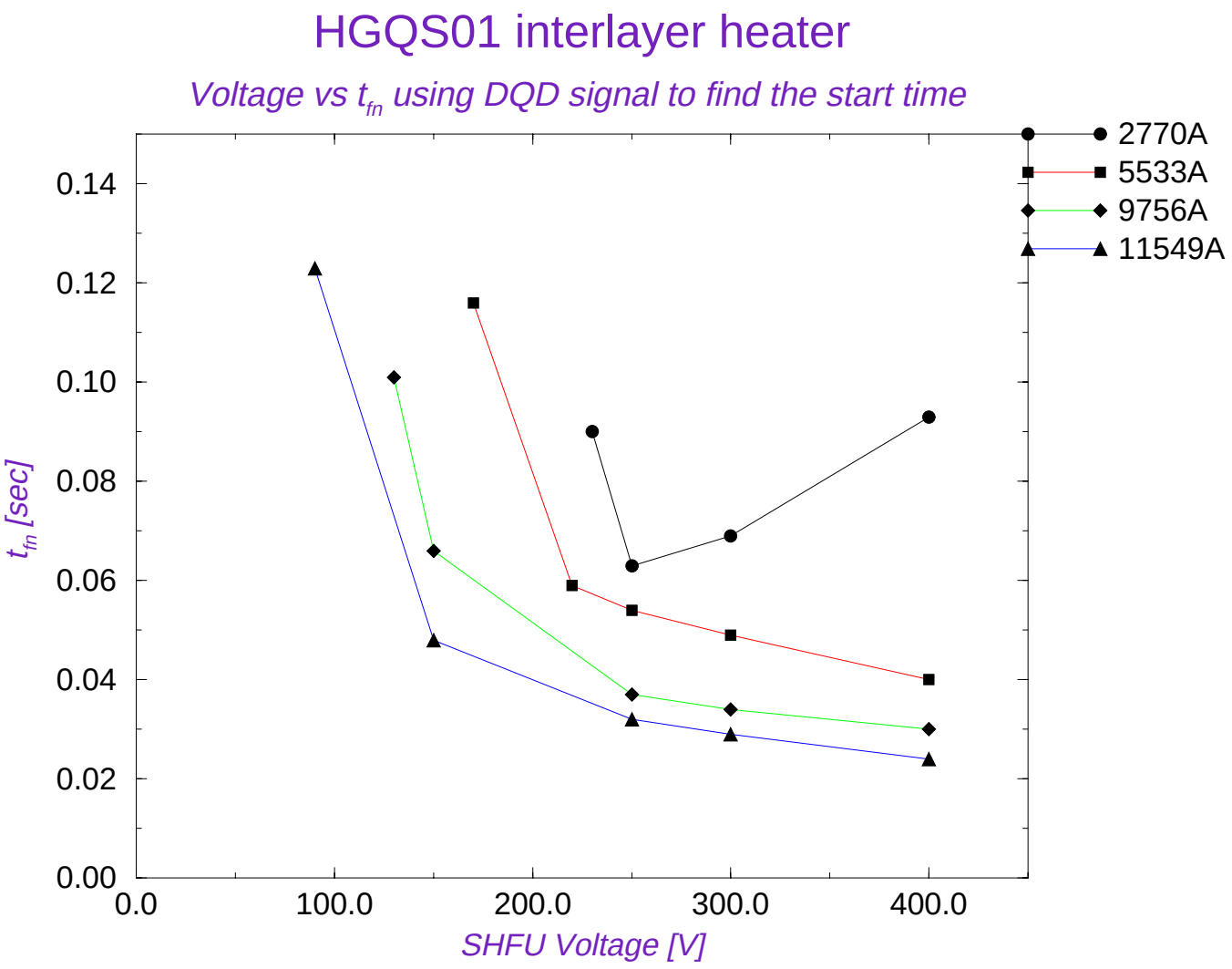

Figure 3.3: Heater induced quenches.t_{fn} is plotted as a function of the SHFU voltage. DQD signal is used to find the quech initiation time (volt_tfn_dqd.eps)

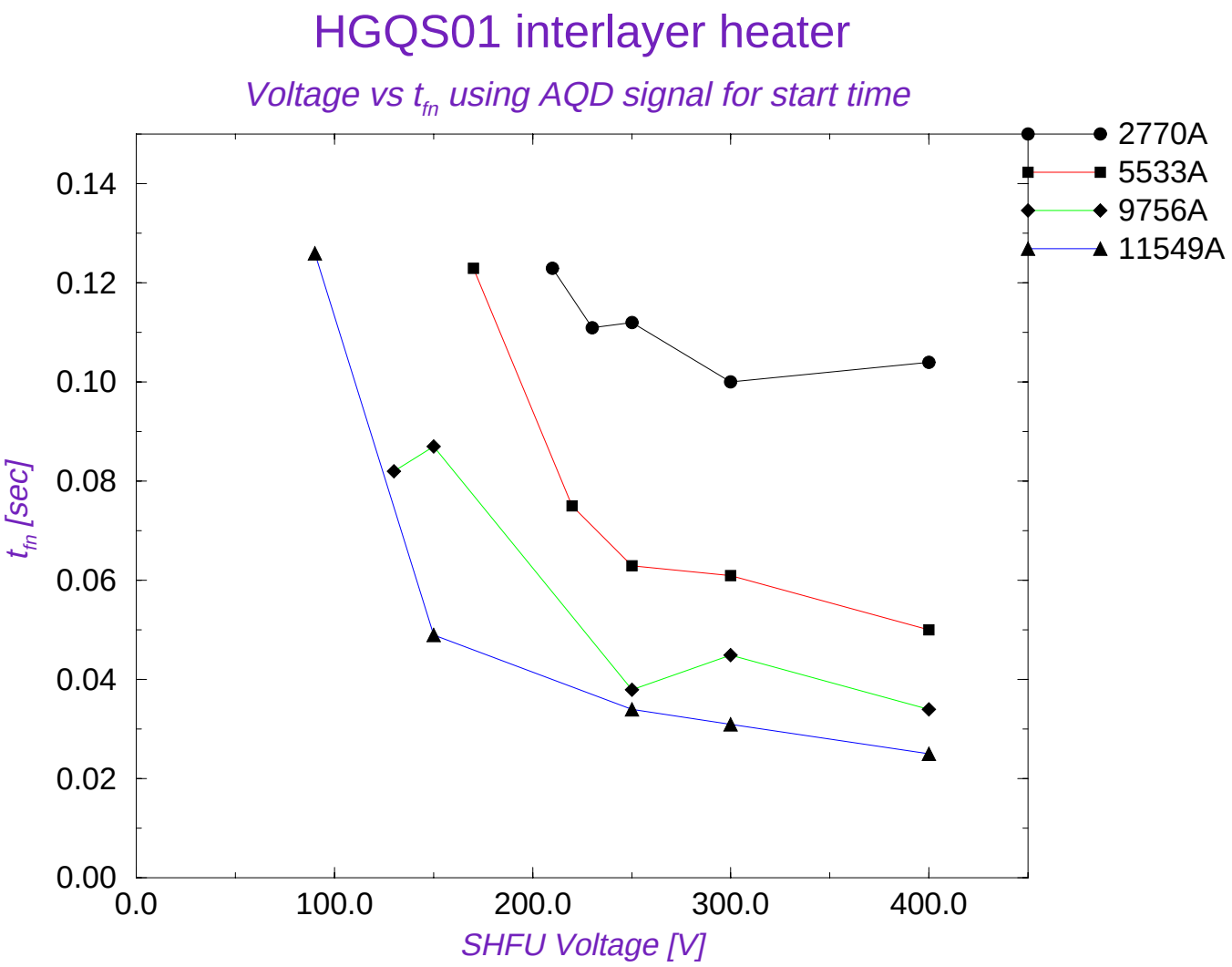

Figure 3.4: Heater induced quenches.t_{fn} is plotted as a function of the SHFU voltage. AQD signal is used to find the quech initiation time (volt_tfn_aqd.eps)

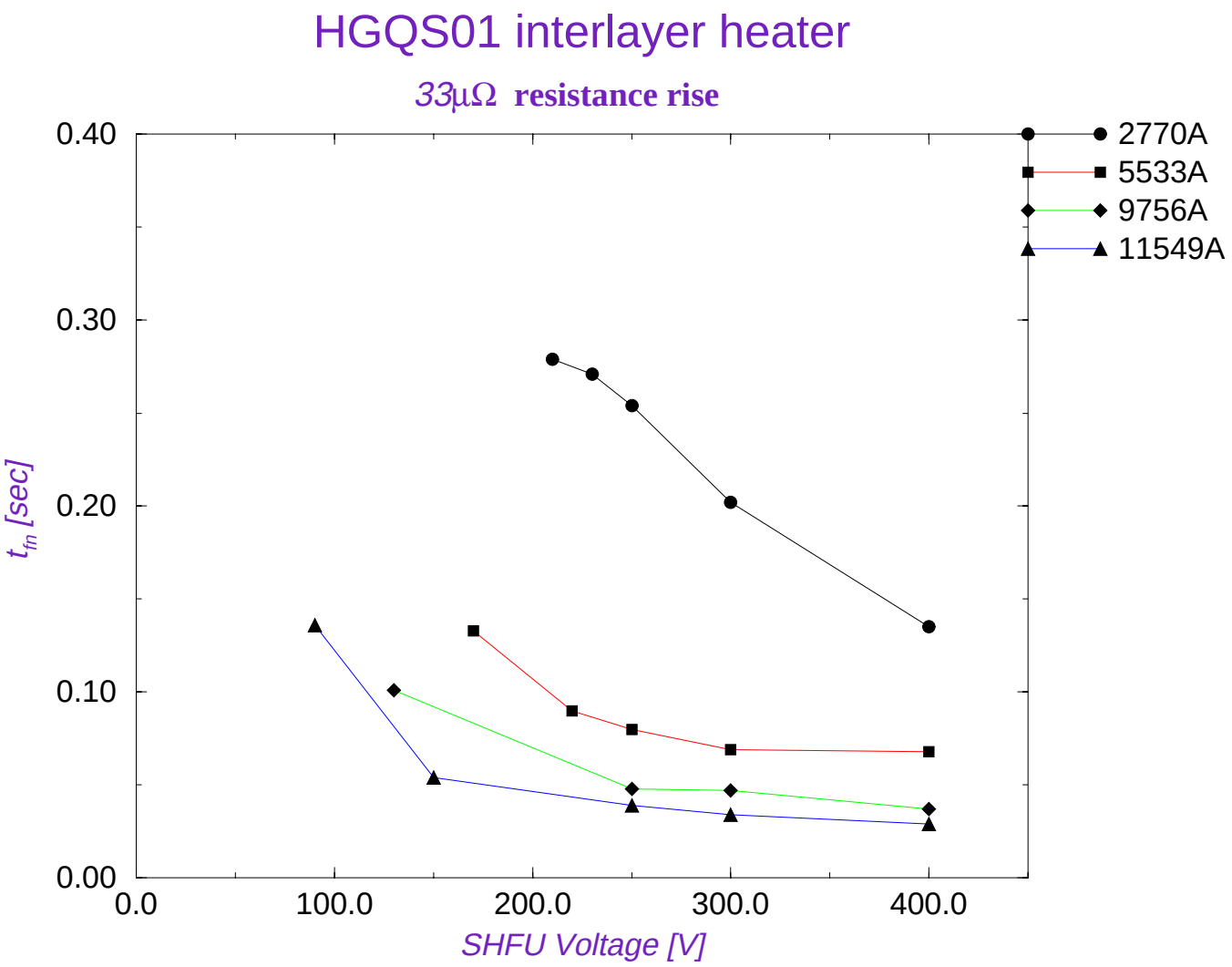

Figure 3.5: Heater induced quenches.t_{fn} is plotted as a function of the SHFU voltage. 8^{th} coil signal is used to find the quench initiation time (volt_tfn_30.eps)

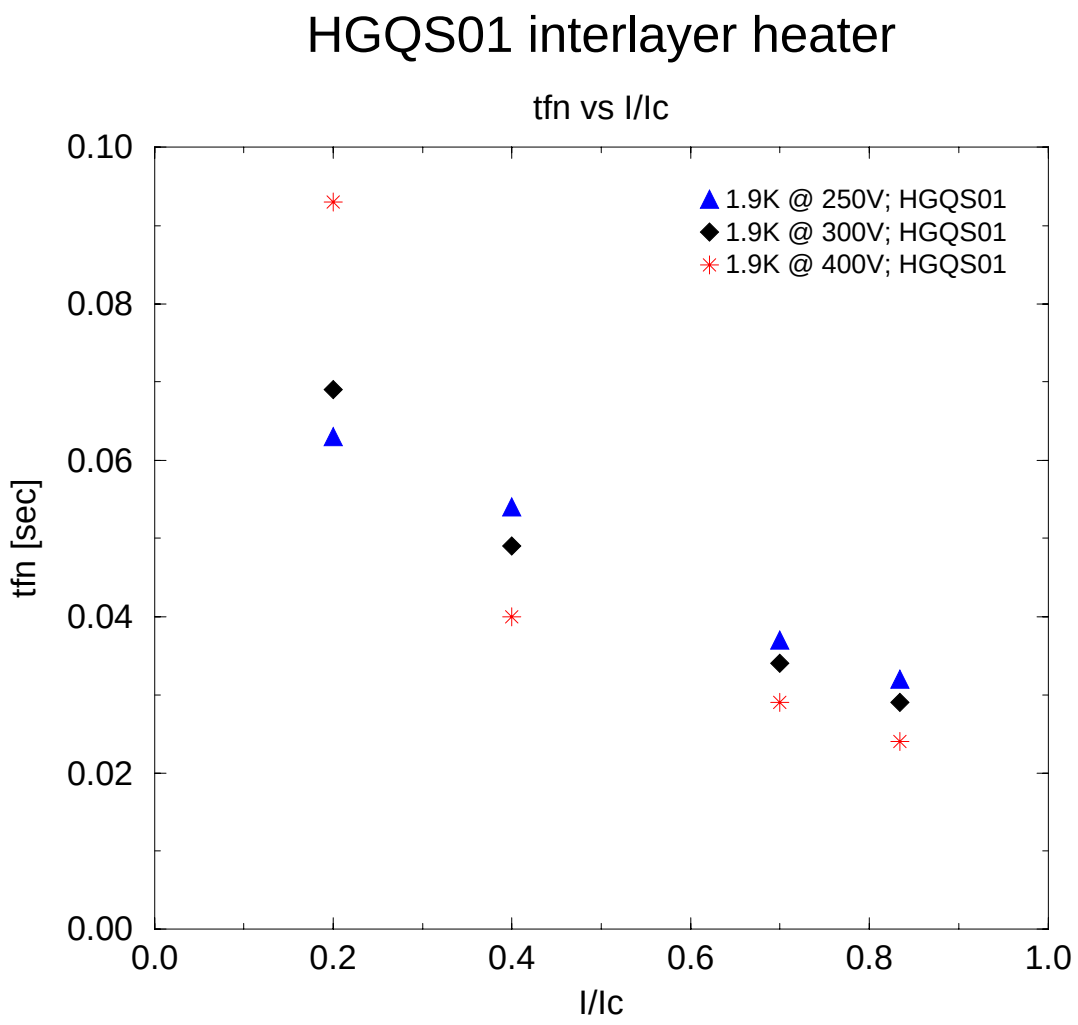

Figure 3.6: t_{fn} is plotted as a function of I/I_c at a fixed SHFU voltages (tfn_ic.eps)

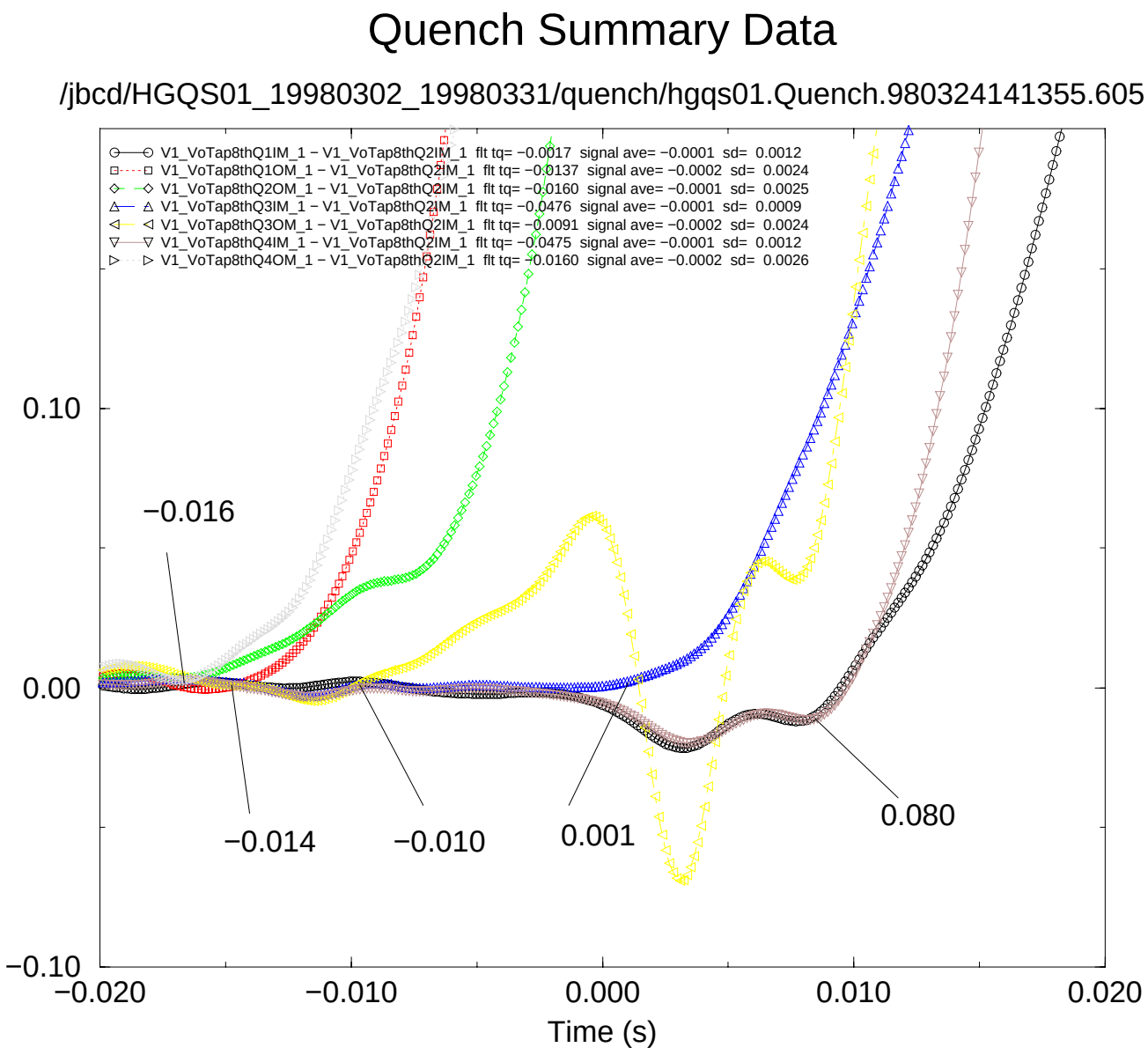

Figure 3.7: 8^{th} coil voltage signals are plotted as a function of time (8thcoil.eps)

Chapter 4

Strain Gauge Results

4.1 Instrumentation Details

Magnet HGQ01 is instrumented with an assortment of strain gauges to measure azimuthal coil stresses and coil end forces. These strain gauges are calibrated at room temperature and at liquid Helium temperature, and are read out during various phases of the magnet construction process, and while during cryogenic testing.

A total of eight beam-type strain gauges are used to measure azimuthal stresses in the straight section of the coils, four mounted at the inner coils, four mounted at the outer coils. Each active strain gauge has a compensating gauge associated with it, whose purpose is to provide an independent measure of the apparent strains induced in the active gauges due to thermal contraction and magneto-resistance effects.

Four capacitance-type strain gauges were also installed in the straight section of the inner coils to measure azimuthal stress. Each of these gauges were installed in such a way that they were in the same collared coil cavity as one of the inner coil beam gauges. Whilst normally a compensating gauge is not needed when using capacitance gauges, a fifth capacitance gauge was mounted in a stress-free manner onto the magnet shell to allow for the correction of any systematic errors that might exist due to differences between the measurement systems used in production and cryogenic testing.

A total of eight bullet-type gauges are used to measure the end forces associated with each inner/outer coil pair. Four bullet gauges are mounted at

the return-end of the magnet, while four are mounted at the lead end. Each bullet gauge consists of two strain gauges whose readings are subsequently averaged to eliminate strains resulting from bending of the transducer structure. The resultant strain is then used to compute the force on the bullet. Two compensating gauges are placed at each end of the magnet, whose readings are averaged in order to provide apparent strain data used in eliminating apparent strains from the active gauges.

Table 4.1 gives the list of coil azimuthal strain gauges, names, and locations for magnet HGQ01, while Table 4.2 lists the same information for the bullet gauges, and Table 4.3 lists this information for capacitance strain gauges.

Table 4.1: HGQ01 Beam Gauges

Production Gauge Name	VMTF Gauge Name	Gauge Type	Gauge Location	Remarks
BGIA009	BmAcQ2IR	Beam, inner, active	Quad 2, RE	Shorted
BGIA010	BmAcQ4IR	Beam, inner, active	Quad 4, RE	Shorted
BGIA016	BmAcQ2IL	Beam, inner, active	Quad 2, LE	
BGIA020	BmAcQ4IL	Beam, inner, active	Quad 4, LE	
BGOA014	BmAcQ2OR	Beam, outer, active	Quad 2, RE	
BGOA015	BmAcQ4OR	Beam, outer, active	Quad 4, RE	
BGOA018	BmAcQ2OL	Beam, outer, active	Quad 2, LE	
BGOA019	BmAcQ4OL	Beam, outer, active	Quad 4, LE	
BGIC001	BmCoQ2IR	Beam, inner, comp.	Quad 2, RE	Comp for BGIA009
BGIC003	BmCoQ4IR	Beam, inner, comp.	Quad 4, RE	Comp for BGIA010
BGIC006	BmCoQ2IL	Beam, inner, comp.	Quad 2, LE	Comp for BGIA016
BGIC009	BmCoQ4IL	Beam, inner, comp.	Quad 4, LE	Comp for BGIA020
BGOC012	BmCoQ2OR	Beam, outer, comp.	Quad 2, RE	Comp for BGOA014
BGOC014	BmCoQ4OR	Beam, outer, comp.	Quad 4, RE	Comp for BGOA015
BGOC020	BmCoQ2OL	Beam, outer, comp.	Quad 2, LE	Comp for BGOA018
BGOC021	BmCoQ4OL	Beam, outer, comp.	Quad 4, LE	Comp for BGOA019

Table 4.2: HGQ01 Bullet Gauges

Production Gauge Name	VMTF Gauge Name	Gauge Type	Gauuge Location	Remarks
BL01A/B	BuQ1R	Bullet, acti	e	Quad 1, RE
BL02A/B	BuQ2R	Bullet, acti	e	Quad 2, RE
BL03A/B	BuQ3R	Bullet, act	ve	Quad 3, RE
BL04A/B	BuQ4R	Bullet, act	ve	Quad 4, RE
BL05A/B	BuQ1L	Bullet, act	ve	Quad 1, LE
BL06A/B	BuQ2L	Bullet, act	ve	Quad 2, LE
BL07A/B	BuQ3L	Bullet, act	ve	Quad 3, LE
BL08A/B	BuQ4L	Bullet, act	ve	Quad 4, LE
BT22	BuCo_1	Bullet, compensator	RE	Comp. for RE bullets
BT23	BuCoR_2	Bullet, compensator	RE	”
BT24	BuCoL_1	Bullet, compensator	LE	Comp. for LE bullets
BT25	BuCoL_2	Bullet, compensator	LE	”

Table 4.3: HGQ01 Capacitance Gauges

Production Gauge Name	VMTF Gauge Name	Gauge Type	Gauge Location	Remarks
HQCGI21	CaQ1IR	Capacitance, active	Quad 1, RE	Opposes BGIA009
HQCGI22	CaQ1IL	Capacitance, active	Quad 1, LE	Opposes BGIA016
HQCGI23	CaQ3IR	Capacitance, active	Quad 3, RE	Opposes BGIA010
HQCGI24	CaQ3IL	Capacitance, active	Quad 3, LE	Opposes BGIA020
HQCGI25	CaCoIR	Capacitance, comp	LE, Shell	

4.2 Test cycle I

4.2.1 Measurement Schedule

Strain gauge readings are performed several times during the magnet construction and testing cycles. Azimuthal coil stresses, measured with beam-type and capacitance strain gauges, are measured during the collaring and yoking/skinning assembly procedures. After the end plates are installed onto the magnet cold mass, the bullet gauges are then installed and the end loading screws torqued to achieve the desired end loads, while the bullet gauges are monitored.

Once cold mass fabrication has been completed, the magnet is moved to the magnet test facility, and prepared for cryogenic testing. Before, during, and after cryogenic testing all strain gauges are monitored. In particular, strain gauge data is acquired while ramping the magnet to the first quench at 4.5K and 1.9K, with subsequent post-training runs made at each temperature in order to detect any significant changes in coil stress levels and distribution. Additionally, several runs were performed where the strain gauge data were monitored at a higher acquisition rate, to better measure the coils stresses as a function of excitation current, and determine if there was any evidence of "fast motion". (Normally, a single scan of all strain gauges is performed at various currents during a measurement cycle, which consists of an "stair-step" ramp to some maximum current, with strain gauge readings being taken at various constant current levels during the up- and down-ramp portions of the cycle.)

Finally, the strain gauges are read out once the cold mass has been warmed back up to room temperature, so that comparisons with pre-cold test data can be made.

4.2.2 Results

The azimuthal coil stress in the straight sections of magnet HGQ01 is summarized in Figure 4.1. This plot shows the azimuthal coil stresses for various operational conditions, as measured by the beam-type strain gauges for the inner and outer coils. (Note that two of the inner coil beam-type gauges were inoperative due to bent connector pins shorting out the gauges.) From this plot the loss of pre-stress between room temperature and cryogenic tempera-

tures, due to thermal contraction of the magnet components, and the further loss of coil stress during excitation resulting from Lorentz forces on the magnet coils, is evident. These data also appear in Tables 4.4- 4.5, along with the capacitance-type strain gauge data for these conditions. Note that due to un-resolved systematic errors in the capacitance gauge measurement systems, the absolute values of the stresses measured by the capacitance gauges do not agree with those measured by the beam gauges - however their relative behaviour agrees remarkably well, as can be seen in Table 4.4.

Table 4.4: Azimuthal Coils Stresses (in psi)

	300K Keyed	300K Yoked	4.5K I=0	4.5K I=9000A	1.9K I=0	1.9K I=11450A	280K Post-Test
Inner Beam Gauges							
Q2L / IB16	13750	11209	5731	2720	5470	920	11054
Q4L / IB20	14666	12599	9402	5952	9042	3333	12259
Q2R / IB09	8574	6461					6005
Q4R / IB10	10109	8268					8000
Inner Coil Average	11775	9634	7567	4336	7256	2127	9330
Outer Beam Gauges							
Q2L / OB18	9799	9443	6808	5680	6905	4554	9263
Q4L / OB19	10597	10226	9671	8296	9988	7088	11420
Q2R / OB14	9148	7824	4889	3756	4768	2875	6727
Q4R / OB15	14395	13569	11506	9826	11640	8126	12908
Outer Coil Average	10985	10266	8219	6890	8325	5661	10080
Capacitance Gauges							
CG21	9478	3862	46663	43000	46600	40800	
CG22	11287	6417	867	-2400	700	-3700	
CG23	9544	3876	-3650	-6600	-3250	-8800	
CG24	9377	6632	26731	23300	26900	21200	
CG Average	9922	5197					

A typical strain gauge run to quench at 1.9K is shown in Figures 4.2- 4.4, which show, respectively, the beam-gauge, return end bullet-gauge, and lead end bullet-gauge measurements as a function of I^2. This first quench at 1.9K occurred at a magnet current of 10364A, with the last strain gauge data taken at 9000A. Notable features include the linear dependence of azimuthal coil stress with I^2, which is to be expected, and the lack of end-loading of the return end bullets until currents of 8000A have been exceeded. This lack of end loading is suspected as a primary contributing mechanism to the significant number of return end quenches observed in this magnet.

A second run to quench at 1.9K is shown in Figures 4.5- 4.7, displaying the same essential features of Figures 4.2- 4.4. Note, however, that as higher currents were reached during this strain gauge data taking run (10,000A), the return end bullet gauges showed not only an increasing load (as expected) but also a greater dependence on I^2 - at the same time that the lead end bullets showed a decreasing sensitivity with I^2. Clearly the loads at the two ends of the magnet are coupled in some fashion. Also, the structure in the lead end bullet data near $I^2 \sim 4x10^7$ appears to be reproducible, implying that there is some physical frictional effect characterizing the motion of the lead end of the magnet cold mass. The initial decrease in end force seen in quadrants 3 and 4 of the lead end is not readily understood - but may be due to noise effects or to mechanical hysteresis in the gauge/end plate manifested at low current.

In addition to the standard stain gauge runs performed at 4.5K and 1.9K (and depicted in Figures 4.2- 4.7), special "fast scans" were also performed, where data was taken "on-the-fly" at approximately 3 second intervals. The results of the first fast scan, which was a run to 10kA, are plotted in Figures 4.8- 4.10. In Figures 4.11- 4.13 are plotted a second fast scan - this time a run to quench at 1.9K (11450A).

In these fast scans the linear dependence of azimuthal coil stress on the square of the magnet current is clearly evident (as shown in 4.8, as is negligible hysteresis. A greater level of hysteresis is evident in the bullet gauge data (specifically Figures 4.9 and 4.10 indicative of friction affecting the mechanics in the end regions of the cold mass. As in previous runs, however, the unloaded condition of the return end below a magnet current of about 6300-7000 A is quite noticeable.

The azimuthal stress data taken during the fast scan to quench ($\sim$ 11450 A) again exhibit extremely good linearity, with consistent behavior among

inner and outer coil gauges. The data for the bullet gauges is also consistent with earlier data, showing the un-loaded condition for the return end, this time indicating contact with the end plate at about 6800-7400 A. There was considerable noise in the current source used for the bullet gauges, necessitating the use of data-smoothing. This noise would normally cancel out of the strain calculation since the compensating gauges utilized the same current source - however one of the compensating gauges for the lead end appeared to be "out-of-phase" with the active gauges, resulting in incomplete cancellation of the current source drift.

Data for one of the capacitance gauges (representative of their overall behaviour) is shown in Figure 4.14, for the "fast scan" strain gauge run to quench at 1.9K. Again, we see excellent linearity in the data, with an uncertainty of about ± 100 psi. The pre-stress loss seen here for capacitance gauge #24 of about 5700 psi compares extremely well with that observed by the corresponding beam gauge (BGIA020) of 5709 psi. The absolute values of coil stress are of course, incorrect, due to imperfect compensation of the systematic differences between measurement systems used in production and cryogenic testing. These differences don't affect the dynamic behavior or sensitivity of the capacitance gauges, since they appear as a "DC offset" to the measured capacitance.

In Figure 4.15 we show the data from the "compensating" capacitance gauge (CG#25) for the same "fast scan". Note the absence of any measurable dependence on magnet current (field) on the measured gauge capacitance, with an average noise level of about 0.2 pF, corresponding to about ± 50 psi. Since this noise level is distinctly less than that observed in the active gauges, one might interpret the higher noise level in the latter as indicative of actual azimuthal coil stress changes, perhaps brought on via frictional effects at the coil/insulation/collar interfaces.

4.2.3 Discussion

While a complete analysis of the strain gauge measurements (including comparison with calculated/expected cold mass behaviour) will be performed in the future, there are still some obvious conclusions that can be drawn from the data for this report.

- There is insufficient end pre-loading, especially at the return end, to preclude the possibility of longitudinal coil motion during energization. This is supported by general quench location observations (8 of 11 positively identified quench locations were coil ends).

- The azimuthal coil loading appears to be sufficient to allow operation at desired gradient, except perhaps for the inner coil in quadrant 2, which shows a stress of about 1000 psi at 11500 A, and which would be unloaded at a current of about 12650 A.

- The inner coils display a greater stress loss as a function of I^2 than the outer coils - by about a factor of 2. This is evident in capacitance gauge and beam gauge data.

- The measured end load as a function of I2 ($\sim 2x10^{-5} lbs/A^2$, for both return and lead ends) differs from the predicted value ($\sim 8x10^{-5} lbs/A^2$) by about a factor of 4. This may be indicative of mechanical interference between the collar/yoke/skin not accounted for in the design, transferring some of the longitudinal loads to the yoke/skin, leading to a lower end force applied to the bullet gauges.

Table 4.5: Changes in Azimuthal Coil Strsses (in psi)

	Yoked–Keyed	300K–4.5K	300K–1.9K	OA-9kA (4.5K)	0A-11450A (1.9K)	Yoked-P.Test (300K)
Inner Beam Gauges						
Q2L / IB16	-2541	-5478	-5739	-3011	-4550	-155
Q4L / IB20	-2067	-3197	-3557	-3450	-5709	-340
Q2R / IB09	-2113					-456
Q4R / IB10	-1841					-268
Inner Coil Average	-2141	-4338	-4648	-3231	-5130	-305
Outer Beam Gauges						
Q2L / OB18	-356	-2635	-2538	-1128	-2351	-180
Q4L / OB19	-371	-555	-238	-1375	-2900	1194
Q2R / OB14	-1324	-2935	-3056	-1133	-1893	-1097
Q4R / OB15	-826	-2063	-1929	-1680	-3514	-661
Outer Coil Average	-719	-2047	-1940	-1329	-2665	-186
Capacitance Gauges						
CG21	-5616			-3663	-5800	
CG22	-4870			-3267	-4400	
CG23	-5668			-2950	-5550	
CG24	-2745			-3431	-5700	
CG Average	-4725			-3328	-5363	

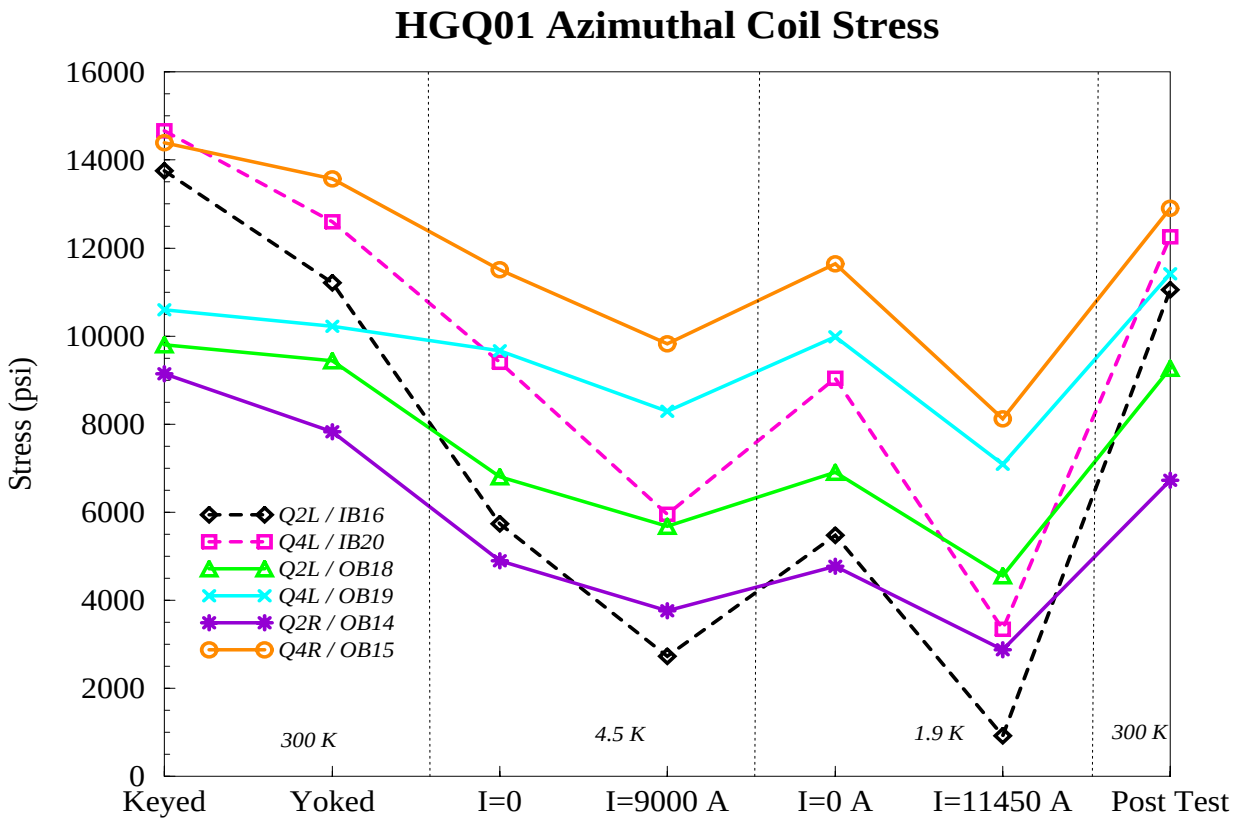

Figure 4.1: Coil stresses measured by inner and outer coil beam-type strain gauges, during various stages of fabrication/testing (Fig1a.ps)

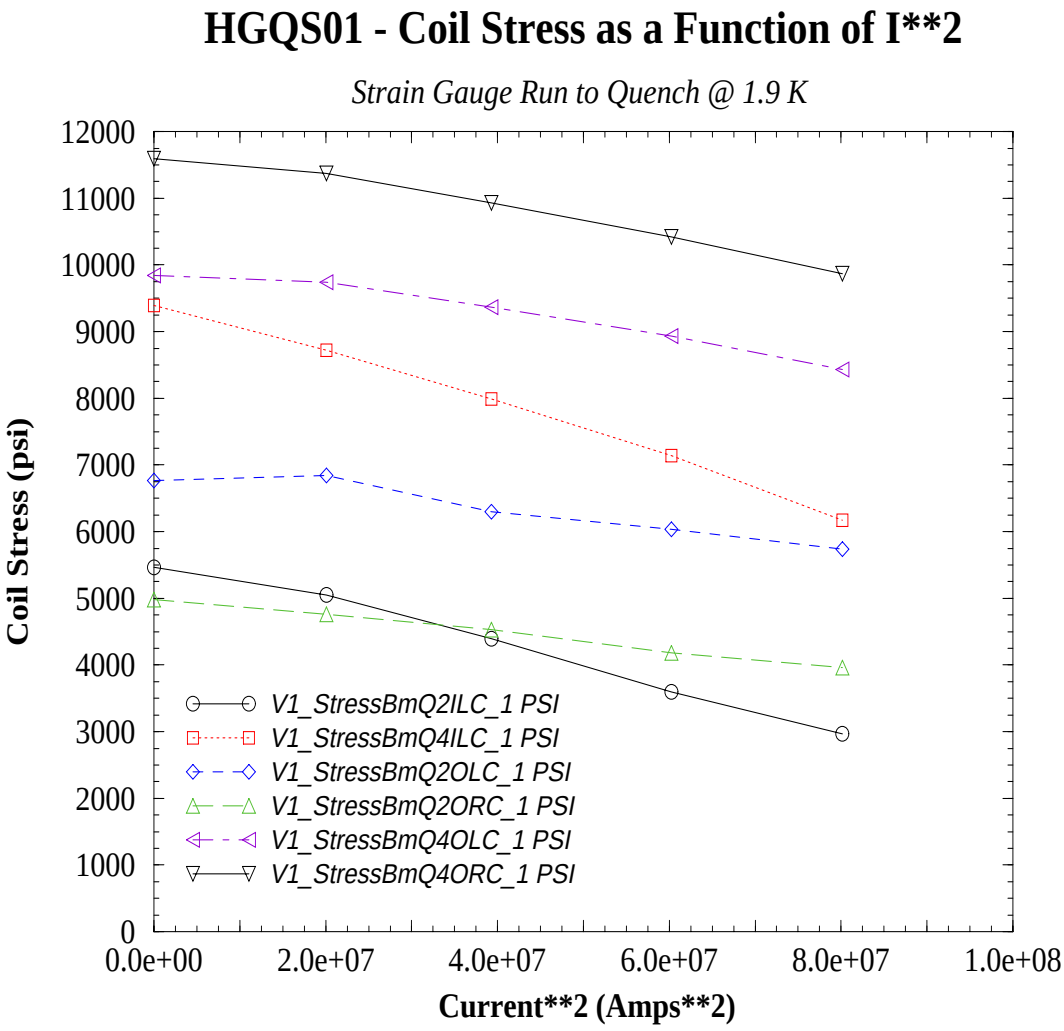

Figure 4.2: Azimuthal coil stresses measured by beam-type strain gauges during first strain gauge data taking run to quench. (Fig2.eps)

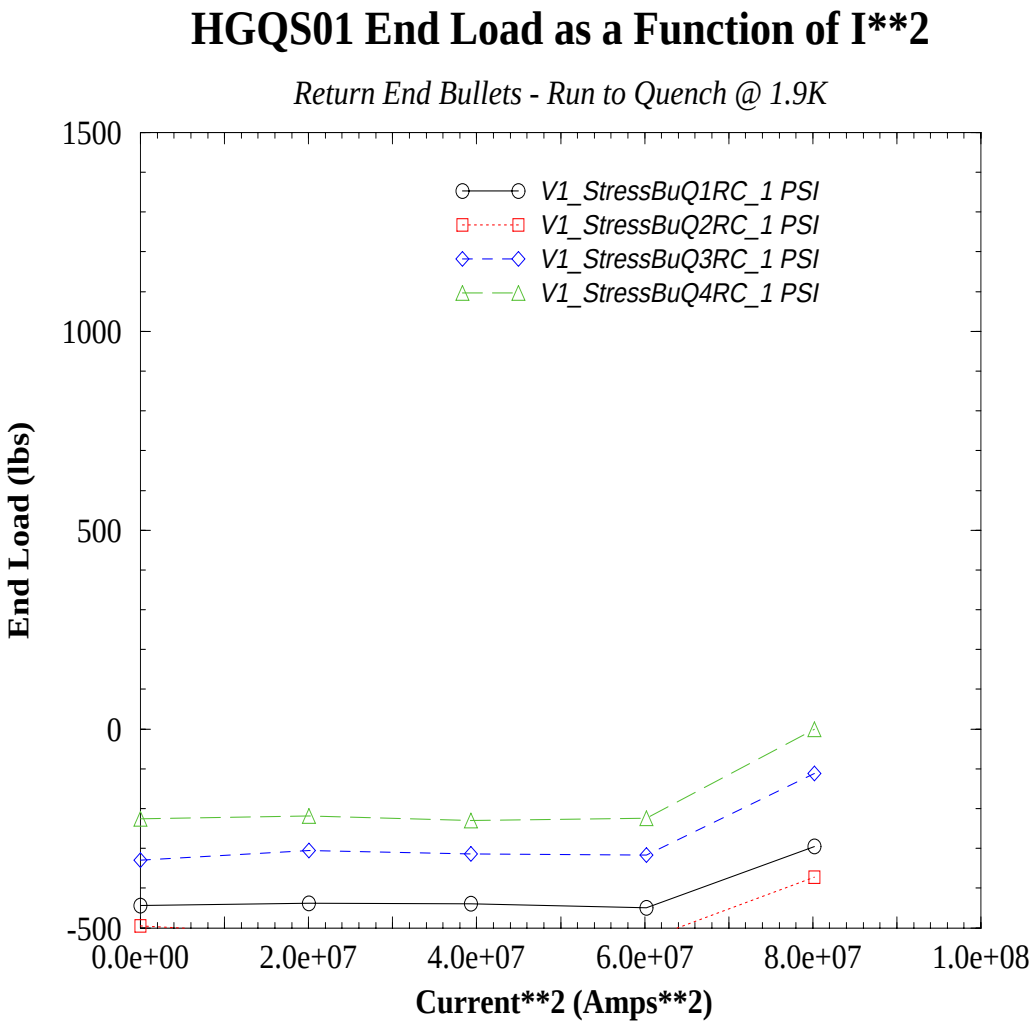

Figure 4.3: End force as measured by return end bullet gauges during first strain gauge data taking run to quench. Note that the return end of the coils does not appear to be constrained until I 8000A (Fig3.eps)

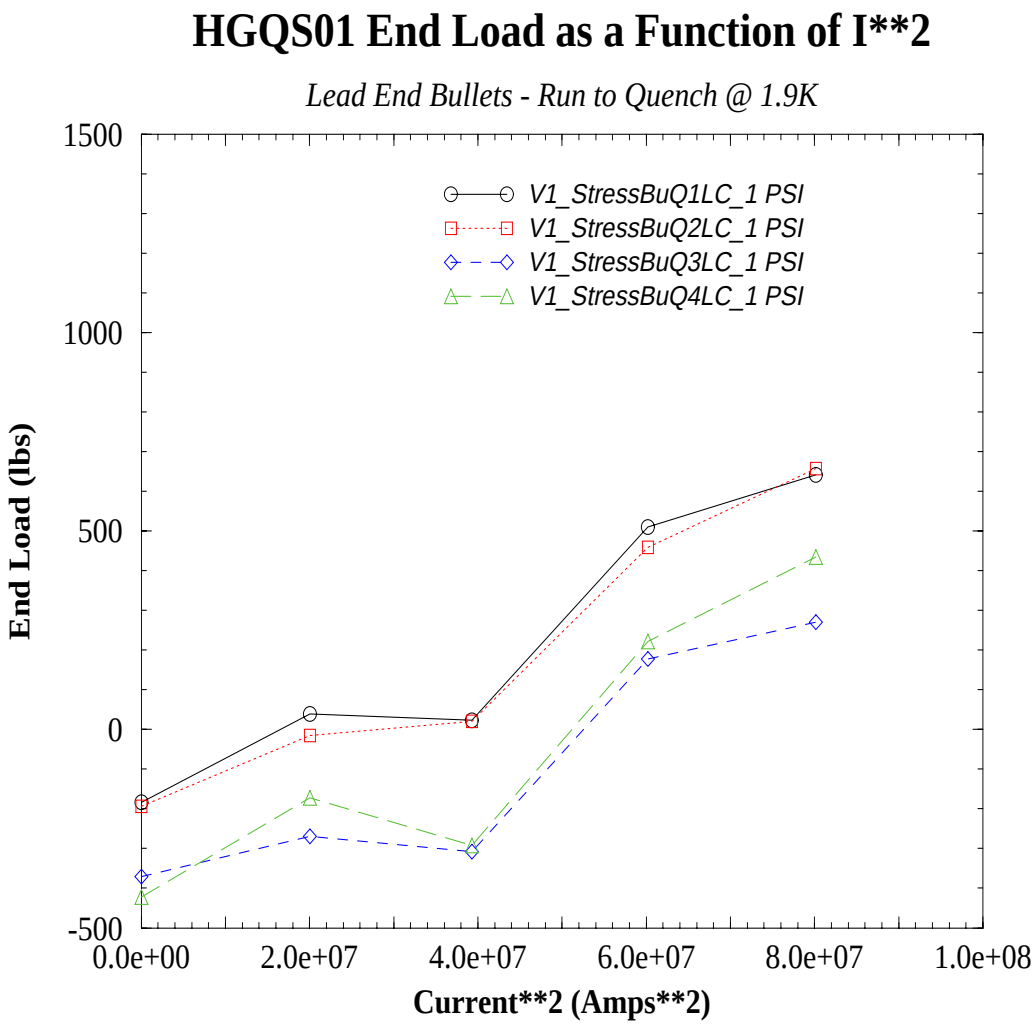

Figure 4.4: End force as measured by the lead end bullet gauges during first strain gauge run to quench. Note that the lead end of the coils does appear to be constrained even at the lowest currents. (Fig4.eps)

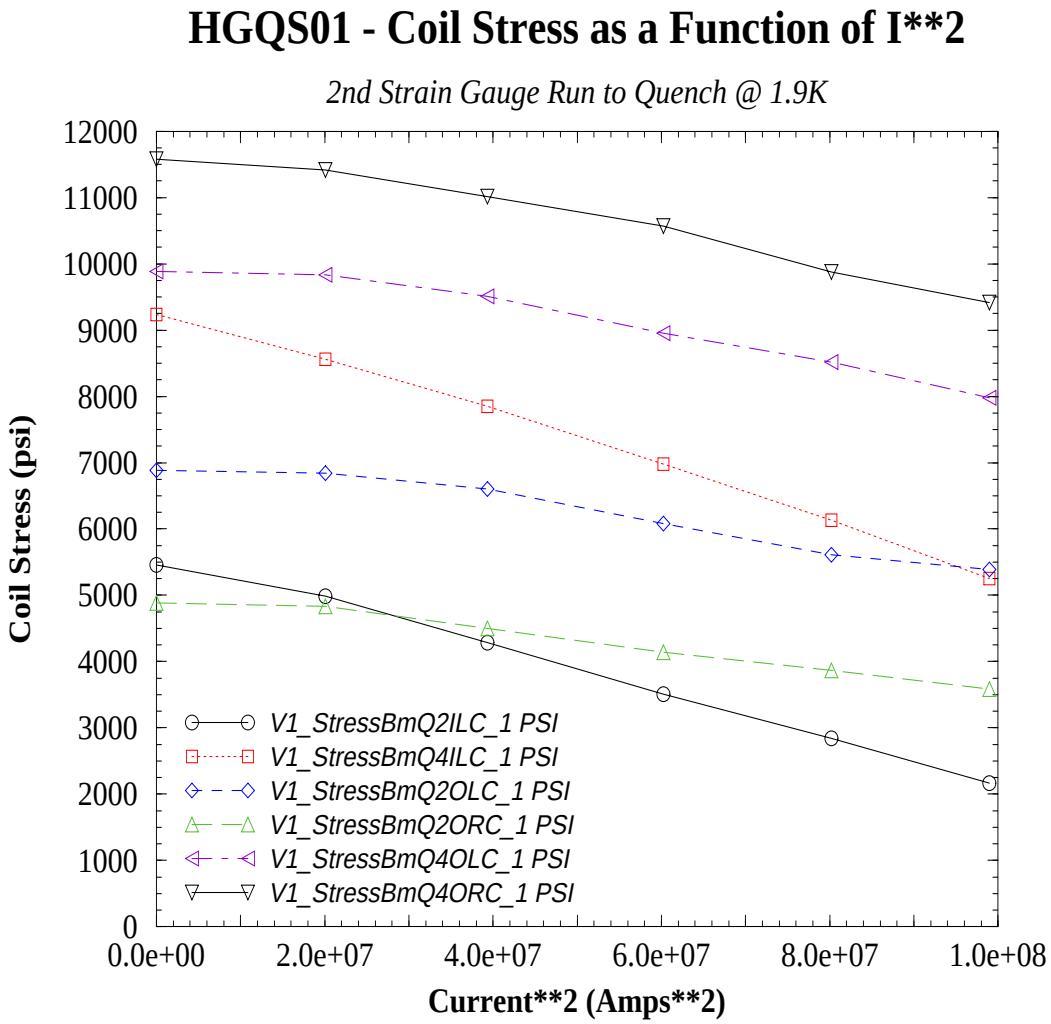

Figure 4.5: Azimuthal coil stresses measured by beam-type strain gauges during second strain gauge data taking run to quench. (Fig5.eps)

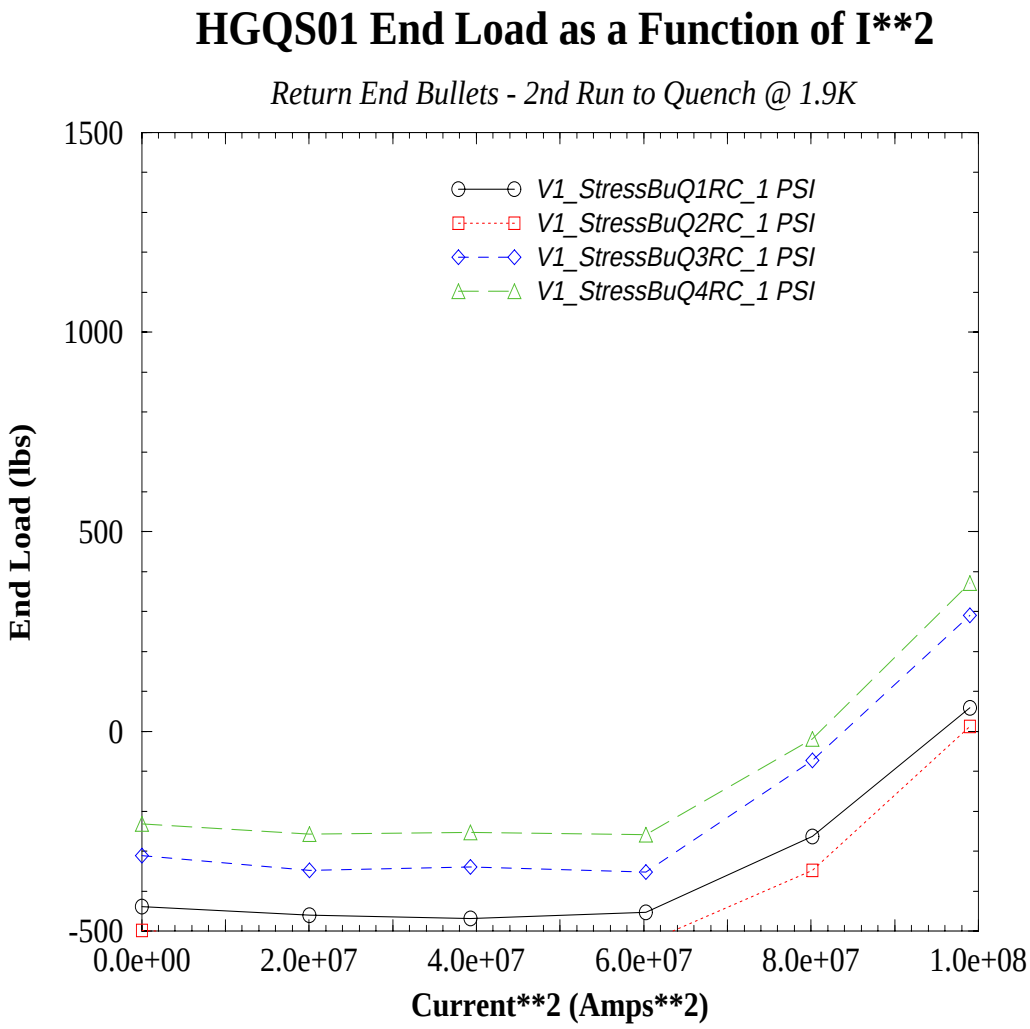

Figure 4.6: End force as measured by return end bullet gauges during second strain gauge data taking run to quench. Again, the return end of the coils does not appear to be constrained until I 8000A (Fig6.eps)

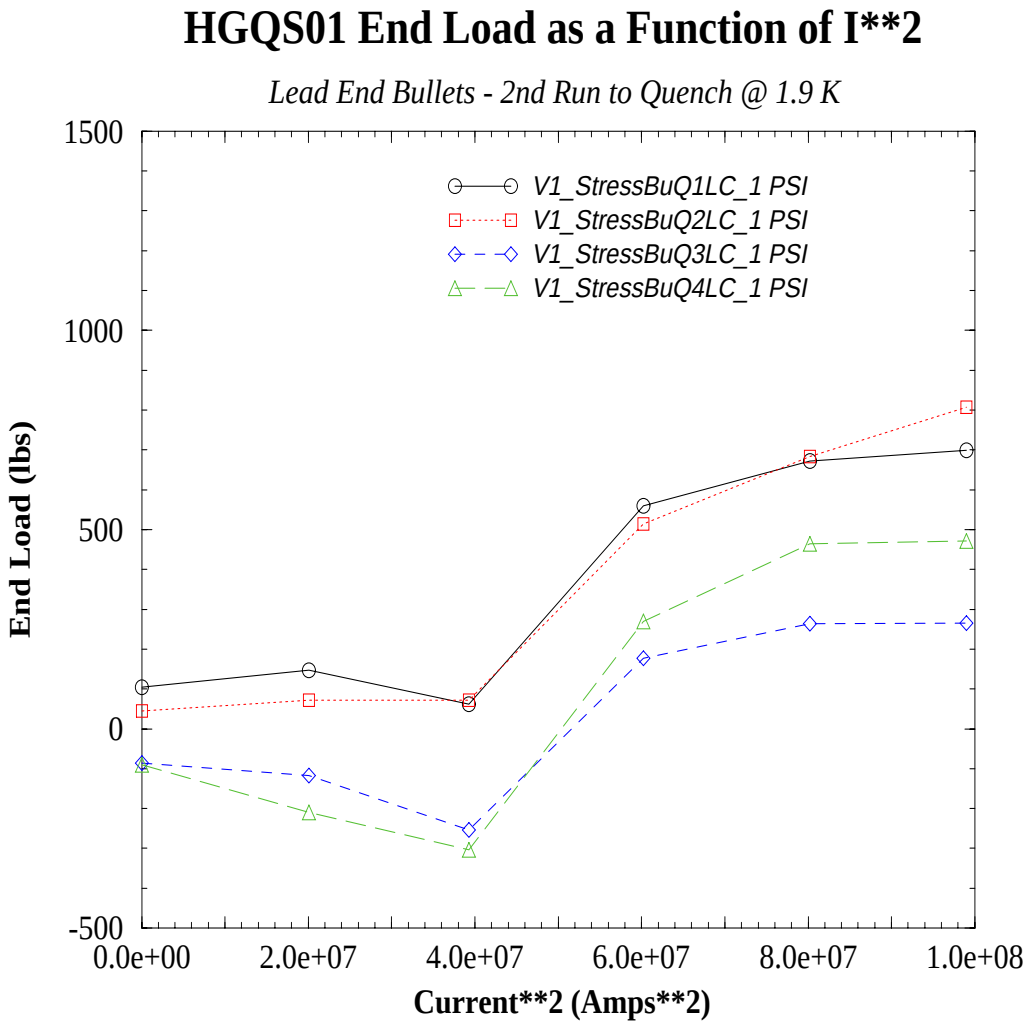

Figure 4.7: End force as measured by the lead end bullet gauges during second strain gauge run to quench. Note that the lead end of the coils does appear to be constrained even at the lowest currents. (Fig7.eps)

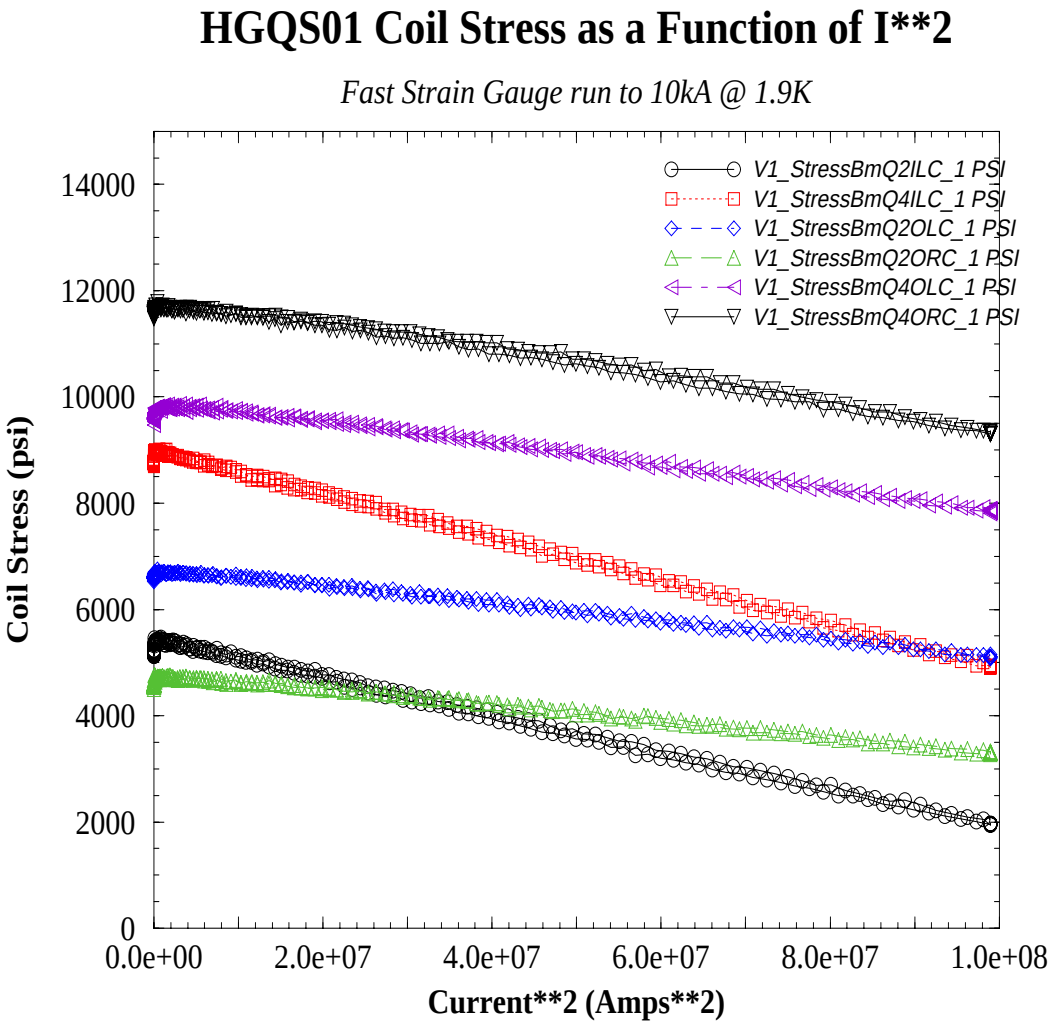

Figure 4.8: Azimuthal coil stresses measured by beam-type strain gauges during fast strain gauge data scan to 10kA. (Fig8.eps)

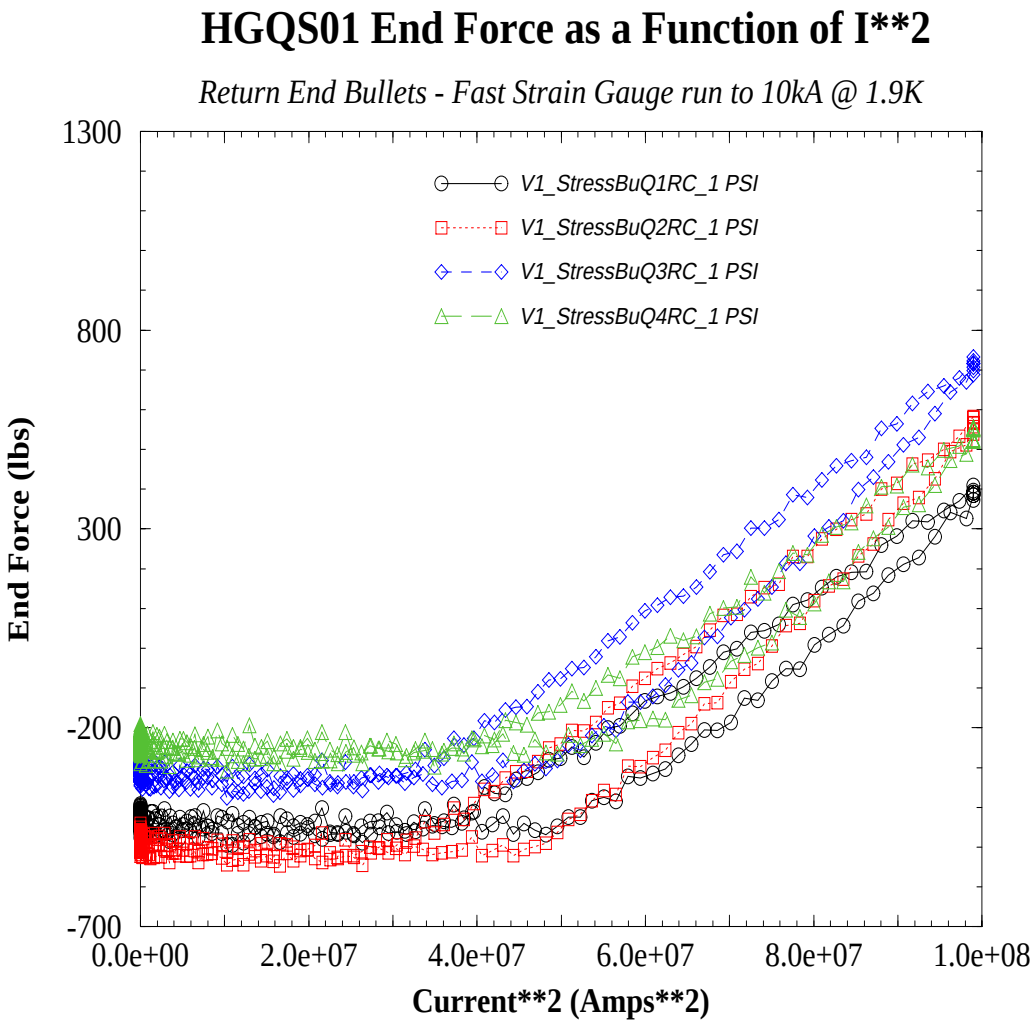

Figure 4.9: End force as measured by return end bullet gauges during fast strain gauge data scan to 10kA. (Fig9.eps)

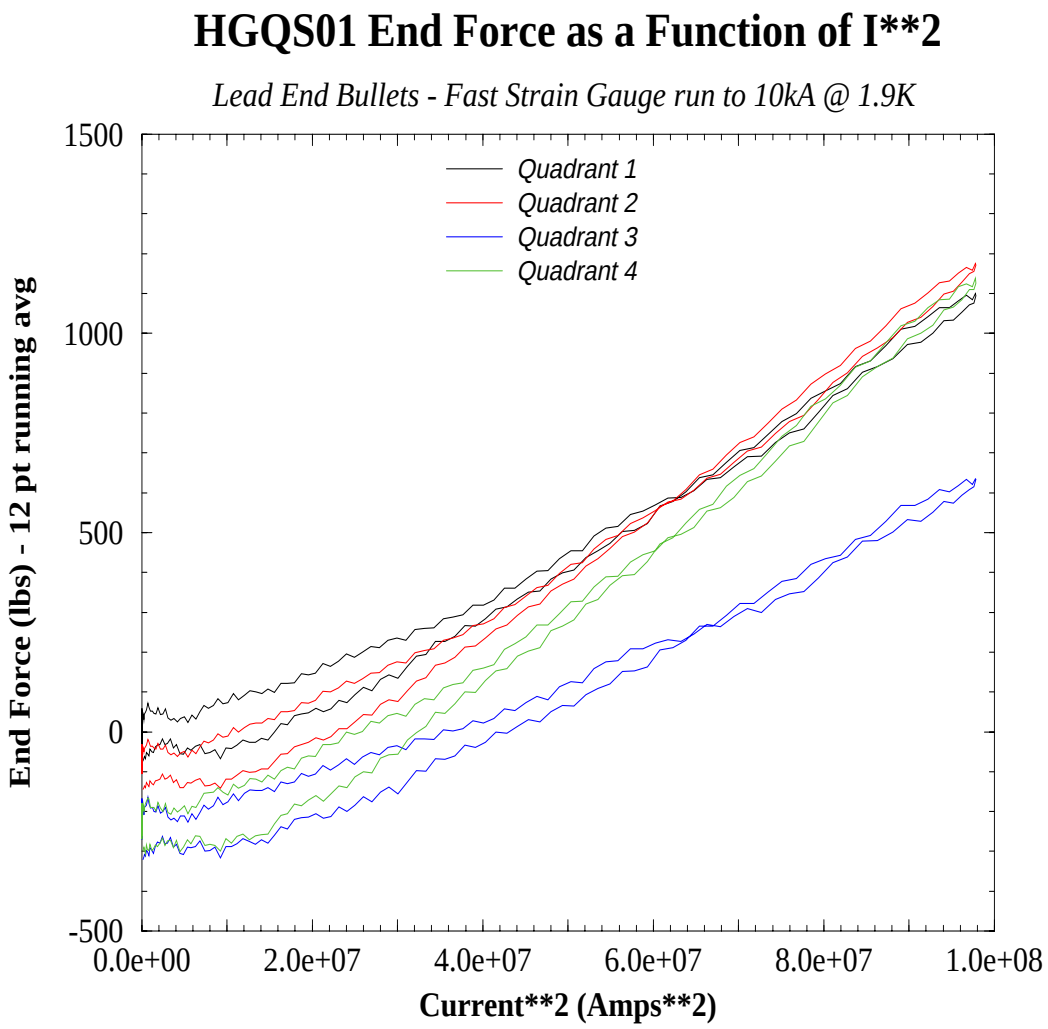

Figure 4.10: End force as measured by the lead end bullet gauges during fast strain gauge run to 10kA. Due to noise from current supply drift, a 12-point running-average algorithm has been applied to the data. (Fig10.eps)

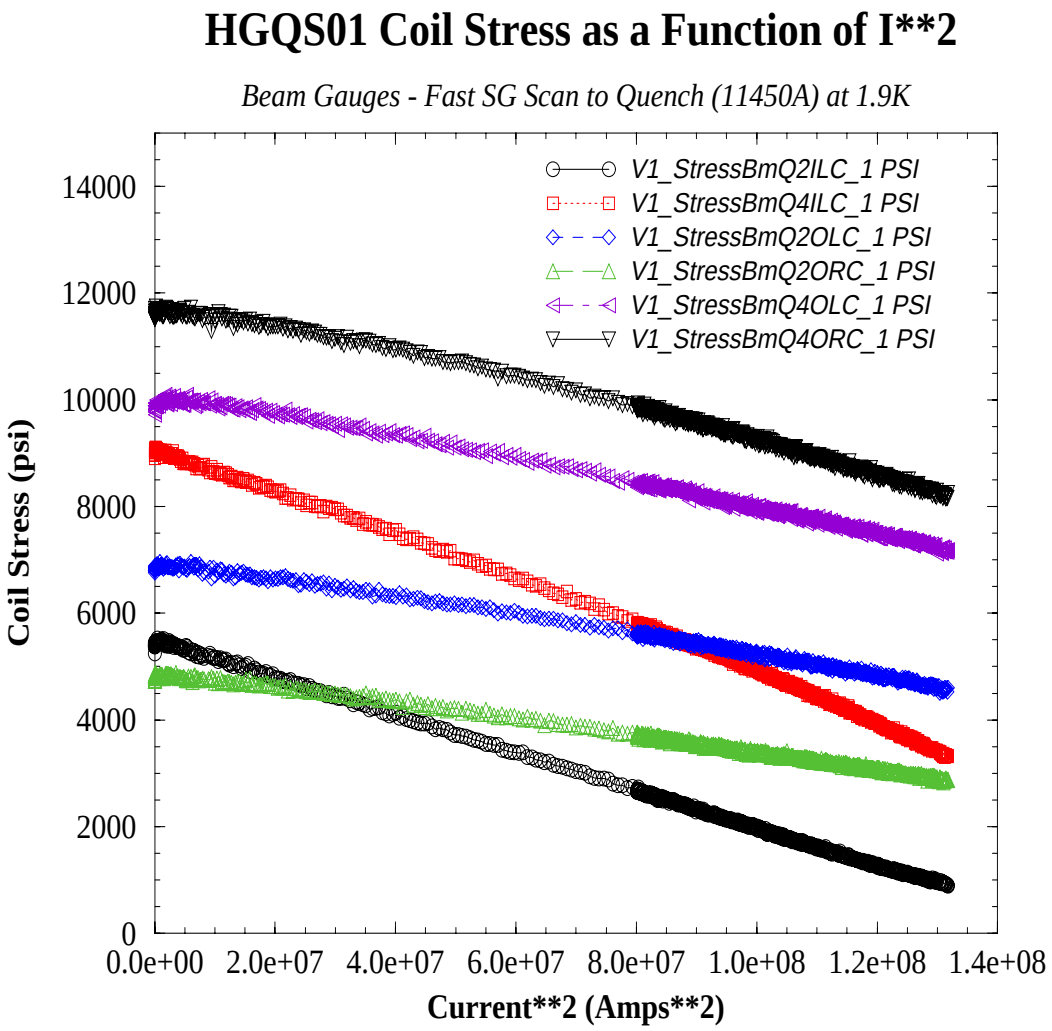

Figure 4.11: Azimuthal coil stresses measured by beam-type strain gauges during fast strain gauge data scan to quench @ 1.9K (11450A). (Fig11.eps)

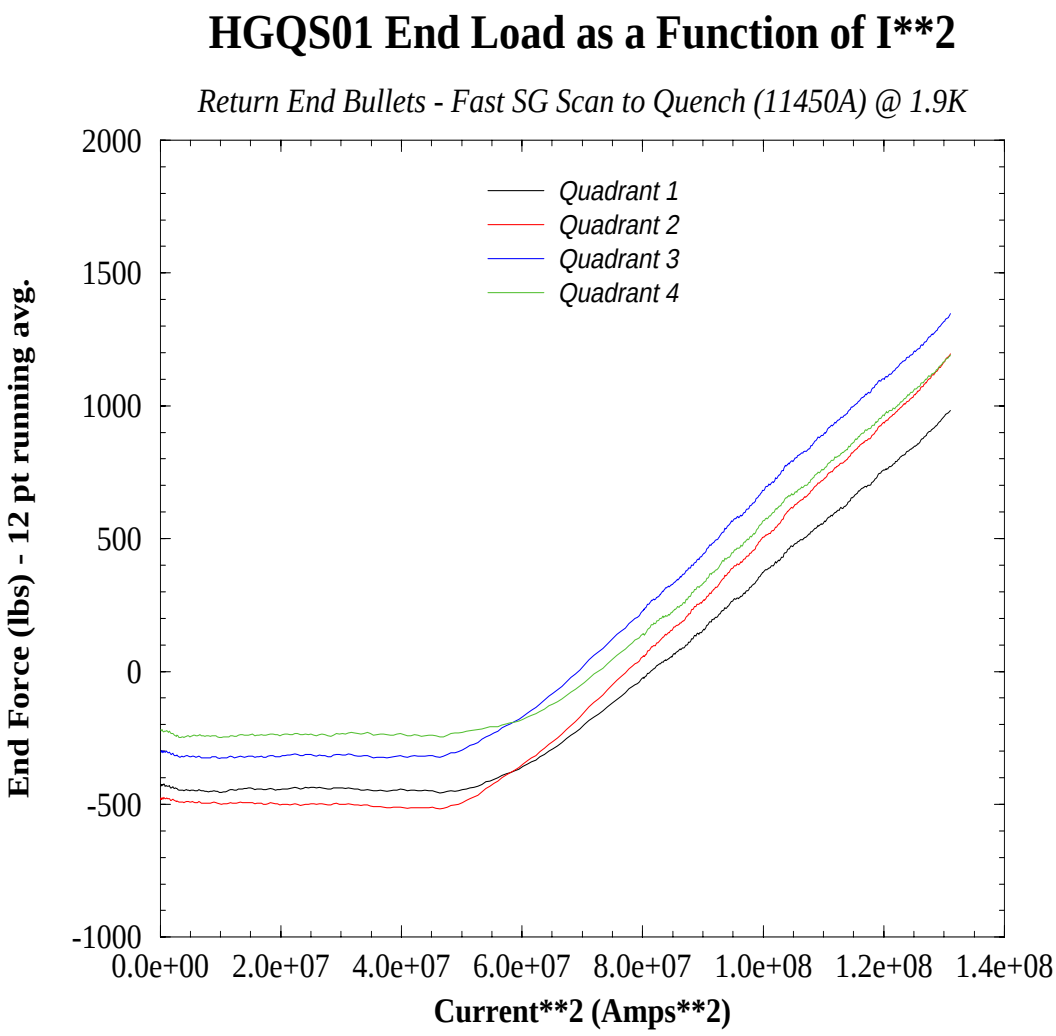

Figure 4.12: End force as measured by return end bullet gauges during fast strain gauge data scan to quench @ 1.9K (11450A). Due to noise from current supply drift, a 12-point running-average algorithm has been applied to the data. (Fig12.eps)

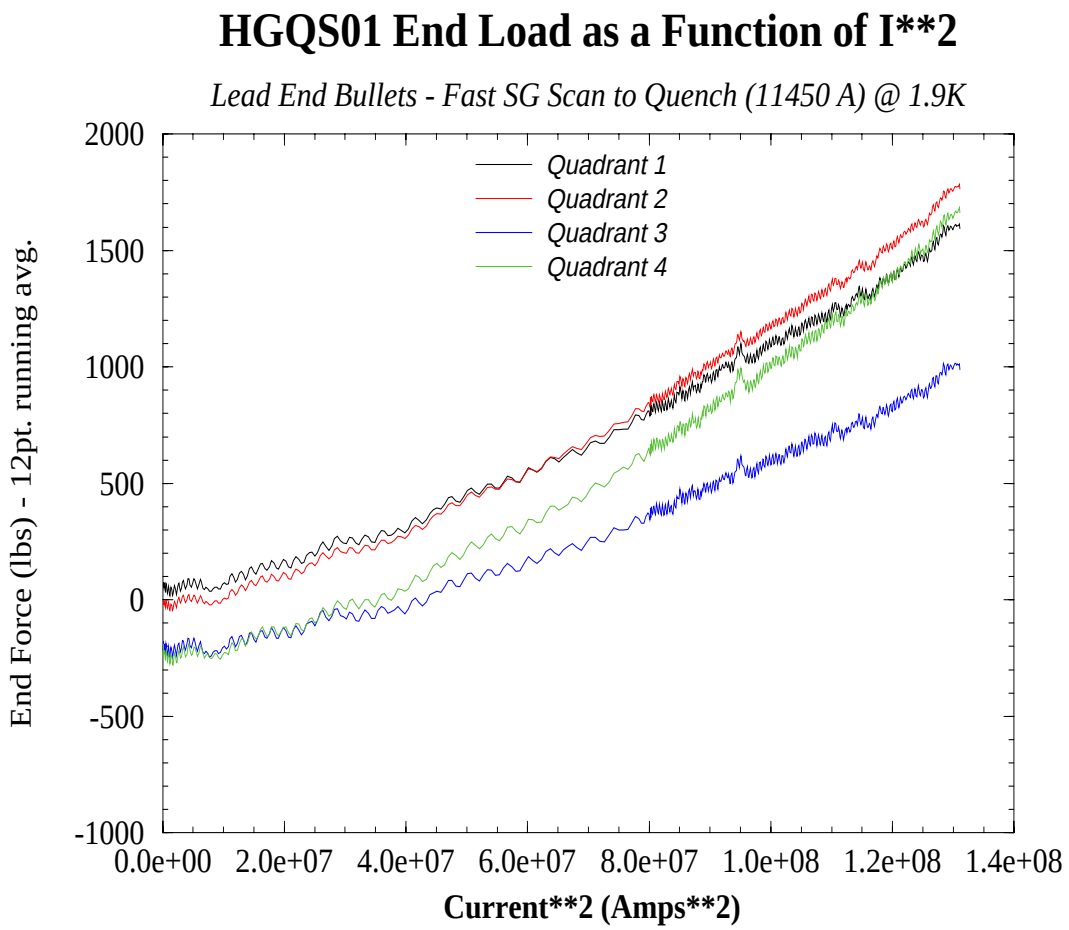

Figure 4.13: End force as measured by the lead end bullet gauges during fast strain gauge run to quench @ 1.9K (11450A). Due to noise from current supply drift, a 12-point running-average algorithm has been applied to the data. (Fig13.eps)

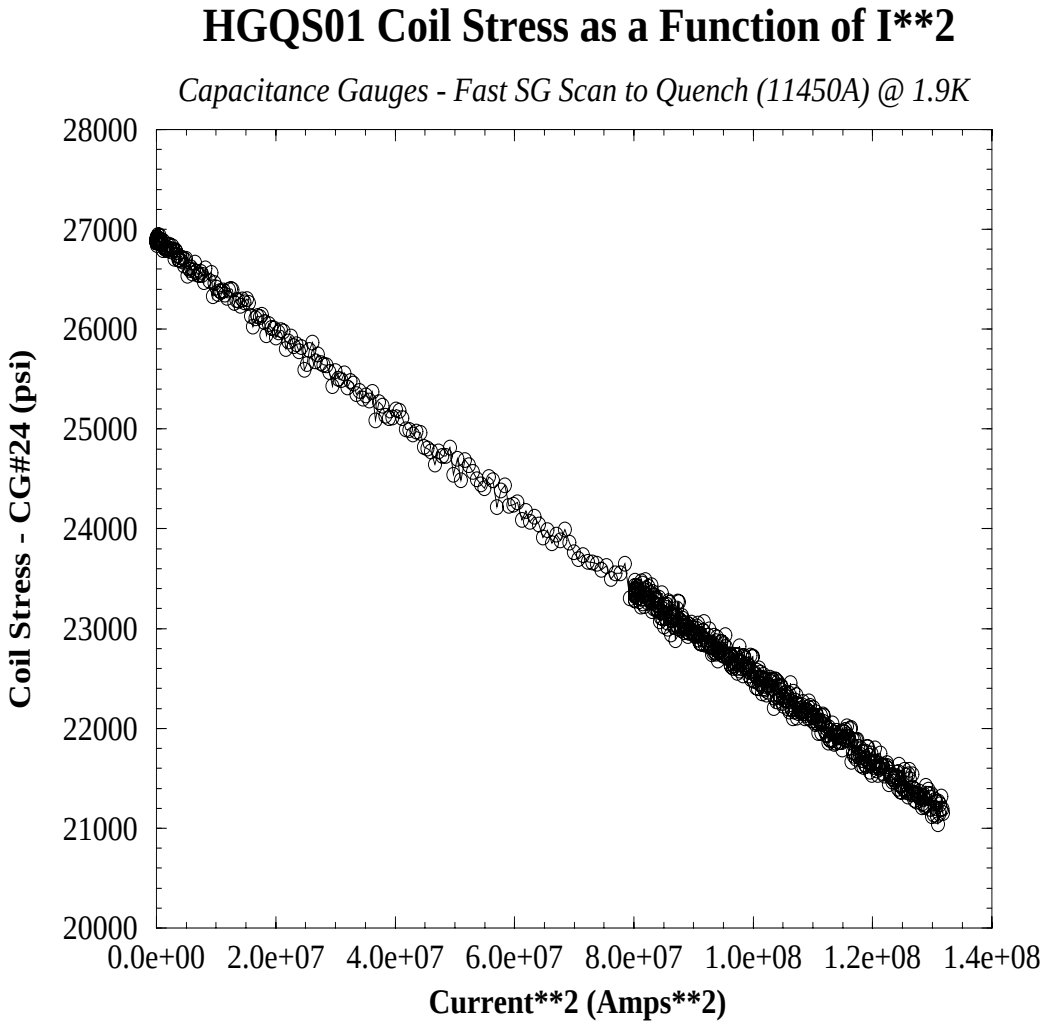

Figure 4.14: Azimuthal coil stress measured by a capacitance gauge during a fast strain scan to quench (11450 A). The absolute value is incorrect due to systematic offsets in the measured capacitance.(Fig14.eps)

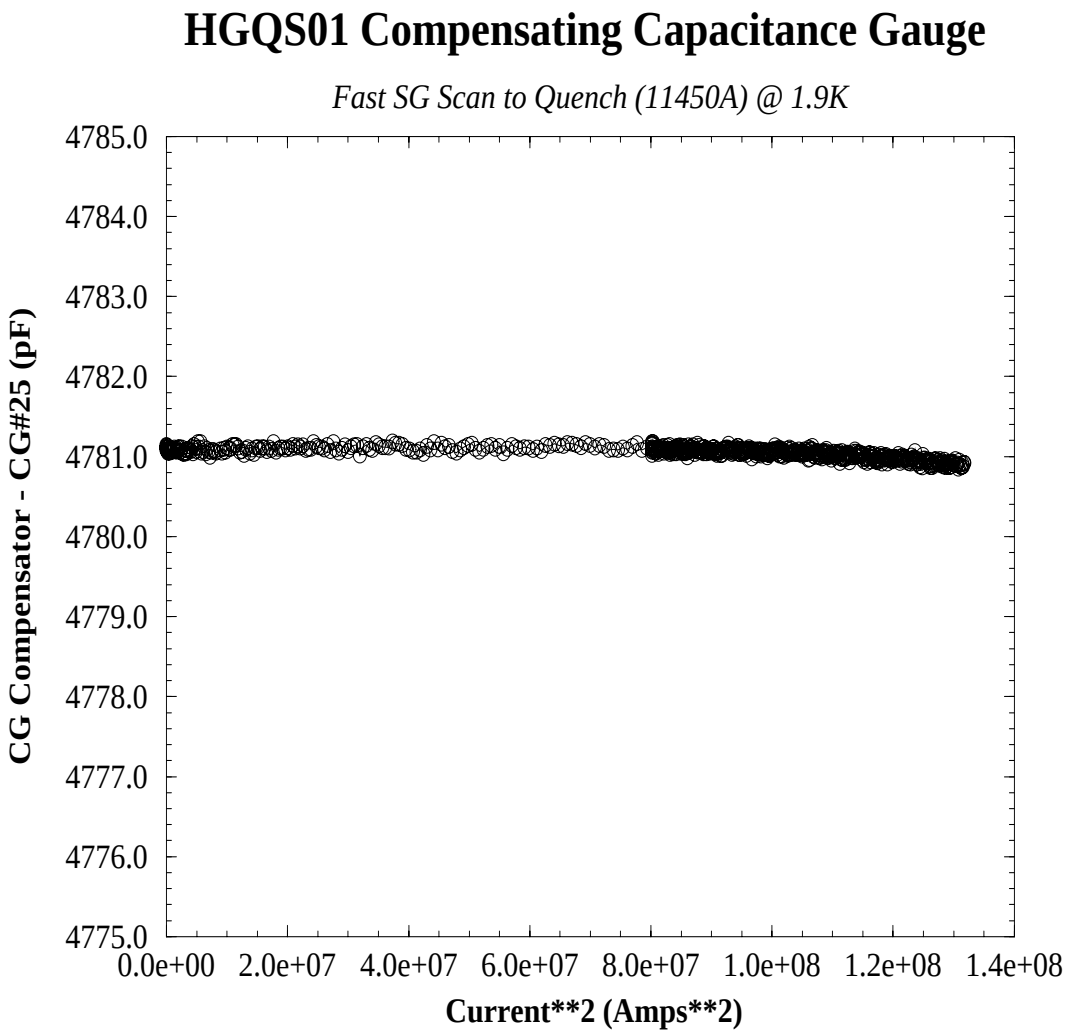

Figure 4.15: Response of the compensating capacitance gauge during a fast strain scan to quench (11450 A). Note the essentially constant value of the capacitance of the gauge during the magnet ramp cycle. (Fig15.eps)

4.3 Test cycle II

A second cryogenic test cycle was undertaken for magnet HGQS01. In addition to a thermal cycle of the cold mass from 1.9K to 300K and back to LHe temperatures, two significant changes were made between test cycles: the return end bullets were torqued further to provide additional pre-load of about 5000 - 6000 lbs (2.22x104 - 2.67x104 N)/bullet, and strain gauges were added to the magnet skin to measure longitudinal and azimuthal strains. A total of 10 gauges were added - 7 active longitudinal gauges, 1 active azimuthal gauges, and one compensating gauge for each direction.

During the second cycle of testing, only the "fast scan" type of strain gauge run was performed, as it was found that continuous data during the ramp cycle was preferred. These fast scans were utilized for both beam, bullet, and skin gauge data acquisition runs. In order to minimize the electrical noise emanating from the capacitance gauge power supply, this supply was turned off during some of the strain gauge runs so that "cleaner" bullet gauge data, for example, could be obtained.

The azimuthal coil stress data measured by beam gauges is summarized in Tables 4.6 and 4.7. These data show that the room temperature, cryogenic, and excited coil stresses durign the 2nd test cycle agree well with those measured during the first test cycle.

In Figure 4.16 we show the azimuthal coil stresses as measured by beam gauges during a typical fast strain gauge run to quench at 1.9K Note that as in the first test cycle, the inner coils lose a greater amount of pre-stress upon excitation than the outer coils, and one might also see some evidence of coil unloading in the inner coil of Quadrant 2 at the lead end, when the magnet current approaches $\sim$ 12,250 A. Figures 4.17 and 4.18 show, respectively , the lead and return end bullet loads during excitation. Both figures show that the bullets experience essentially linear lading with square of the excitation current, and that, unlike test cycle #1, the ends of the coils have positive load applied to them even at zero current. (Note also that the data in Figure 4.17 have been processed to eliminate the noise picked up from the capacitance gauge excitation source.) Figure 4.19, which shows the inner coil stress in quadrant 1 as measured by a capacitance gauge which "opposes" the beam gauge in quadrant 2 at that location (i.e., measures essentially the same coil stress as that beam gauge) also shows some evidence of coil unloading as the magnet current approaches $\sim$ 11,800 A - in reasonably good agreement with

the behavior measured by the complementary beam gauge. As this coil is also the coils which shows the lowest level of zero-current pre-load, this behavior is not unexpected, nor observed in the other, more highly pre-loaded coils.

The longitudinal shell gauge data is presented in Figure 4.20, which shows the compensated strains as a function of the square of the excitation current, for the strain gauges mounted in a longitudinal orientation on the cold mass shell near the return end. The various gauges show an increase in shell strain from 10 to 60 μ over the current range 0 - 11375 A. (These data were taken during a run to quench at 2.5K, hence the lower maximum current.)

4.4 Summary of HGQS01 Mechanical Behavior - TC1 & TC2

- Test cycle #1 mechanical behavior summary :

  Average Inner Coil Cool-Down Loss : $4300 - 4600 psi (30 - 32 MPa)$
  Average Outer Coil Cool-Down Loss : $1900 - 2000 psi (13 - 14 MPa)$

  Average Inner Coil Lorentz Loss : $3.9 - 4.0 x 10^{-5} psi/A^2 (2.7 - 2.8 x 10^{-7} MPa/A^2)$
  Average Outer Coil Lorentz Loss : $1.7 - 2.0 x 10^{-5} psi/A^2 (1.2 - 1.4 x 10^{-7} MPa/A^2)$

  Average Lead End Lorentz Force : $2.0 x 10^{-5} lbsf/A^2 (9.0 x 10^{-5} N/A^2)$
  Average Return End Lorentz Force : $2.1 x 10^{-5} lbsf/A^2 (9.3 x 10^{-5} N/A^2)$

- Test cycle #2 mechanical behavior summary:

  Average Inner Coil Cool-Down Loss : $4700 - 5000 psi (33 - 35 MPa)$
  Average Outer Coil Cool-Down Loss : $2000 psi (14 MPa)$

  Average Inner Coil Lorentz Loss : $4.1 - 4.3 x 10^{-5} psi/A^2 (2.8 - 3.0 x 10^{-7} MPa/A^2)$
  Average Outer Coil Lorentz Loss : $1.9 - 2.0 x 10^{-5} psi/A^2 (1.3 - 1.4 x 10^{-7} MPa/A^2)$

  Average Lead End Lorentz Force : $2.3 x 10^{-5} lbsf/A2 (1.0 x 10^{-4} N/A2)$
  Average Return End Lorentz Force : $2.2 x 10^{-5} lbsf/A2 (9.8 x 10^{-5} N/A2)$

- Skin Strains (longitudinal) :

  Return End averge strain : $31 \pm 11 \pm 1 \mu\epsilon$ (errors are statistical & systematic) (calc. from end load : 33 $\mu\epsilon$)

  Lead End average strain : $14 \pm 3 \pm 1 \mu\epsilon$ (errors are statistical & systematic) (calc. from end load : $35 \mu\epsilon$)

  (Skin gauges were not optimally placed to observe longitudinal variations. This has been remedied in magnet HGQS02)

- Predictions (from DOE Review materials) :

  Inner Coil Cool-Down Loss : 600 psi (4MPa)

  Outer Coil Cool-Down Loss : 1450 psi (10 MPa)

  Inner Coil Lorentz Loss : $4.4x10^{-5}psi/A^2(3.0x10^{-7}MPa/A^2)$

  Outer Coil Lorentz Loss : $2.9x10^{-5}psi/A^2(2.0x10^{-7}MPa/A^2)$

  End Lorentz Force : $8.2x10^{-5}lbsf/A^2(3.6x10^{-4}N/A^2)$

4.5 Conclusions and Observations

Azimuthal coil stresses appear to be marginally satisfactory - the lowest preloaded coil may be showing signs of unloading at Imax . This should be addressed in subsequent model magnet fabrications.

Original end support appeared to be insufficient - however while the longitudinal support was improved for test cycle #2 by adding load to the return end bullets, this did not have any noticeable effect on quench behavior/localization. This would suggest that improved radial/azimuthal support is required, perhaps by radial or azimuthal shimming at the coil ends.

Longitudinal forces during excitation appear to be about 1/4 predicted values. The most likely explanation for this is that some of the longitudinal forces in the coils are being reacted by other components of the mechanical assembly, rather than just the end plates/skin.

Cool-down loss appears to be greater (significantly so on the inner coil) than predicted. This information should be used to re-evaluate the thermal properties of the coils as used in ANSYS or other calculations.

Azimuthal Lorentz forces observed during magnet excitation match predictions reasonably well - however inner coils show greater loss.

The dynamic behavior of the capacitance gauges used to measure inner coil stresses of this magnet agree well with the corresponding beam gauges. However, due to parasitic and systematic contributions to the measured capacitance, absolute coil stress data is presently available using this technique. This problem should be addressed by standardizing measurement and wiring systems, and/or by exploring design/configuration options.

Table 4.6: Azimuthal Coils Stresses (in psi) - Test Cycle II

	300K Pre 2n TC	4.5K I=0	4.5K I=9710A	1.9K I=0	1.9K I=12520A
Inner Beam Gauges					
Q2L / IB16	11135	5345	2076	4996	491
Q4L / IB20	9208	5525	2595	5286	611
Q2R / IB09	6072	8507	4285	8141	1468
Q4R / IB10	8222	13627	7939	13181	3109
Inner Coil Average	8659	8251	4224	7901	1420
Outer Beam Gauges					
Q2L / OB18	9516	6898	5218	6801	3970
Q4L / OB19	11640	9901	8077	9869	6426
Q2R / OB14	5312	3475	2221	3377	1389
Q4R / OB15	13085	11254	9007	11539	7220
Outer Coil Average	9888	7882	6131	7897	4751

Table 4.7: Changes in Azimuthal Coil Strsses (in psi) - Test cycle II

	300K–4.5K	300K–1.9K	0A-9710A (4.5K)	0A-12520A (1.9K)
Inner Beam Gauges				
Q2L / IB16	-5790	-6139	-3269	-4505
Q4L / IB20	-3683	-3922	-2930	-4675
Q2R / IB09	2435	2069	-4222	-6673
Q4R / IB10	5405	4959	-5688	-10072
Inner Coil Average	-408	-758	-4027	-6481
Outer Beam Gauges				
Q2L / OB18	-2618	-2715	-1680	-2831
Q4L / OB19	-1739	-1771	-1824	-3443
Q2R / OB14	-1837	-1935	-1254	-1988
Q4R / OB15	-1831	-1546	-2247	-4319
Outer Coil Average	-2006	-1992	-1751	-3145

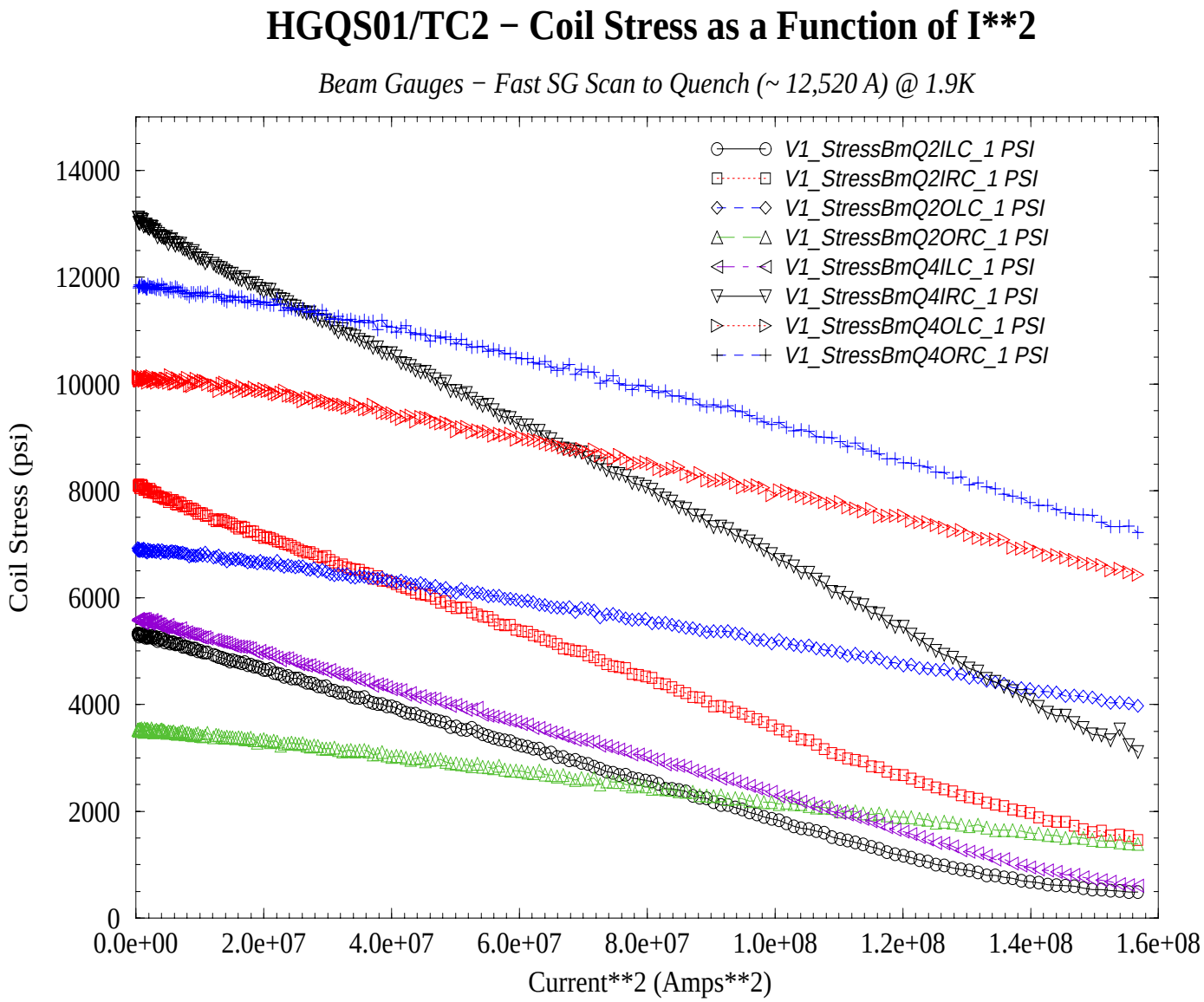

Figure 4.16: Azimuthal coil stresses as measured by beam gauges during a typical fast strain gauge run. (=FigA.eps)

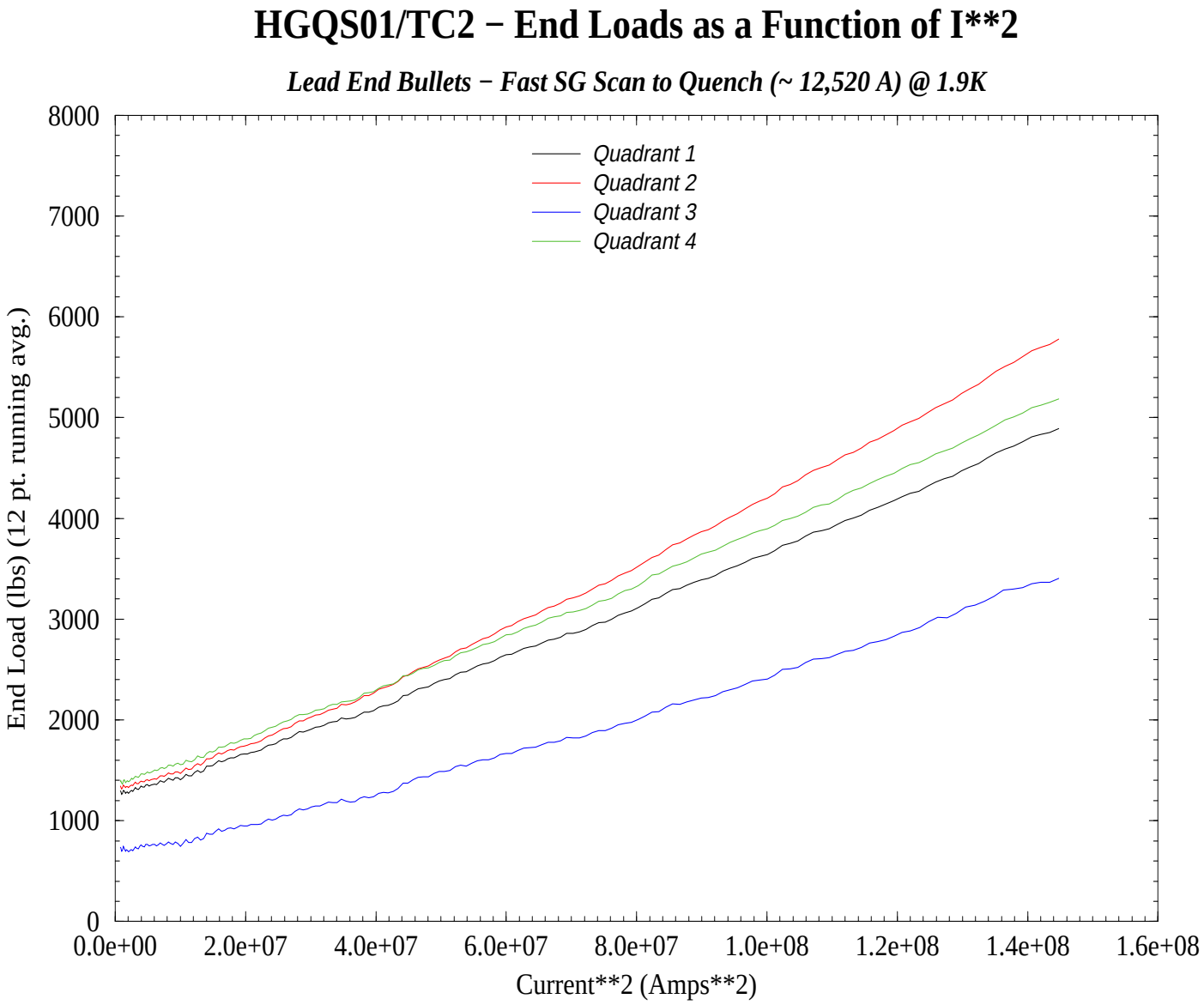

Figure 4.17: Lead end bullet loads during excitation. (FigB.eps)

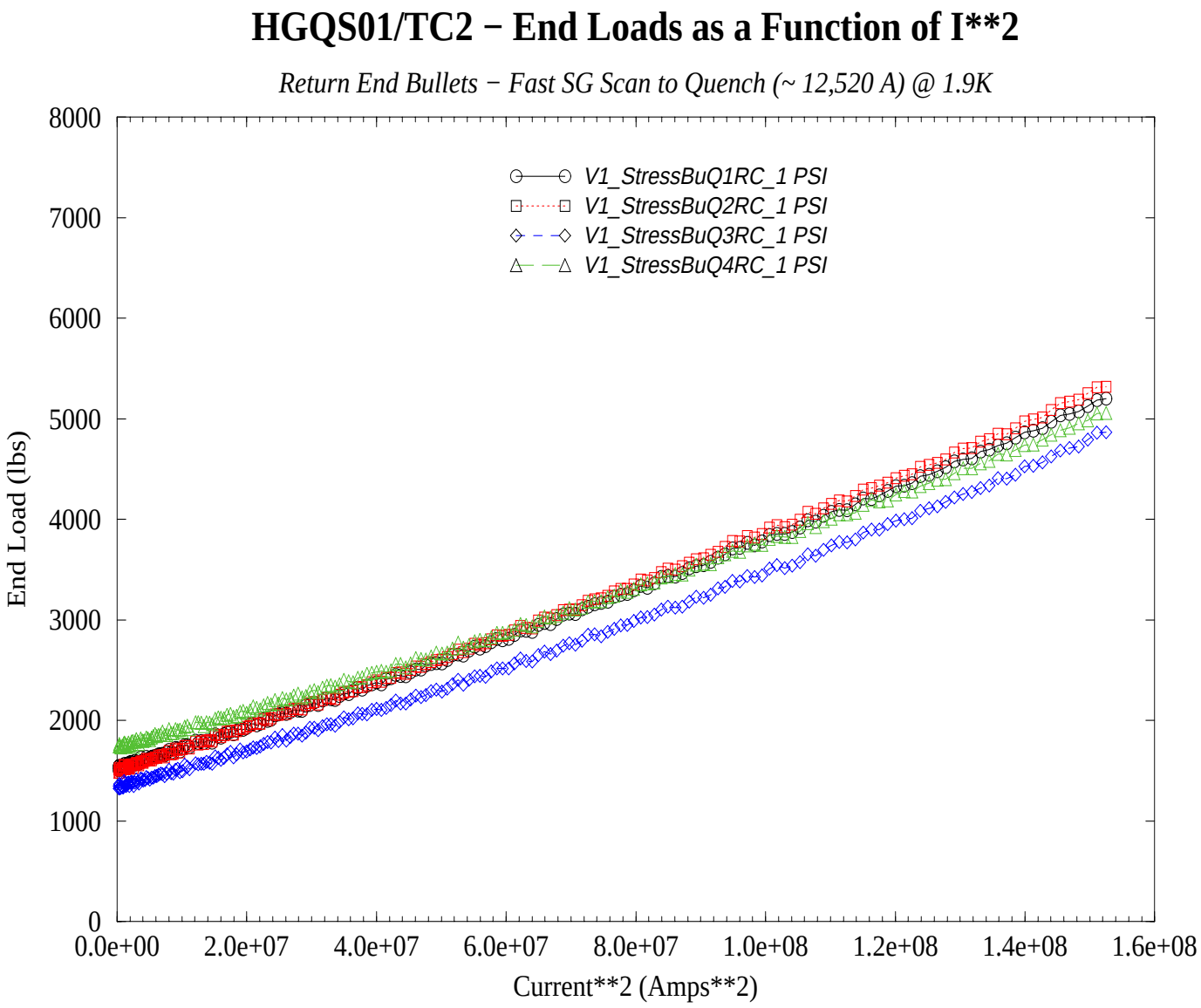

Figure 4.18: Return end bullet loads during excitation. (FigC.eps)

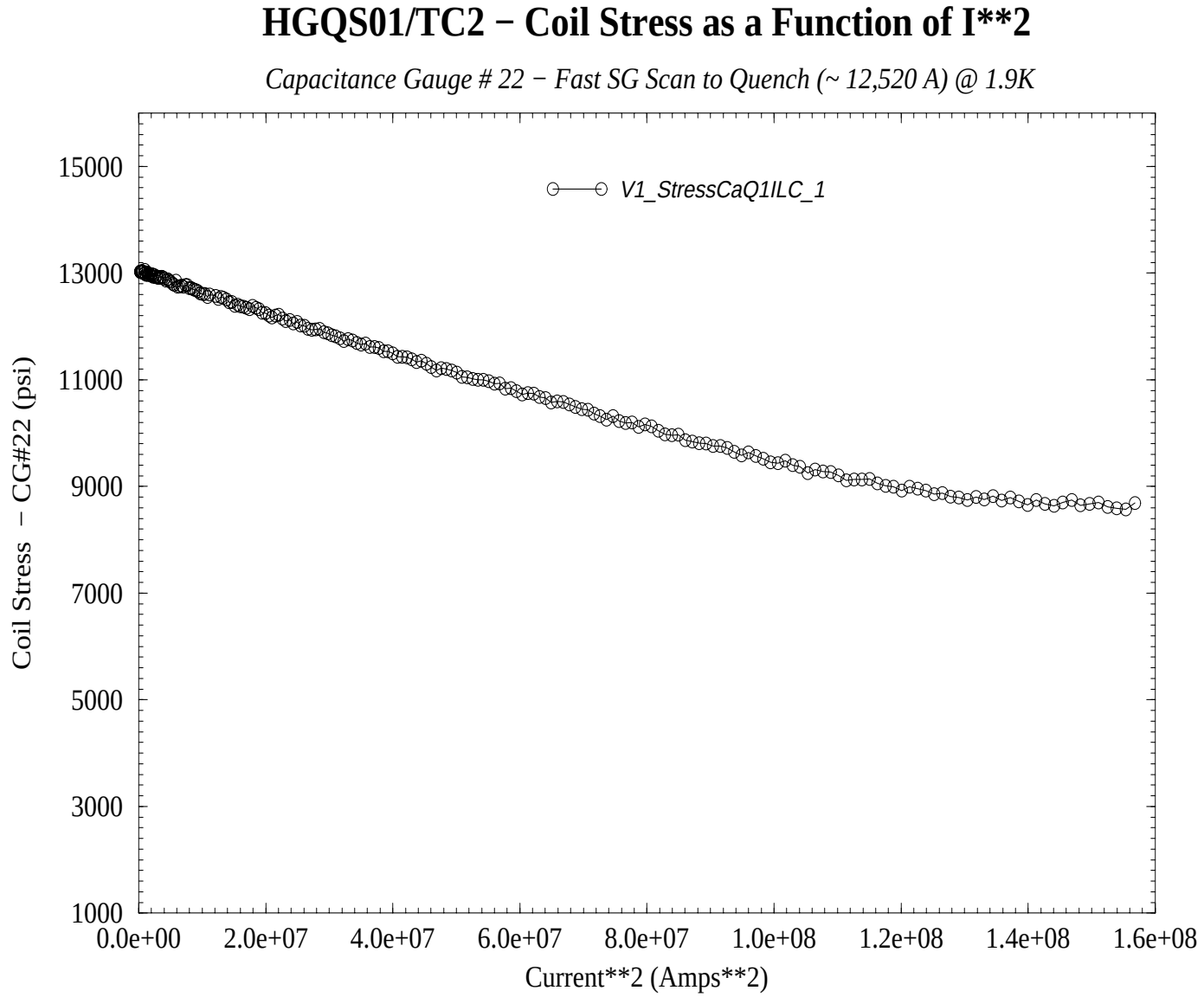

Figure 4.19: Shows the inner coil stress in quadrant 1 as measured by a capacitance gauge. (FigD.eps)

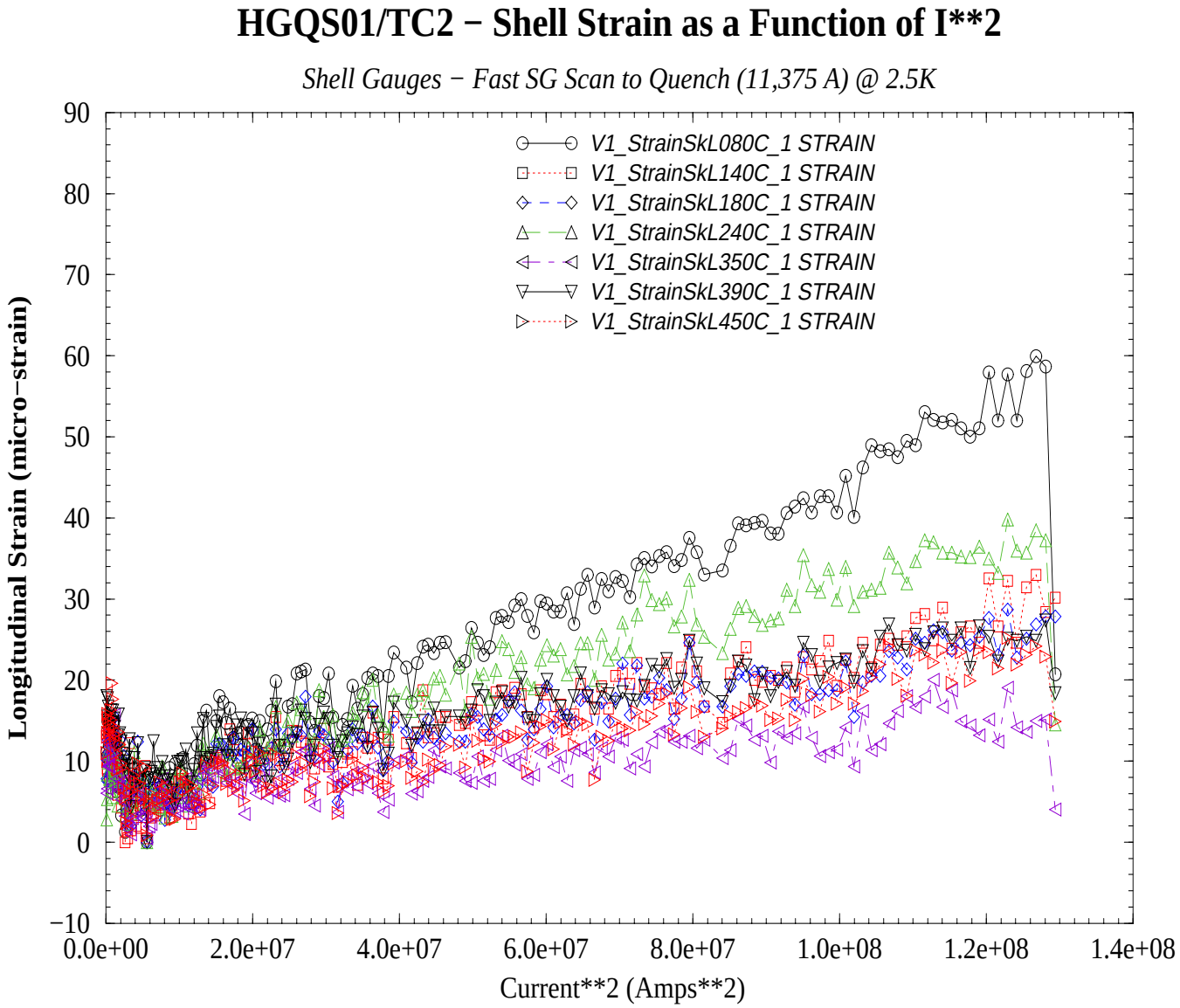

Figure 4.20: Shows the compensated strains of the longitudinal shell gauge data as a function of the square of the excitation current. (FigE.eps)

Chapter 5

Magnetic Measurements

5.1 Measurement System

Magnetic measurements on HGQS01 were performed using the tangential, vertical drive, rotating coil system obtained from the SSCL. It should be noted that quadrupole magnets measured with this probe for the SSCL at Babcock and Wilcox (where this coil was predominantly used) were of 40mm-50mm aperture, and consequently the probe is not optimal for measurements of the 70mm aperture HGQ magnets. A probe optimized to the HGQ aperture is to be commissioned soon.

The probe has nominal diameter of 1 in. and length 0.25 m, and has 5 windings on a machined ceramic coil form: tangential, 2 dipole buck, and 2 quadrupole buck windings. The opening angle of the tangential coil is 15°. Other coil parameters are summarized in the following table:

Winding	N turns	L(m)	Radius(m)	Ang Offset(rad.)
TAN	30	0.25	0.012379	0.433544
Q Buck1	3	0.25	0.012339	0.000000
Q Buck2	3	0.25	0.012336	0.867089
D Buck1	3	0.25	0.012338	5.856985
D Buck2	3	0.25	0.012332	1.293288

This probe is connected via G-10 and stainless steel drive shaft to an external drive on the vertical test sled. Note that the length of the warm

finger limits the travel at the far (non-lead) end of the magnet so that full end scans could only be done at the lead end.

Field measurements are taken with the 'mfm' data acquisition system, where probe rotation speed is $\sim$ 0.3 Hz, and the voltages generated are sampled 128 times per rotation using HP3458 DVM's; each sample is an integration over one line cycle (0.0167s). Closed loop feedback through an op-amp holds the coil angular velocity constant at the 1% level. Data from each winding are saved independently and bucking is performed digitally. For measurements at low field, pre-amplifiers with gain of 128 are applied to the signals upstream of the DVM's.

In all measurement analyses, the probe is centered in the transverse plane using the feed down from quadrupole to dipole.

Further system, operations, and analysis information is available at
http://tsmtf.fnal.gov/ dimarco/sscl_systems.html.

5.2 Measurements

The magnetic measurements performed on HGQS01 during the first thermal cycle are listed in Appendix C. The magnet was then warmed to room temperature and removed from the dewar. Load on the magnet ends was increased, and an harmonic shim was removed. The magnet was again cooled. The magnetic measurements performed on HGQS01 during the second thermal cycle are listed in Appendix D. One change was made in measurement procedure for the second thermal cycle. The edges of the steps of the stairstep measurements were sharpened in an attempt induce eddy currents.

The measurements characterize the magnetic behavior of HGQS01 in the following areas:

- Variation of multipoles/field strength as a function of current and ramp rate: measurements of multipole hysteresis at various ramp rates and maximum currents (CLP), and stairstep (SSL) measurements.

- Axial variation of multipoles/field strength and field angle: z-scans (ZSC) in steps of 10 inches in the body as well as a fine scan (LES) in 1 inch increments at the lead end.

- Time dependence of multipoles at "injection" porch: measurements as a function of duration at pre-cycle flattop and maximum pre-cycle flattop current (ACL).

5.3 Data

Below are representative plots and summaries of harmonics from the main areas of measurement. Note that a coordinate rotation is performed on the data so that the quadrupole component of each measurement is always pure normal; consequently, plots of the normal and skew quadrupole are not shown (always being exactly 10000 and 0 respectively). Field harmonics are reported at a reference radius of 10 mm. [1]

A complete set of plots for all measurements can be found at
http://tsmtf.fnal.gov/ dimarco/HGQS01_test_data.html

5.3.1 Current dependence

Transfer function to 11kA

Figure 5.1 shows the transfer function obtained from measurements ZSC-2kA-T45 and ZSC-6kA-T45. Also plotted are field angle and the transverse plane probe offsets determined from the feed down of quadrupole to dipole. Characteristic of the transfer function is the decrease at higher currents from iron saturation. A twist in the magnet of 7 mrad/m can be seen. The field angle increases with distance from the return end plate corresponding to a counterclockwise twist viewed from the return end. There is also an apparent tilt in the warm bore of 1 mm from top to bottom.

[1] Those tables of harmonics given in this section are given for a reference radius of 17mm, the LHC standard, in Appendix B.

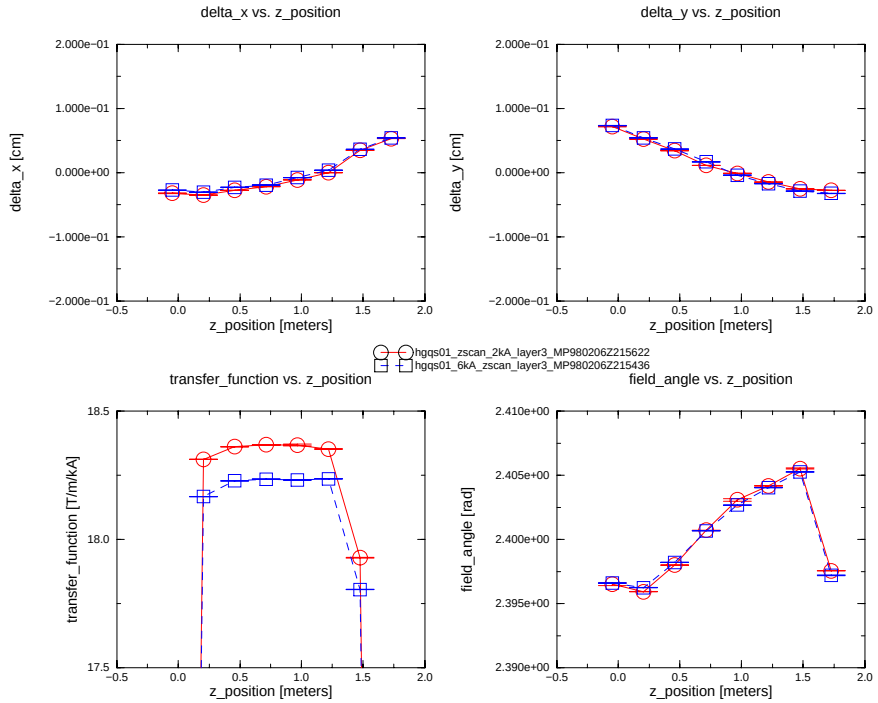

Figure 5.1: Transfer function.

Field harmonics to 11kA

Table 5.1 summarizes the field harmonics in the magnet body. Data were measured at $z = 0.818$ m.

Tables 5.2 and 5.3 summarize the field harmonics measured in axial scans of the magnet.

	2kA (u) mean	2kA (u) error	2kA (d) mean	2kA (d) error	6kA mean	6kA error	11kA mean	11kA error
b3	0.350	0.0148			0.410	0.0050	0.440	0.014
b4	0.130	0.0040			0.140	0.0018	0.140	0.002
b5	-0.100	0.0024			-0.085	0.0017	-0.073	0.014
b6	-0.480	0.0031	-0.400	0.0025	-0.450	0.0018	-0.440	0.013
a3	0.460	0.0150			0.450	0.0062	0.380	0.134
a4	0.720	0.0035	0.670	0.0037	0.710	0.0032	0.710	0.003
a5	0.022	0.0013			0.025	0.0014	0.020	0.002
a6	-0.000	0.0018			-0.002	0.0009	-0.002	0.006

Table 5.1: Field harmonics at 2kA, 6kA, 11kA measured during the first thermal cycle. Where there is a difference between the field during up ("u") and down ("d") ramp, separate values are given. Otherwise the value given is the average of both up and down ramp data. (Data are averaged over the range ± 100 A around the nominal value The change in field with current over that range is negligible.) The quoted error is $\sigma/\sqrt{(N)}$, where N is the number of points included in the average.

End regions

Figure 5.2 shows the transfer function and the field angle obtained from measurement LES-6kA-T45. Figure 5.3 shows the transfer function and the field angle obtained from measurement LES-6kA-T19-TC2. The shape of the transfer function in the end region is the same. There is, however, a difference 29 mm between the two coordinate systems. This is after our best attempts to establish the same z axis origin for measurements from the two thermal cycles. We consider measurements from the second thermal cycle to be in the reference frame describe in [1]. We know, and it is obvious, from the discrepancy in the two figures that data from the first thermal cycle does not have the same z axis origin, and we have abandoned the attempt to understand why. We believe, however, that all measurements from the first thermal cycle have the same z axis origin. [2]

[2]One possibility is that the probe drive mechanics slipped during measurement. However, the warm $z$scans made before and after the cold measurements of the first thermal

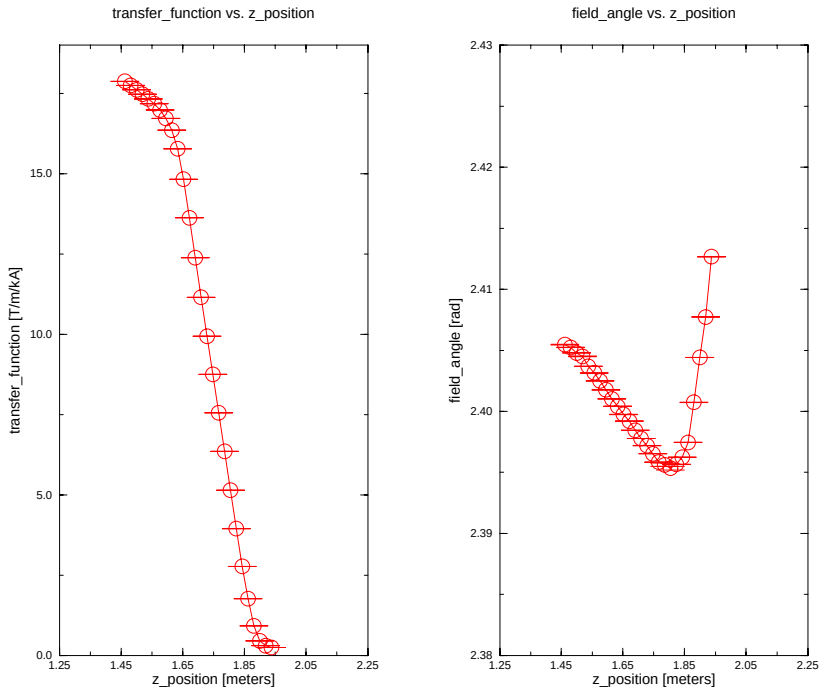

Figure 5.2: Transfer function and field angle as a function of z in the lead end measured during the first thermal cycle of the magnet.

5.3.2 Effect of the Removal of the Harmonic Shim

Table 5.4 gives the measured and predicted change [2] in the magnetic field harmonics for the removal of the shim. Predicted values agree well with those measured. TCI data is from measurement CLP-Z0-11kA-10As-T19; and TCII data, from CLP-Z0-11kA-10As-T19-TC2.

---

cycle overlay exactly the data from the end scan. A slippage in the drive system is, thus, not possible.

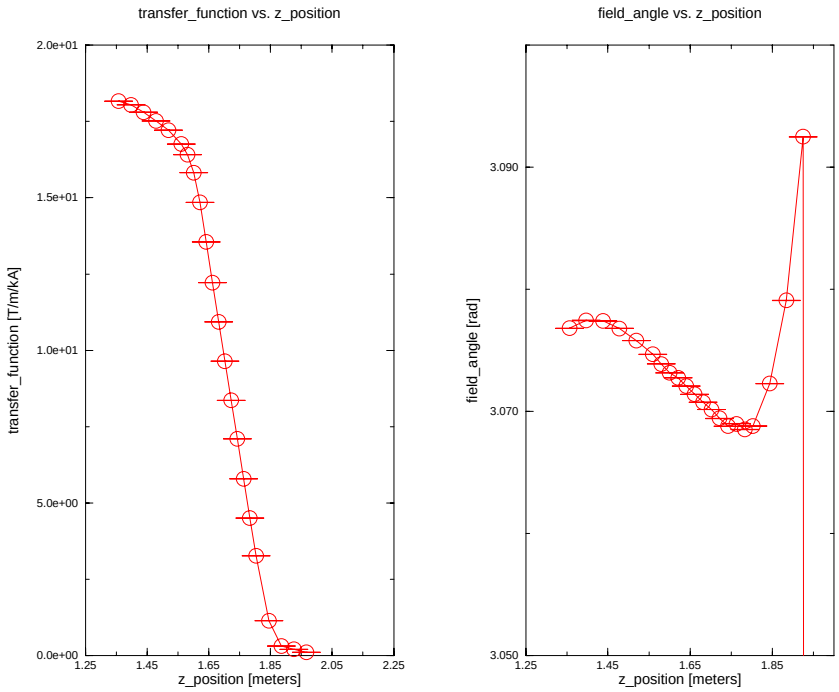

Figure 5.3: Transfer function and field angle as a function of z in the lead end measured during the second thermal cycle of the magnet.

5.3.3 Time Dependence

"Stairstep" Measurements

No change in harmonics during the stairstep was observed.

Field angle to 11kA

Figure 5.4 shows the field angle as a function of current at 10A/s and 40A/s ramp rates. These data were obtained from measurements CLP-Z0-11kA-10As-T19 and CLP-Z0-11kA-40As-T19. Since a rotation is performed on the data so that the quadrupole component is always pure normal, this ap-

parent change in the field angle of the quadrupole stems from the presence of a skew quadrupole term. Here clear ramp rate dependence of a skew quadrupole contribution is observed as a hysteresis in field angle with magnitude of the hysteresis half-width at 2000A being about 1mrad/10A/s (1 mrad corresponds to 20 units of skew quadrupole).

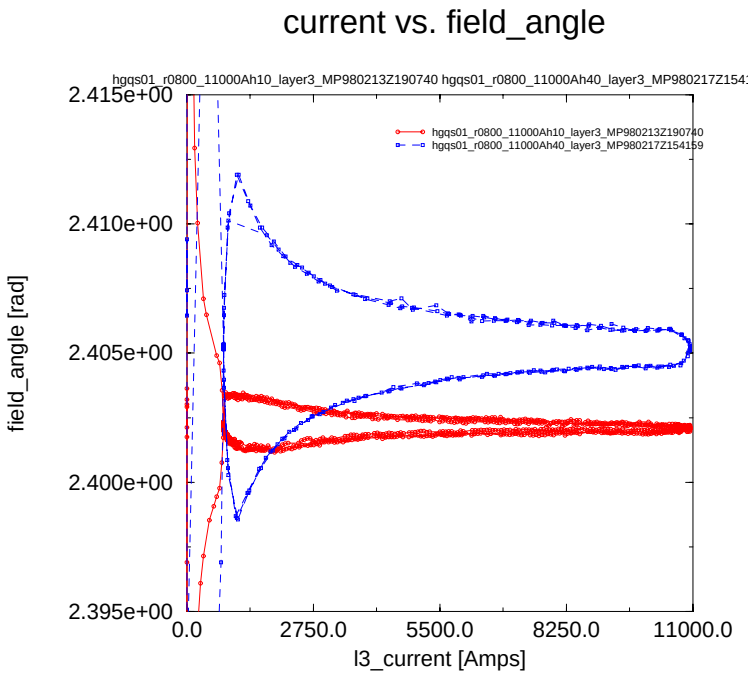

Figure 5.4: Field angle as function of current at 10A/s and 40A/s (fieldangle_vs_current.eps) Note that the 'cusp' which forms at $\sim 800A$ is caused by the parabolic decceleration/acceleration of the power supply when stopping/starting a ramp.

Accelerator cycle ramps

Figures 5.5 show the change in harmonics as a function of time while at the 800A 'injection porch' of measurement ACL-11kA-T19-30m-TC2. This measurement had a 5 min. pre-cycle flattop at a current of 11kA. There is a decay of 0.3 units in the octupole. No change in the dodecapole is observed. No change in harmonics at injection was observed during the first thermal cycle.

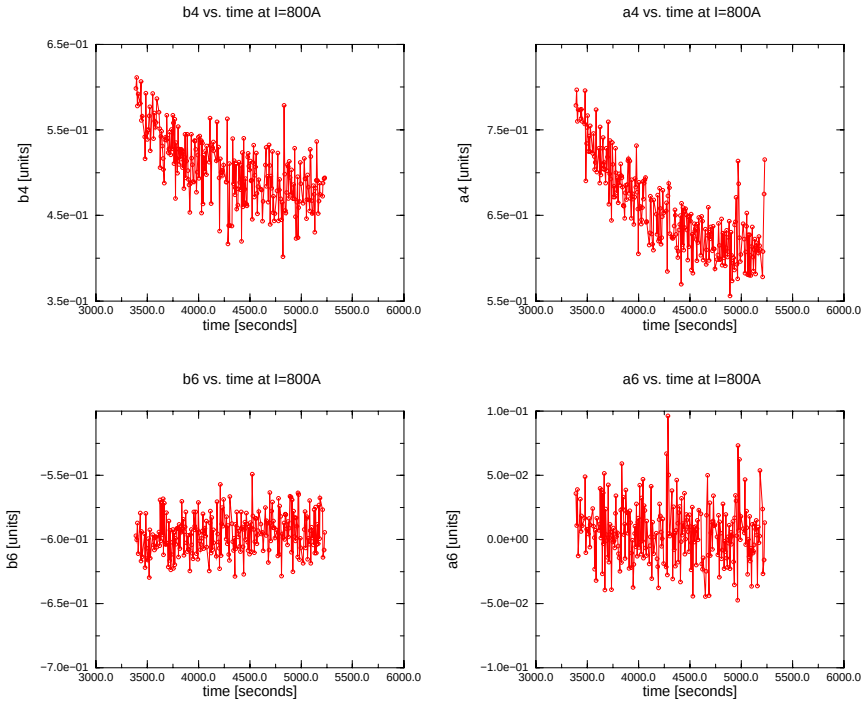

Figure 5.5: Selected field harmonics at the nominal injection current of 800 A.

5.4 Measurement Uncertainty

Analysis is underway to understand the level of measurement uncertainty. No quantitive statement can be made at this time although some feeling for the level of uncertainty can be gained by looking at the point-to-point variation in, for example, Fig. 5.5. This apparent jitter is not yet understood. We are also still investigating the warm-cold correlation between multipole measurements.

5.5 Summary

We make the following observations about the magnet as built (TCI).

- Axial variation is observed at the level of 0.5 units in several low order multipoles ($b_3,\ b_4, a_3,\ a_4$)
- Normal and skew harmonics for $n \geq 8$ are less than, or on the order of, 0.0025 units at any axial position in the body of the magnet.
- Harmonics generally showed little change as a function of current.
- There is very little time dependent behavior exhibited by the multipoles.
  - Measurements made at different ramp rates show no dependence of the hysteresis width of multipoles on ramp rate. Also, multipoles show no significant change when ramping stops during stairstep measurements.
  - There is, however, a ramp-rate dependent skew quadrupole which decays very quickly when ramping stops. This appears in the data as a change in field angle (see Figure 5.4). The magnitude of this effect at 2000A is about 20 units of a_n (or equivalently 1 mrad) per 10A/s ramp rate.
  - No time variation of multipoles during the injection plateau of accelerator cycles was observed in measurements made during the first thermal cycle.

- As expected, the iron yoke contributes 10% to the magnet field. Iron saturation reduces the field by a few percent at high current.
- There is a small twist along the magnet (appx. 7 mrad/m).

The field measured during the second thermal cycle was produced by the removal of the shim which we comment on below. One interesting feature of the second set of measurement was the change in octupole seen while at injection current in the accelerator cycle. This was not seen during the first thermal cycle but is presumably not related to the removal of the shim.

Agreement between calculated and measured fields in the lead end of the magnet is good with and without the shim. [3] The observed change in the field caused by the removal of the magnetic shim also agrees well with the calculated change in field.

	TCI mean	10A error	TCI mean	2kA error	TCI mean	6kA error
b3	0.557	0.4978	0.390	0.5238	0.499	0.5029
b4	-0.074	0.0889	0.028	0.0499	0.037	0.0498
b5	-0.060	0.0303	-0.049	0.0224	-0.044	0.0215
b6	-0.291	0.2313	-0.280	0.2031	-0.258	0.2048
b7	0.005	0.0040	-0.000	0.0021	-0.001	0.0027
b8	-0.004	0.0029	-0.000	0.0006	0.001	0.0007
b9	0.004	0.0025	-0.000	0.0003	0.000	0.0008
b10	0.001	0.0023	-0.004	0.0014	-0.004	0.0017
a3	-0.093	0.2315	0.150	0.1095	0.173	0.1081
a4	0.764	0.2803	1.005	0.1964	1.019	0.1946
a5	-0.001	0.0295	0.018	0.0212	0.019	0.0209
a6	0.051	0.0391	-0.012	0.0128	-0.017	0.0123
a7	-0.007	0.0071	-0.002	0.0017	-0.002	0.0011
a8	0.008	0.0078	-0.000	0.0010	0.001	0.0006
a9	-0.002	0.0046	-0.001	0.0005	-0.000	0.0005
a10	0.006	0.0041	0.000	0.0002	-0.000	0.0003

Table 5.2: Field harmonics averaged over the length of the magnet from axial scan data at 10A, 2kA, 6kA measured during the first thermal cycle. Data is averaged over 1.8 m of the magnet. The quoted error is $\sigma/\sqrt{(N)}$, where $N = 8$, and is intended to give some indication of the variation in field along the length.

	TCII mean	10A error	TCII mean	6kA error	TCII mean	11kA error
b3	0.706	0.4464	0.492	0.4273	0.405	0.4244
b4	0.275	0.0696	0.248	0.0861	0.148	0.0689
b5	-0.066	0.0328	-0.046	0.0274	-0.051	0.0264
b6	-0.133	0.2822	-0.168	0.2747	-0.155	0.2800
b7	-0.011	0.0097	0.001	0.0043	-0.001	0.0024
b8	-0.003	0.0128	0.002	0.0020	0.000	0.0007
b9	-0.002	0.0056	0.000	0.0004	-0.000	0.0005
b10	-0.005	0.0026	-0.004	0.0015	-0.003	0.0010
a3	1.074	0.6989	1.730	0.5193	1.065	0.4004
a4	0.742	0.2162	1.054	0.1564	1.036	0.1690
a5	-0.063	0.0568	0.011	0.0377	0.015	0.0334
a6	-0.031	0.0763	-0.006	0.0084	-0.011	0.0064
a7	-0.008	0.0097	-0.001	0.0014	-0.002	0.0016
a8	-0.004	0.0078	0.001	0.0016	0.002	0.0019
a9	-0.009	0.0071	0.001	0.0004	-0.000	0.0009
a10	-0.000	0.0015	-0.000	0.0004	-0.000	0.0003

Table 5.3: Field harmonics averaged over the length of the magnet from axial scan data at 10A, 6kA, 11kA measured during the second thermal cycle.

	measured				
	800 A			11kA	
n	Δb_n (u)	Δb_n (d)	Δa_n	Δb_n	Δa_n
3	0.22		2.86	0.00	1.40
4	0.33	0.47	0.15	0.13	0.09
5	0.03		-0.03	0.03	-0.03
	predicted				
	800 A			11kA	
n	Δb_n		Δa_n	Δb_n	Δa_n
3	0.44		2.68	0.04	1.57
4	0.38		0.12	0.19	0.10
5	0.04		-0.04	0.02	-0.02
6	-0.002		-0.007	-0.0004	-0.003

Table 5.4: Difference in field harmonics measured in the two thermal cycles caused by the removal of the magnetic shim. ($\Delta b_n = b_n^{TCII} - b_n^{TCI}$, etc.) The uncertainty on the measured values is 20-40% at low current and 10% or less at high current. Allowing for measurement uncertainty, no difference is measured in the $n = 6$ component of the field. The predicted value is also small. Where there is a difference between up ("u") and down ("d") ramp data, both values are given. If no difference is observed, the measured value is given in the up ramp column.

Chapter 6

Splice Resistance Measurements

This summary describes measurements of coil splice resistances made during the first thermal cycle of HGQS01 in the vertical magnet test facility in the Fermilab Technical Division.

6.1 Introduction

During the magnet fabrication, voltage taps were placed directly on either side of each splice between coils, specifically to measure the voltage drops across the splices. A splice resistance is given by the ratio of measured voltage drop across the splice to the measured magnet current (by Ohm's Law).

6.2 Method

Measurement of the magnet current was made via a calibrated Holec transductor located on the negative bus of the power supply which is connected directly to the magnet (see "Power Schematic" figure also available on the VMTF web page at

http://tsmtf.fnal.gov/ tartagli/VMTF/Doc/VMTF.html)

The transductor signal was digitized by a Pentek data logger, in sych with the splice Voltage measurements. The estimated absolute error on the

current is about 1 part in 10000.

The splice Voltages were conditioned using a specially configured (high gain = 1000) Isolation Amplifier, which fed the amplified signals into a Pentek data logger for digitization.

The data were recorded using the VMTF data acquisition system, which controlled the power supply ramp and measurement sequence. The splice data were taken in conjuction with "strain gauge" runs, in which the current was ramped up to a series of increasing levels, and data were taken during a 10-second "flat top" at each of the levels. Data were also taken at (less frequent) flat top levels on the downgoing ramp. Only one digitized measurement of the splice voltage and current was recorded at each level during a given strain gauge run.

6.3 Analysis

Plots of Splice Voltage versus current were created and least-squares fits were made using the program XMGR. The fitted slopes give the splice resistance directly. However, it was quickly noticed that some of the splices show a lot of scatter, while others are quite well correlated to the current. The reason for this is not yet known, but may be due to problems with some of the wiring (perhaps not properly twisted for noise rejection), or with noise in the Amplifier or digitizer channels. Further tests in the 2nd thermal cycle will attempt to resolve the noise problems. For this analysis, data from all of the strain gauge runs (at a given magnet temperature) were combined to give better statistical determination of the fitted slopes.

6.4 Results

Results are summarized in Figure 6.1- 6.9 and in Table 6.1 Tables and plots of the fits are also available on the web at:

http://tsmtf.fnal.gov/ tartagli/HGQ/HGQ_RSplice.html

Table 6.1: Splice resistance summary

Splice	R(4.3K)	R(1.9K)
Q1I-Q1O	.699 ± .044	.699 ± .036
Q2I-Q2O	.527 ± .055	.611 ± .074
Q2O-Q4I	.647 ± .147	.612 ± .126
Q3I-Q1O	.649 ± .135	.331 ± .114
Q3I-Q3O	.643 ± .159	.665 ± .323
Q4I-Q4O	.281 ± .097	.283 ± .096
Q4O-Q3O	.864 ± .055	.840 ± .059

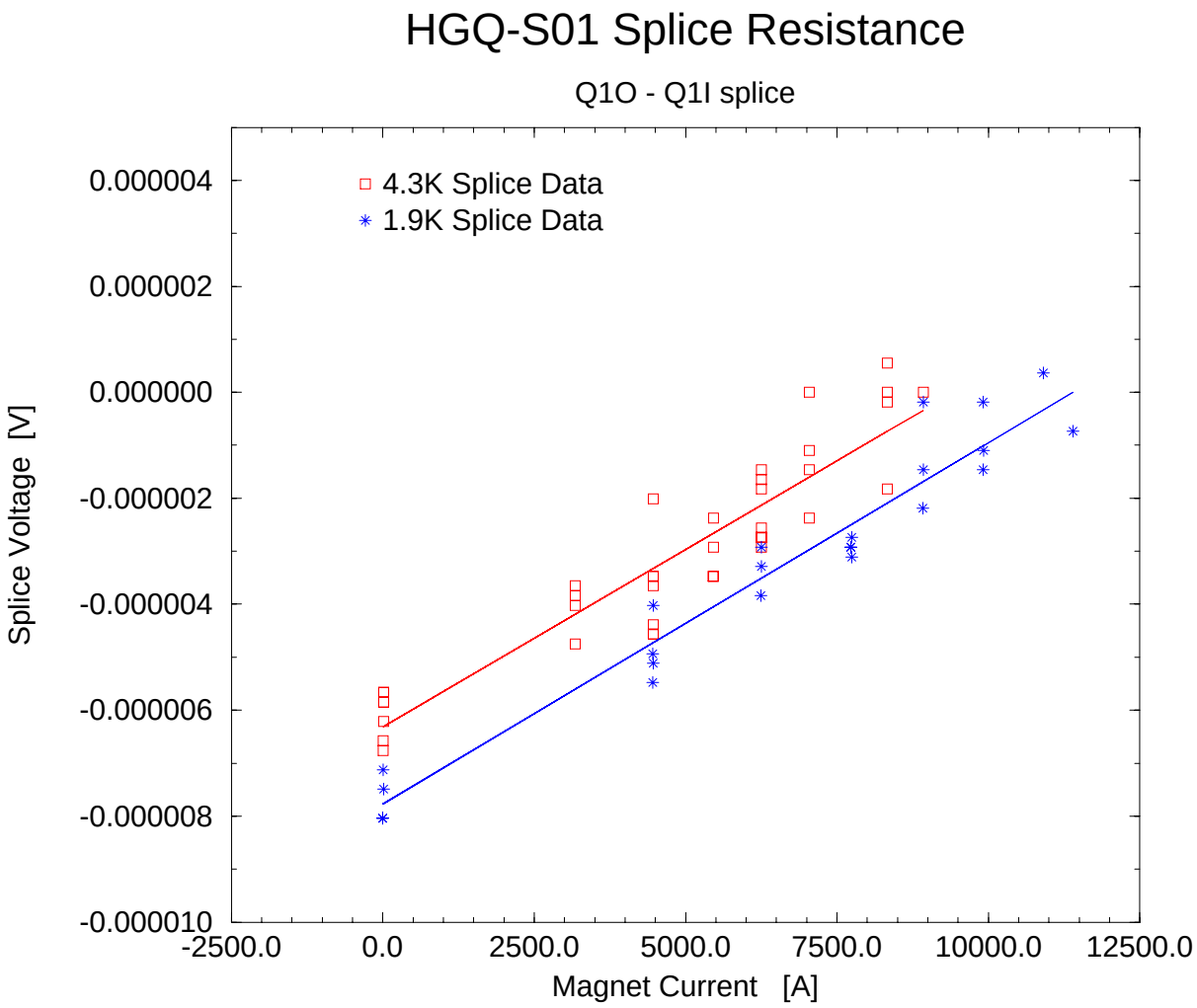

Figure 6.1: Qudrant 1 inner to quadrant 1 outer splice

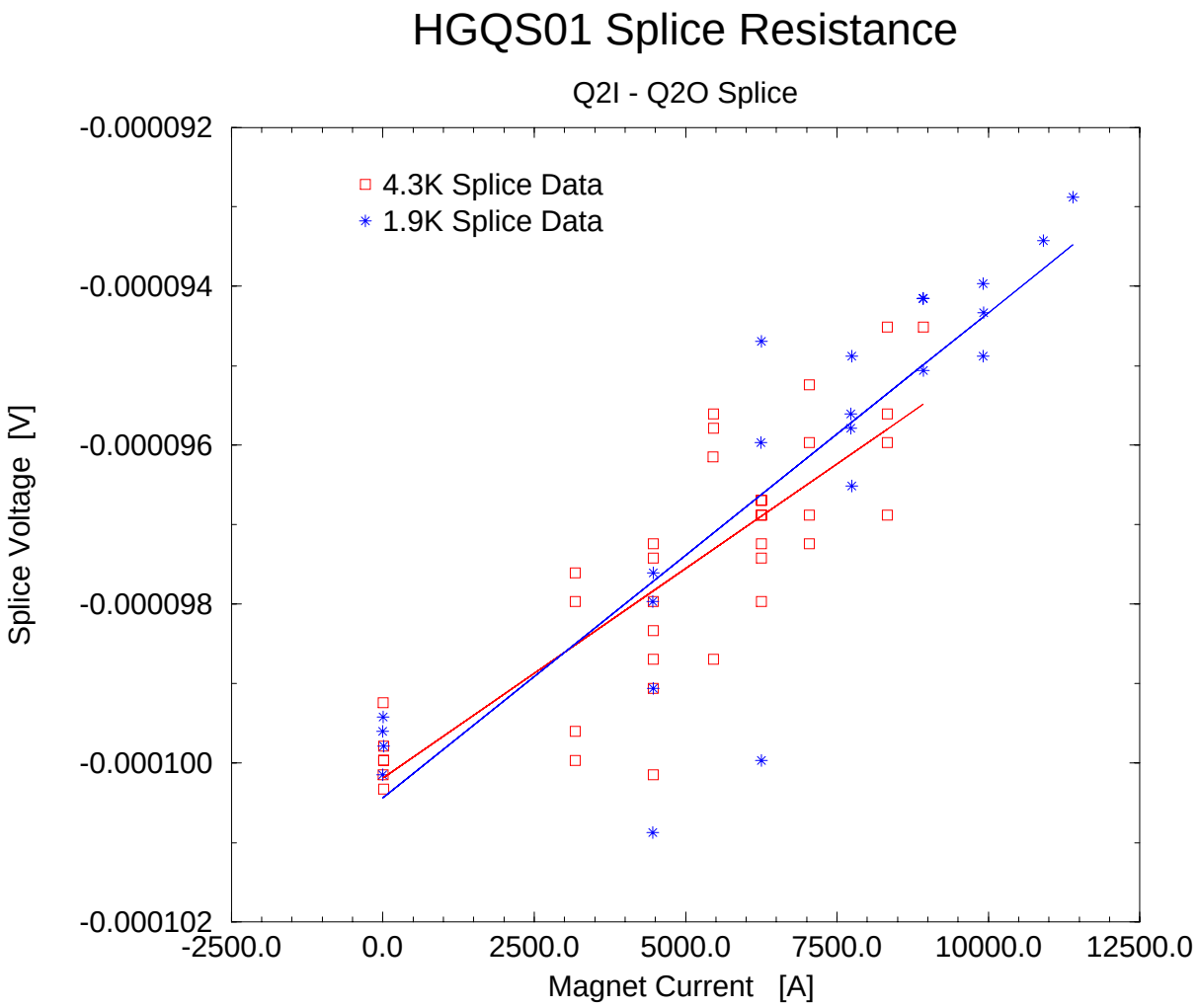

Figure 6.2: Qudrant 2 inner to quadrant 2 outer splice

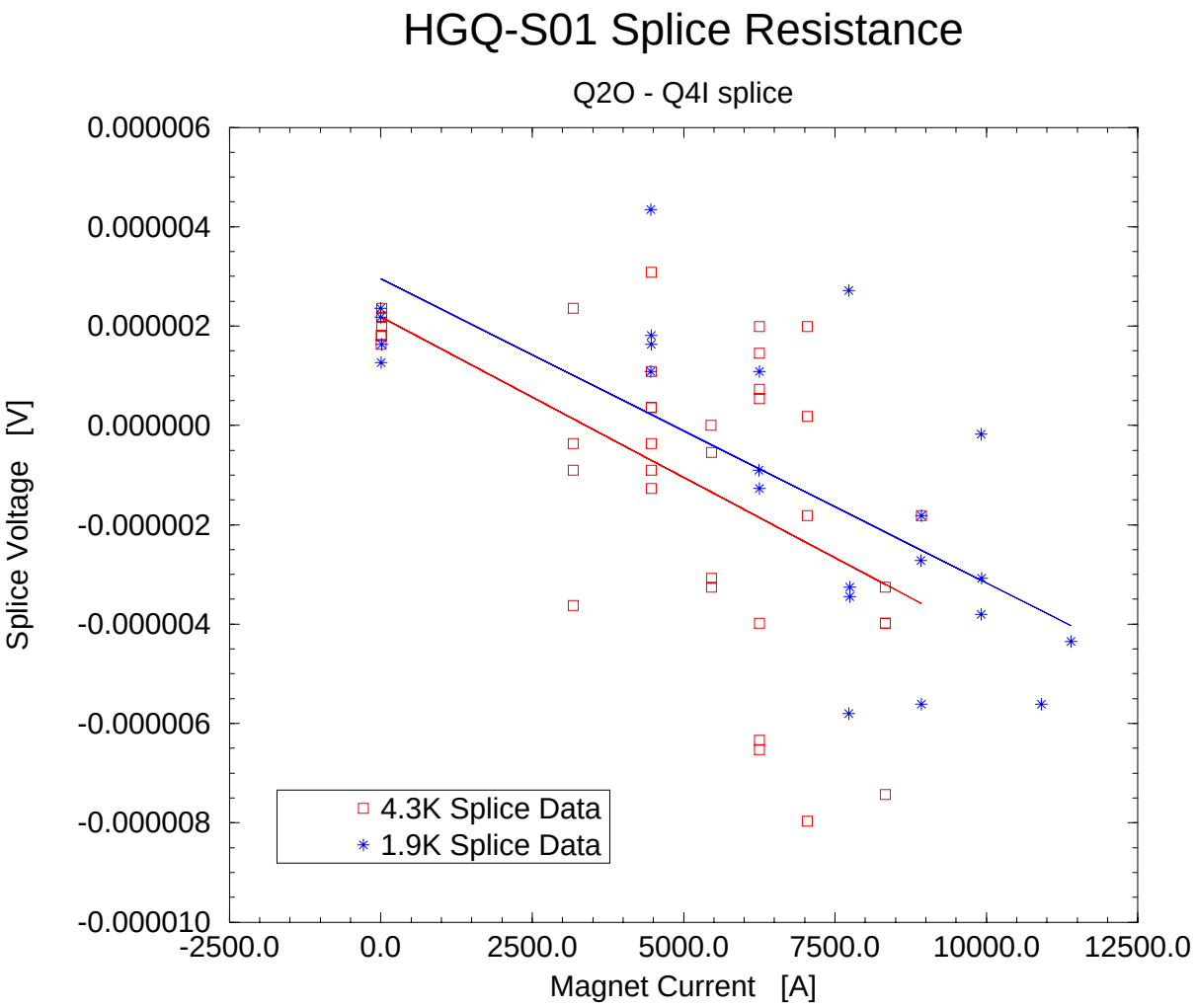

Figure 6.3: Qudrant 4 inner to quadrant 2 outer splice

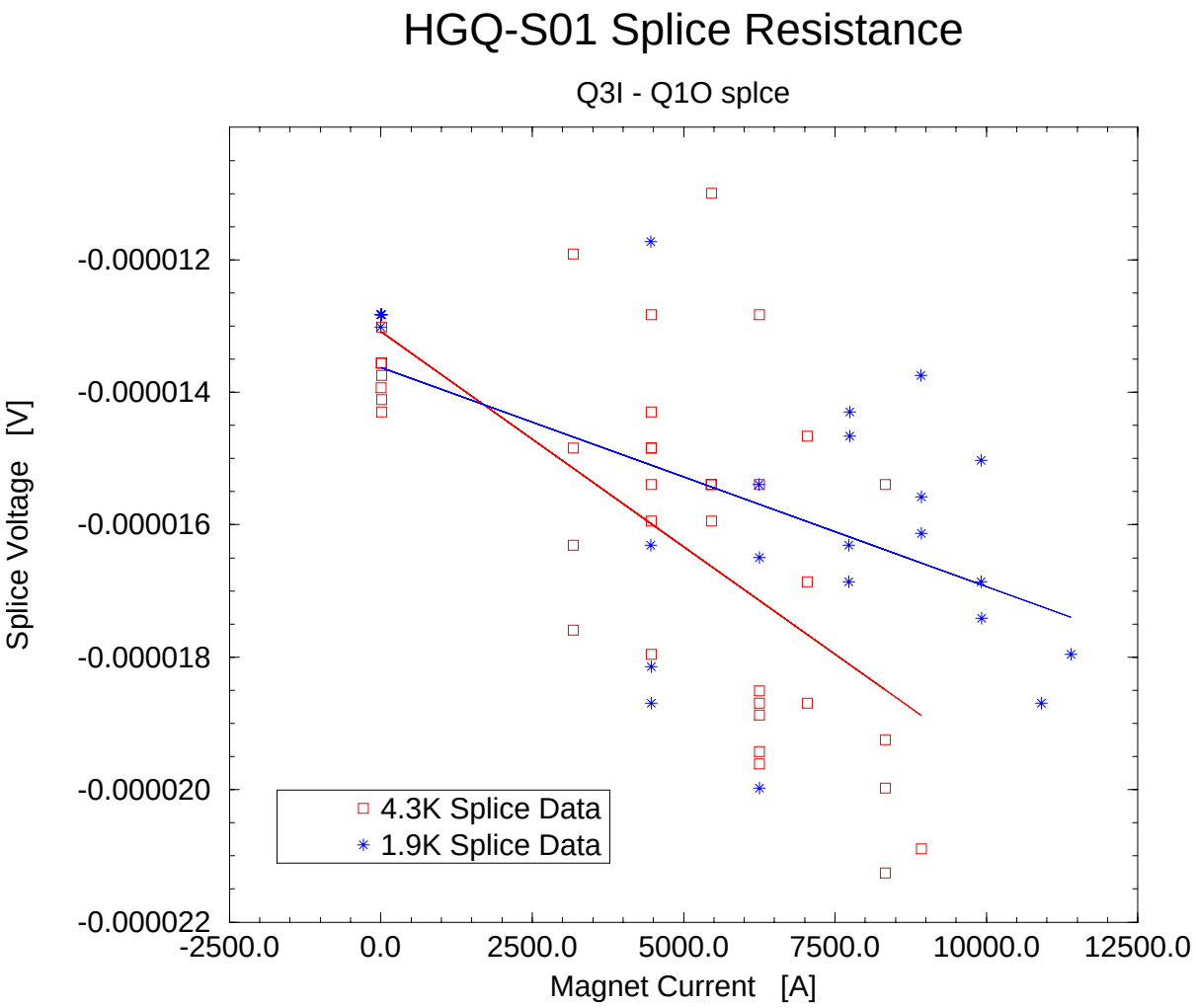

Figure 6.4: Qudrant 3 inner to quadrant 1 outer splice

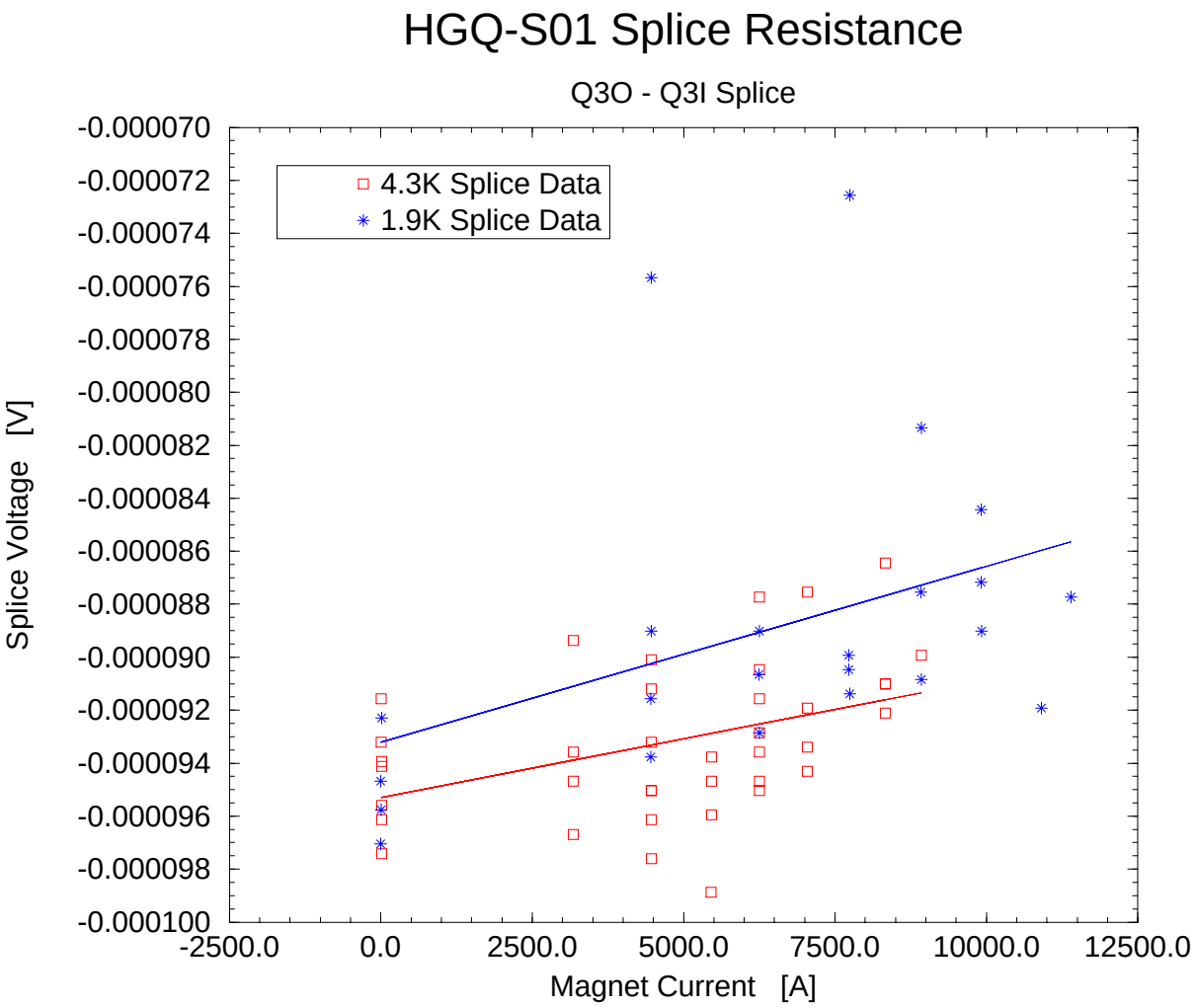

Figure 6.5: Qudrant 3 inner to quadrant 3 outer splice

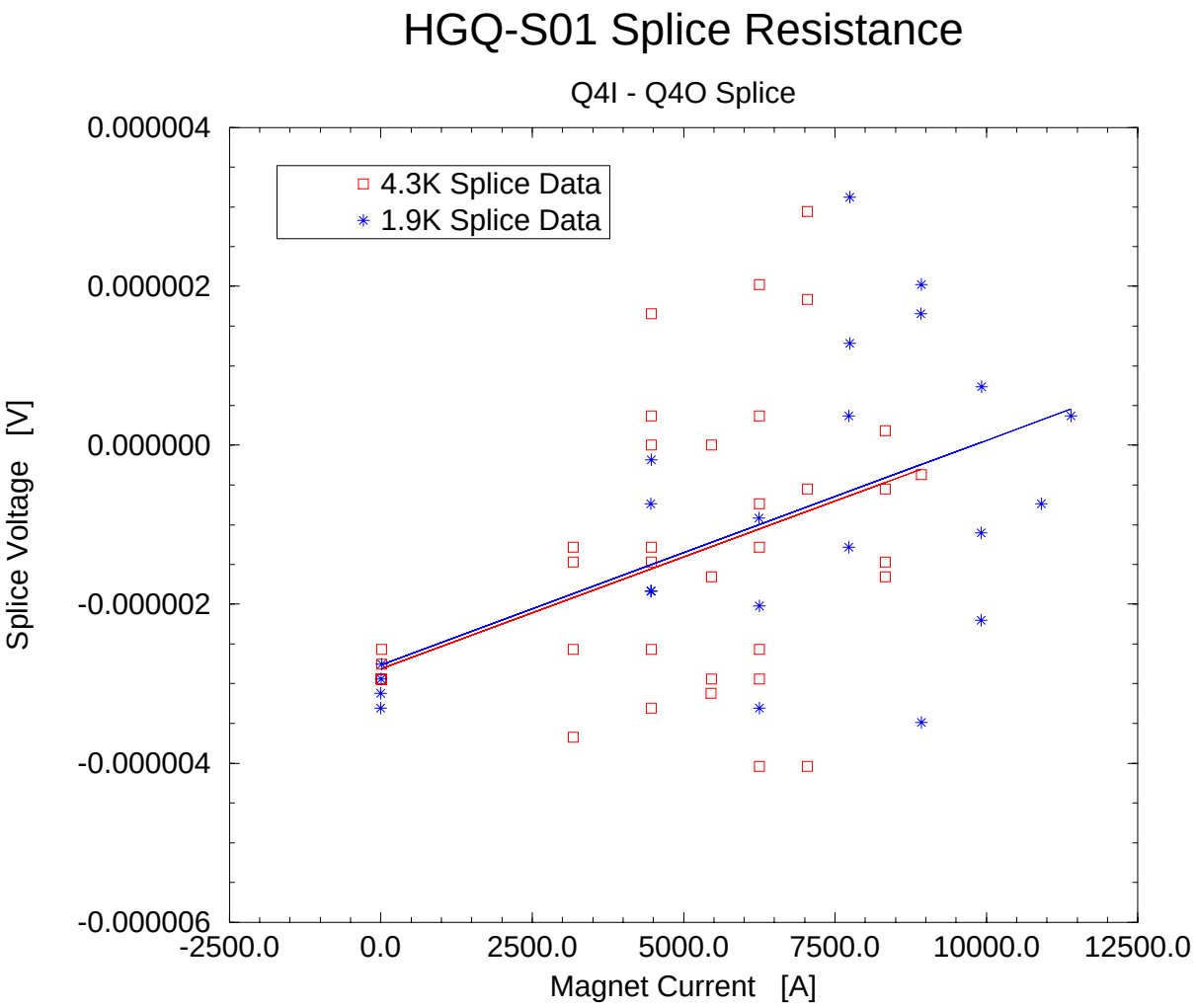

Figure 6.6: Qudrant 4 inner to quadrant 4 outer splice

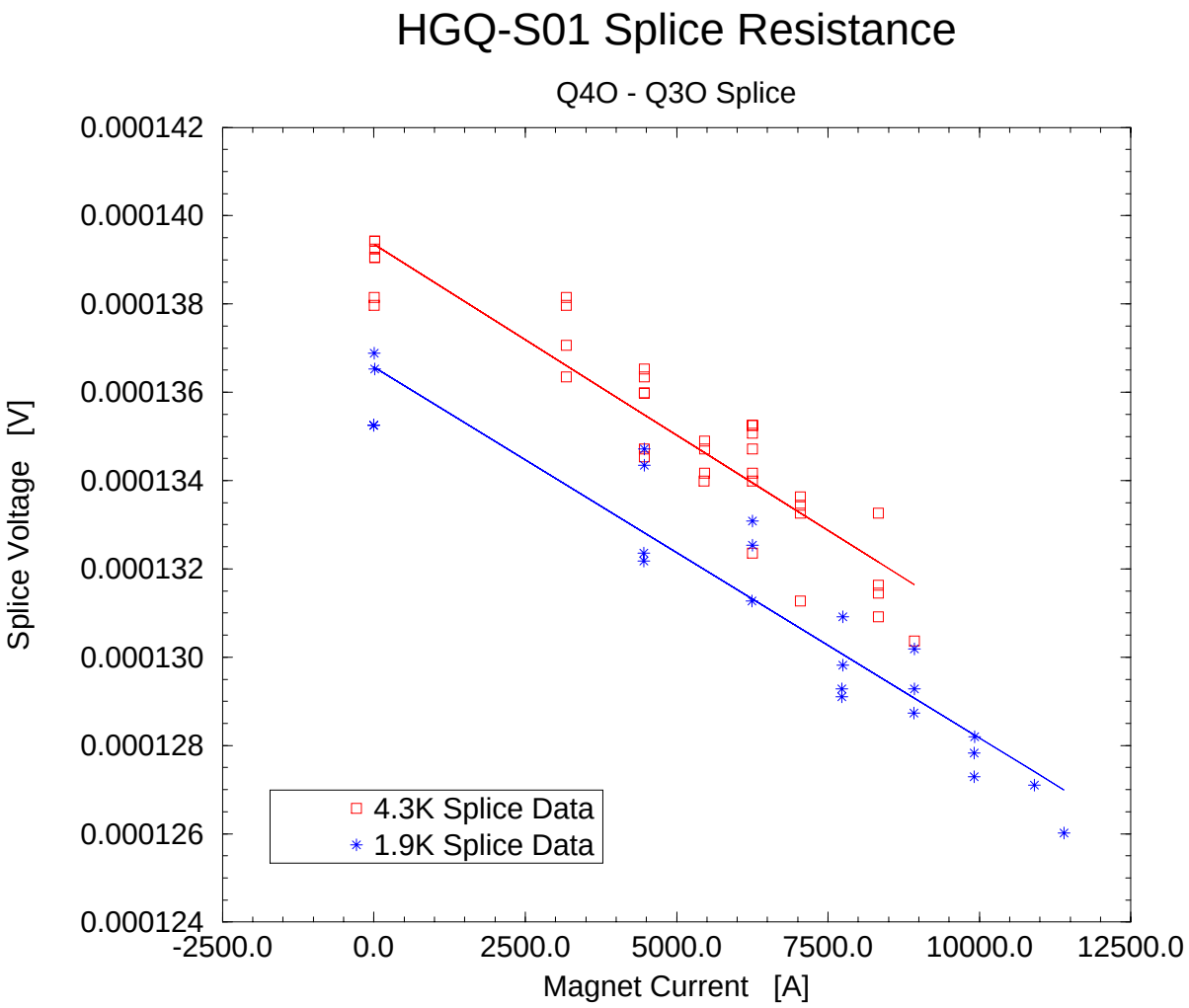

Figure 6.7: Qudrant 4 outer to quadrant 4 outer splice

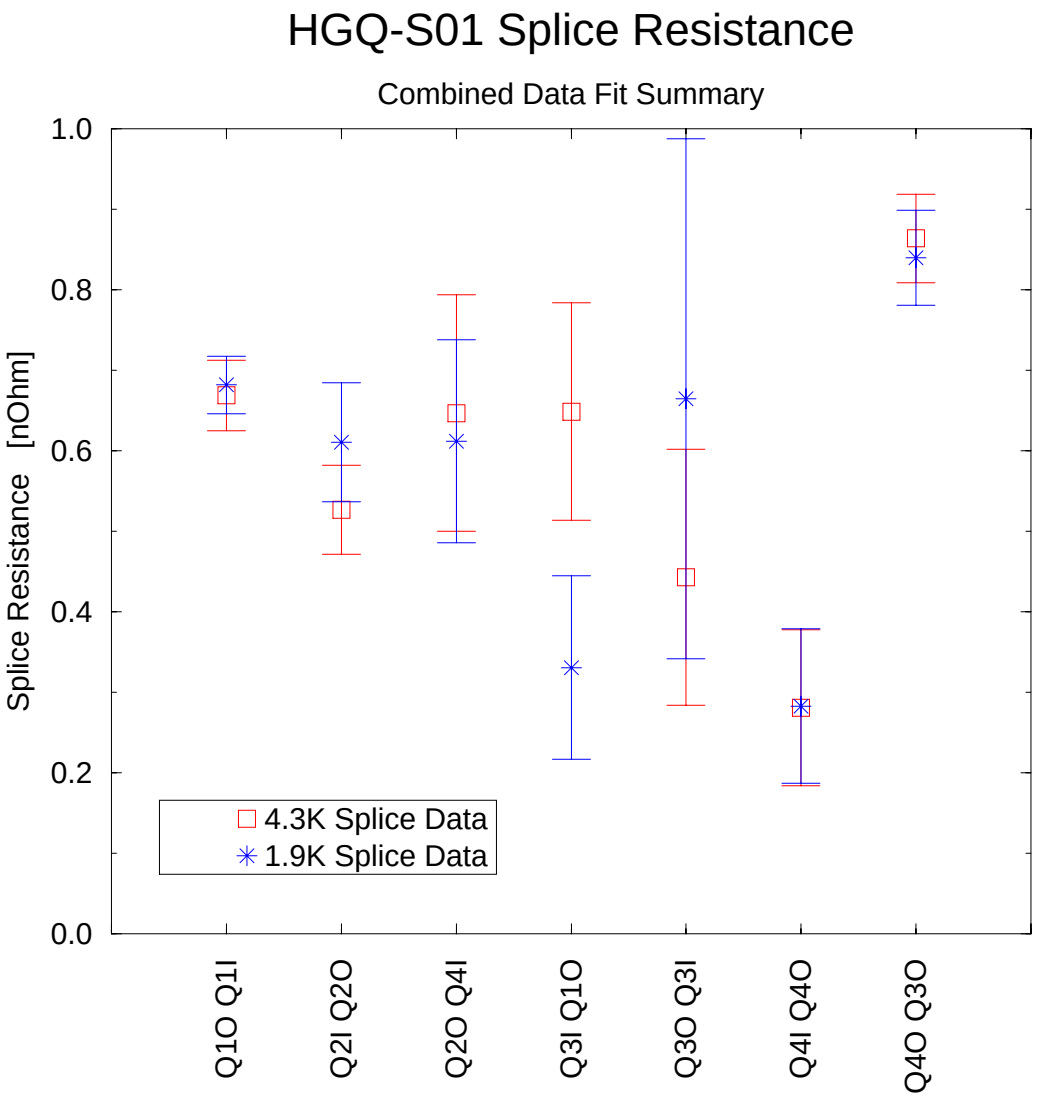

Figure 6.8: Summary of the splice resistance measurement

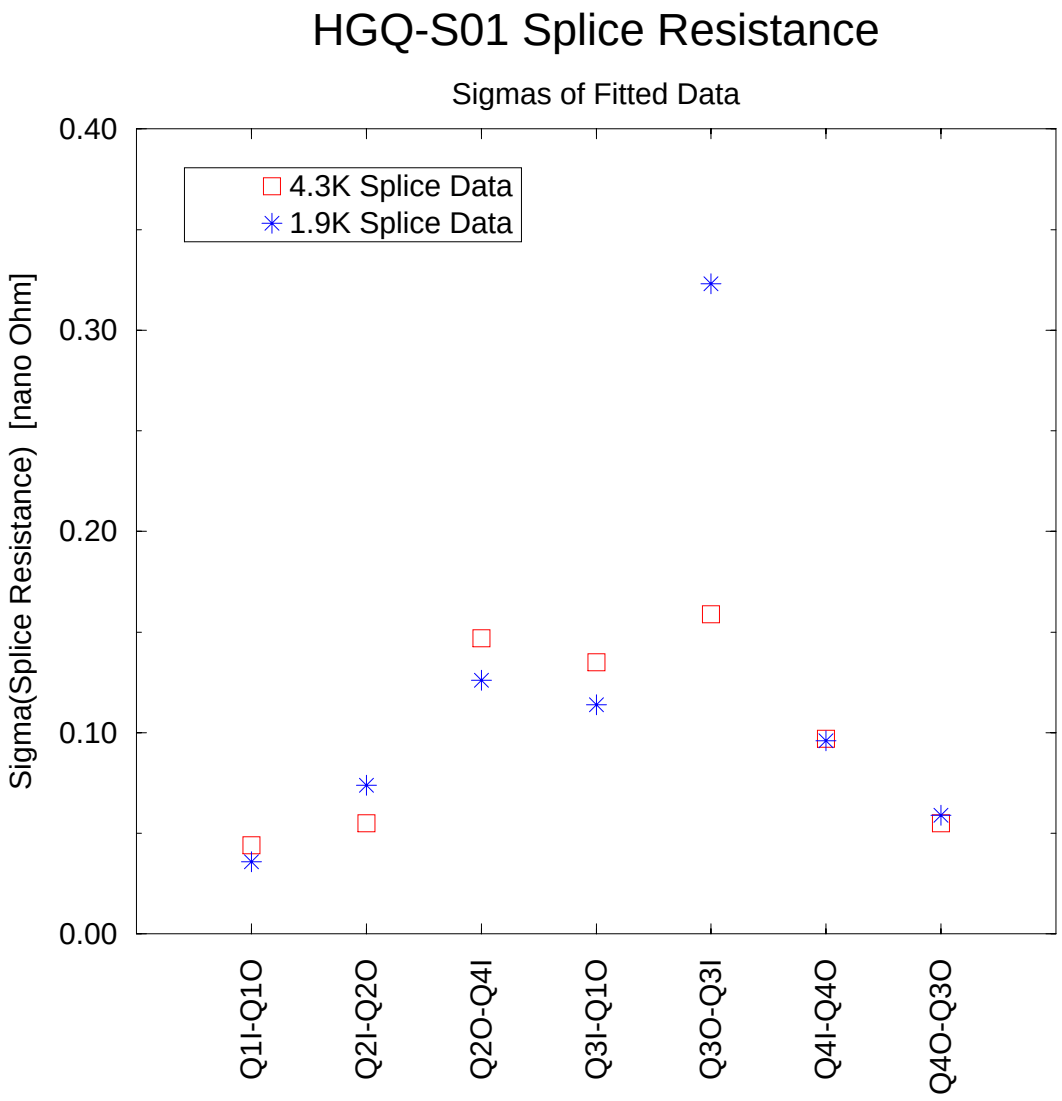

Figure 6.9: Sigma distribution of the fitted data

Chapter 7

RRR study

This chapter summarizes the residual resistance ratio (RRR) measurements performed at the end of the second test cycle. RRR is determined by measuring the the coil resistance and temperature during magnet warm up.

Measurements of magnet resistance were made using a 4-wire technique at a current of 10A. Current was supplied by a Hewlett Packard Power Supply and voltages measured through the magnet voltage taps (see chapter 1). Both voltage and current measurements were made using HP3458A DMMs. For measurement of temperature we used Carbon-Glass sensors in the vicinity of the magnet. Two sensors were used, one of them closer to the top of the magnet and the other closer to the bottom. Note that these sensors were in fact reading the gas temperature and therefore one would expect the actual magnet temperature to be somewhat different.

Figures 7.1 and 7.2 compare the resistances of the eighth coils, measured while the magnet was gradually warming up, against the calculated the room temperature resistances. For these plots, the average temperature of the top and bottom carbon glass sensors was used. We observed that the parameterization curve constrained by the resistance values measured at the lower temperatures does not agree well with the data measured at the higher temperatures. However, the magnet resistance around 20 K is not strongly temperature dependent and therefore the error in RRR introduced by basing measurements on these points is not significant ($< 10\%$).

Note that the RRR value for the inner coil (~ 140) is significantly larger than that of the outer coil (~ 55). This is not necessarily a surprise since the inner and outer cable strands are made from completely different billets.

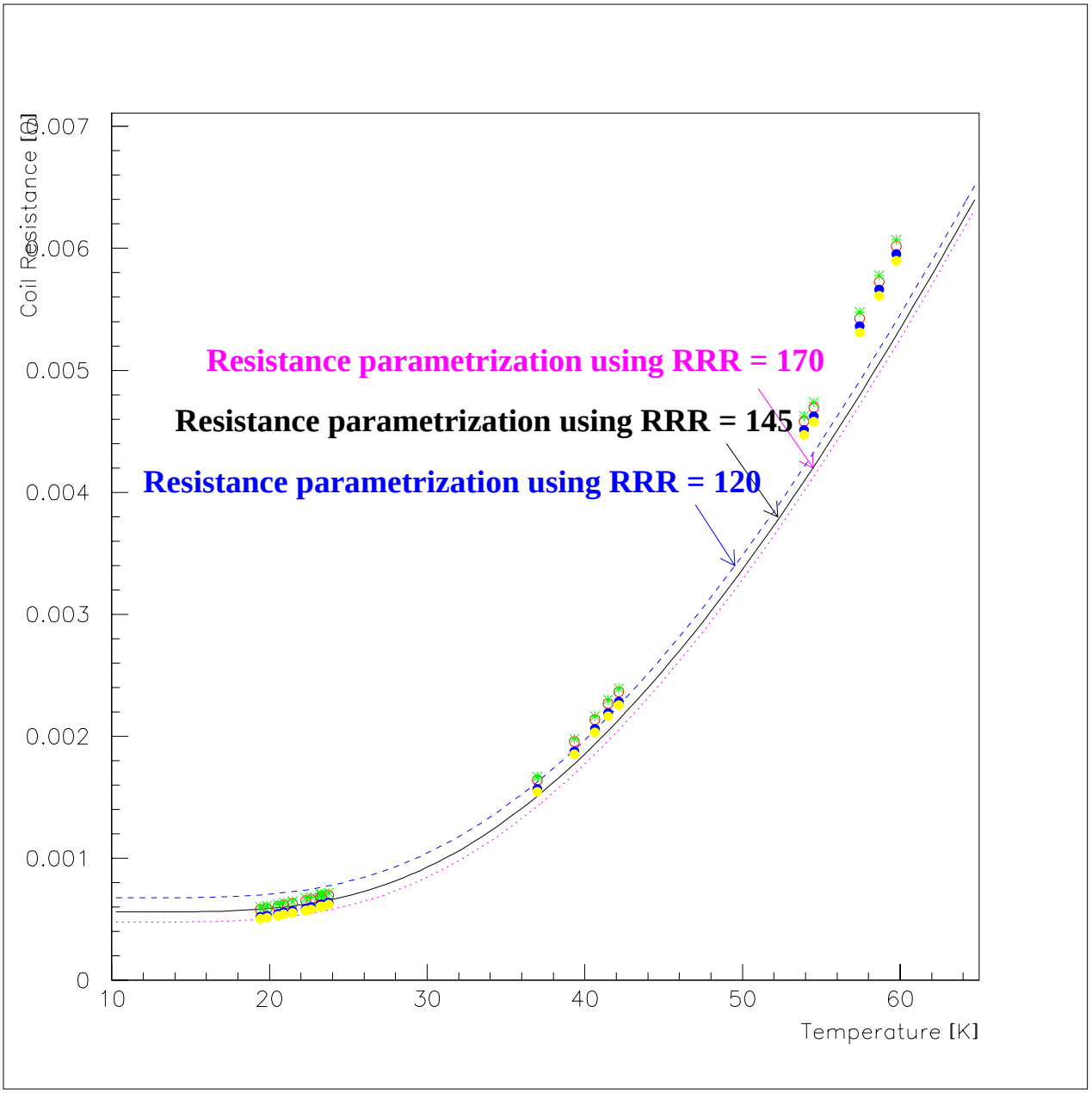

Figure 7.1: Inner coil resistance temperature dependence comparison with parametrization. (rrr1.ps)

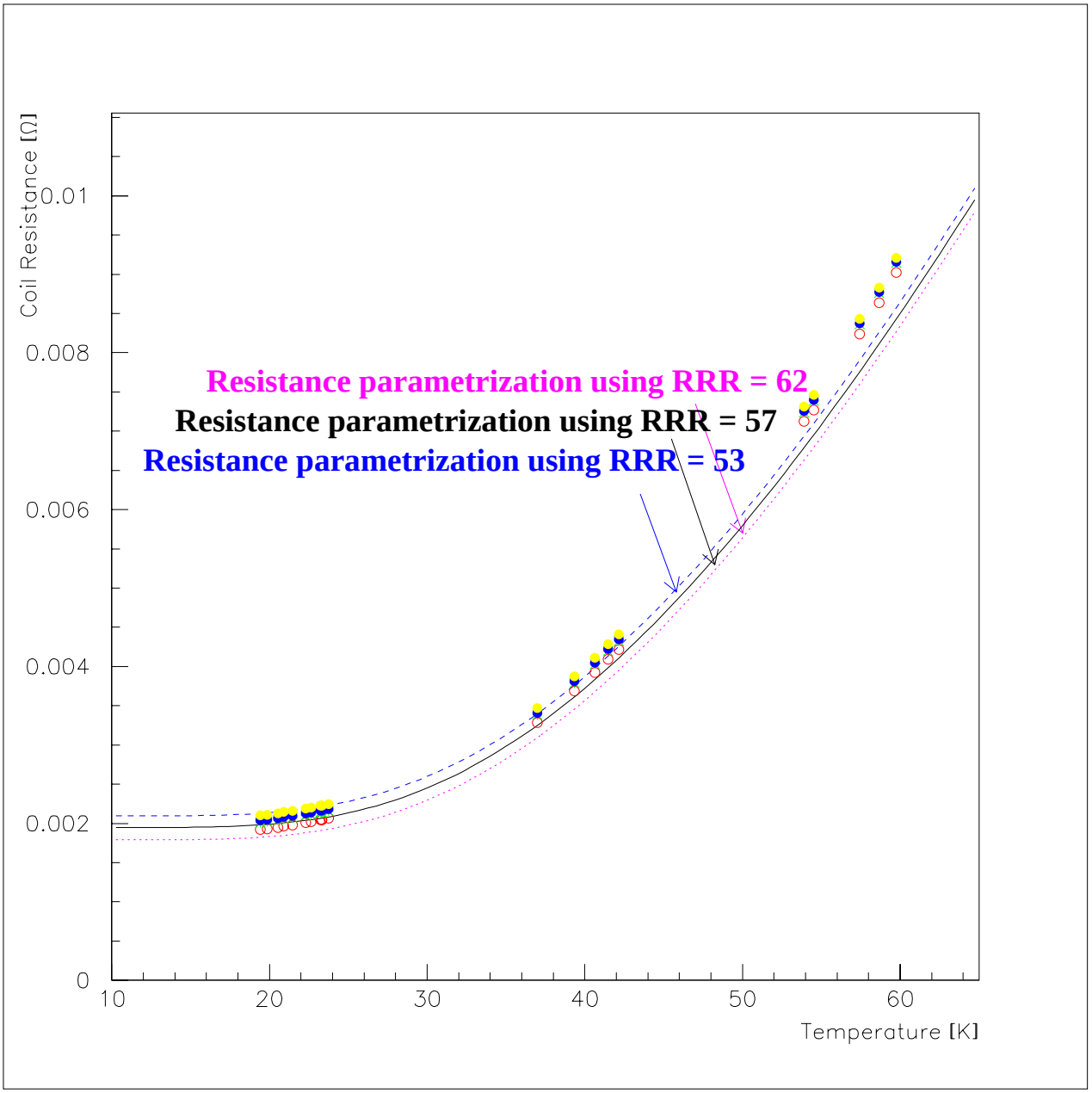

Figure 7.2: Outer coil resistance temperature dependence comparison with parametrization. (rrr2.ps)

Chapter 8

Snapshot events

8.1 Introduction

During the first set of quench tests at 1.9K, the magnet HGQS01 exhibited unusual behavior: the quench detection system was triggered by a half-coil voltage difference exceeding 100mV, yet analysis of the quench characterization voltage tap data did not reveal any signature of resistive voltage growth normally associated with a quench. A total of four such "ramp-to-quench" power tests were performed, with successively higher quench thresholds or reduced ramp rate, in which no actual quench occurred in the magnet. Finally, at a threshold of 400mV, the first real quench at 1.9K was observed at a current of 10364 Amps. Careful study was made of the data and power system to eliminate the possibility that these "glitches" were caused by the power supply, or other noise outside the magnet. The conclusion was that something inside the magnet, such as coil motion, must be responsible for these inductive voltage glitches.

8.2 Snapshot Data

In order to study this phenomenon further, a special data acquisition mode of the digital quench detection (DQD) system was enabled to capture selected quench detection signals when certain threshold conditions were met. This mode is known as a "snapshot scan", because it captures voltage traces for a relatively short (100ms) time window surrounding the trigger event, and

saves those "quench" data to a file. Meanwhile, it does not interfere with the usual quench detection and characterization electronics, which remain active in case a real quench occurs (and is triggered at a higher threshold than the snapshot). The snapshot scan operates within the digital quench detection scan. It therefore has access to the same signals used by DQD to identify quenches: these are the magnet current, the rate of change of magnet current ("Idot"), the whole coil voltage, the individual half-coil voltages, and the "ground resistor" voltage indicating current to ground. These signals are sampled at approximately 2KHz and buffered for fast quench analysis and data saving. The snapshot was automatically disabled whenever the quench system was reset. It was then enabled manually before each power test via a unix script, in which a threshold and minimum time between snapshots were specified. The minimum time between snapshots was kept at 10 seconds, which is close to the limit for the system to save the data. The threshold values were varied somewhat between 50mV and 150mV. During the second thermal cycle, the threshold was kept at 100mV. The snapshot scan was enabled for essentially all of the up- and down-ramps of the power supply, during strain gauge runs, ramp to quench tests, and magnetic measurement cycles, at 1.9K and 4.5K operations during the first and second thermal cycles of HGQS01. We observe that the snapshots were triggered only during 1.9K operation of the magnet, all of which are seen only in the half-coil voltage difference.

8.3 Snapshot Results

The snapshot data reveal that the glitches exhibit remarkably repeatable behavior! In Figure 8.1(8.2) we plot the peak half-coil voltage difference, versus the magnet current on the up(down)-ramp at the time the snapshot was triggered, for data taken during the first and second thermal cycles. (Only the first 9 quenches have been studied in the 2nd thermal cycle, and only one of these contained down-ramps; the others were all ramps to quench). We find, for the first thermal cycle, that the glitches occurred at very nearly the same currents on each ramp, with the sign and magnitude of these signals being very repeatable, and the sign of the glitches changing with a reproducible pattern. We also observe that glitches occurring on the down-ramp start and end at lower currents than on the up-ramp. A typical voltage trace is shown

in Figure 8.3. We find that the voltage traces themselves have structure that is repeatable from one ramp to the next. There is no obvious increase in the number of snapshots triggered at the lower (50mV) threshold. There appears to be some significant qualitative change in this glitch behavior during the second thermal cycle, which can be clearly seen in Figure 8.1 and 8.2. Some of the current values at which glitches occur have changed, and the sign of some of these has also changed. Recall that additional pre-stress was added to the return end bullets between thermal cycles, so mechanically the magnet is slightly different for the 2nd test. The first four glitches triggered the quench detection system, and therefore have the full quench characterization voltage tap data saved. Preliminary studies of these data have not come to any solid conclusion, so additional analysis effort is required to make sense of these data.

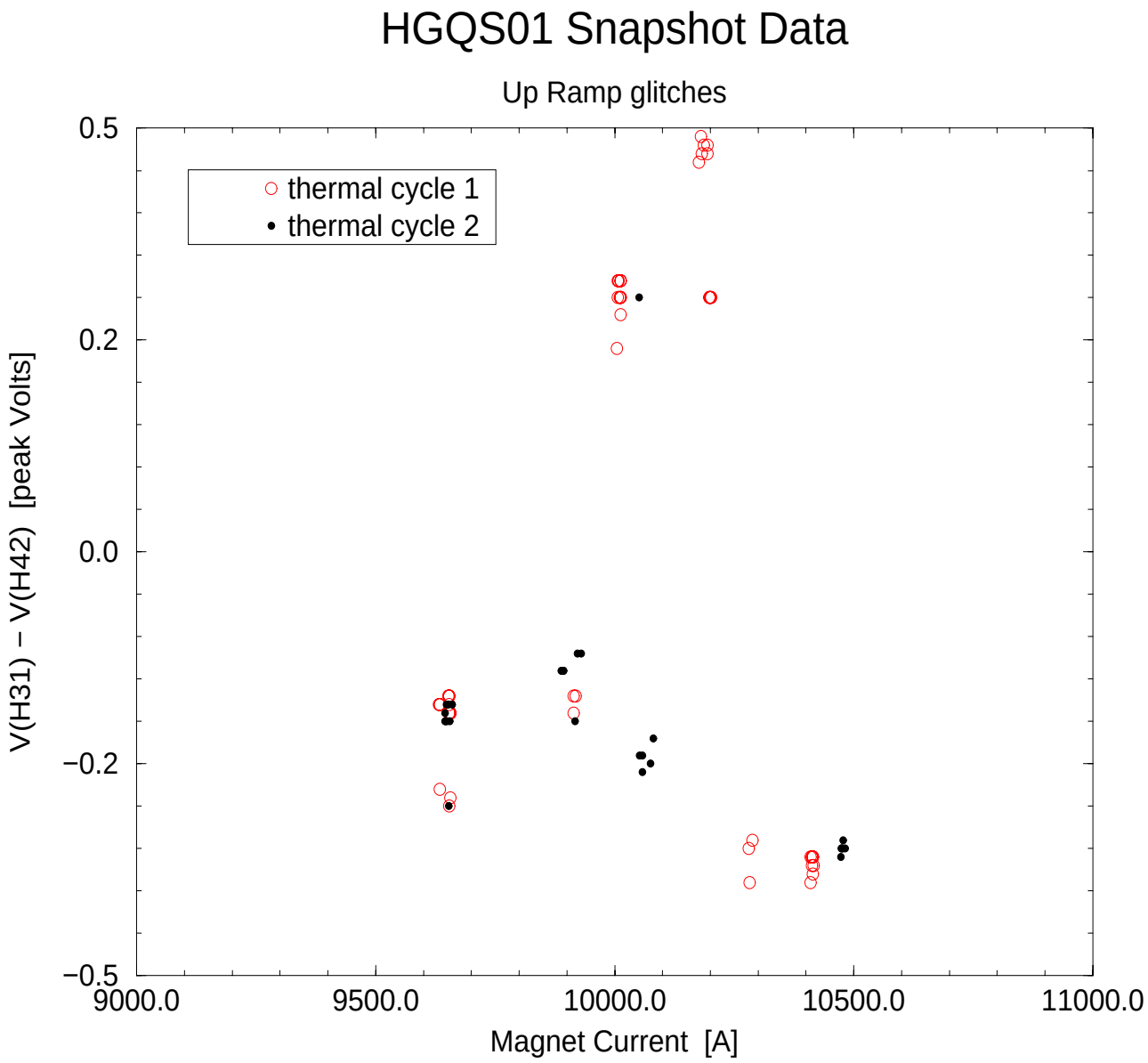

Figure 8.1: Half coil voltage difference versus magnet current for up-ramp snapshots. (upramps.eps)

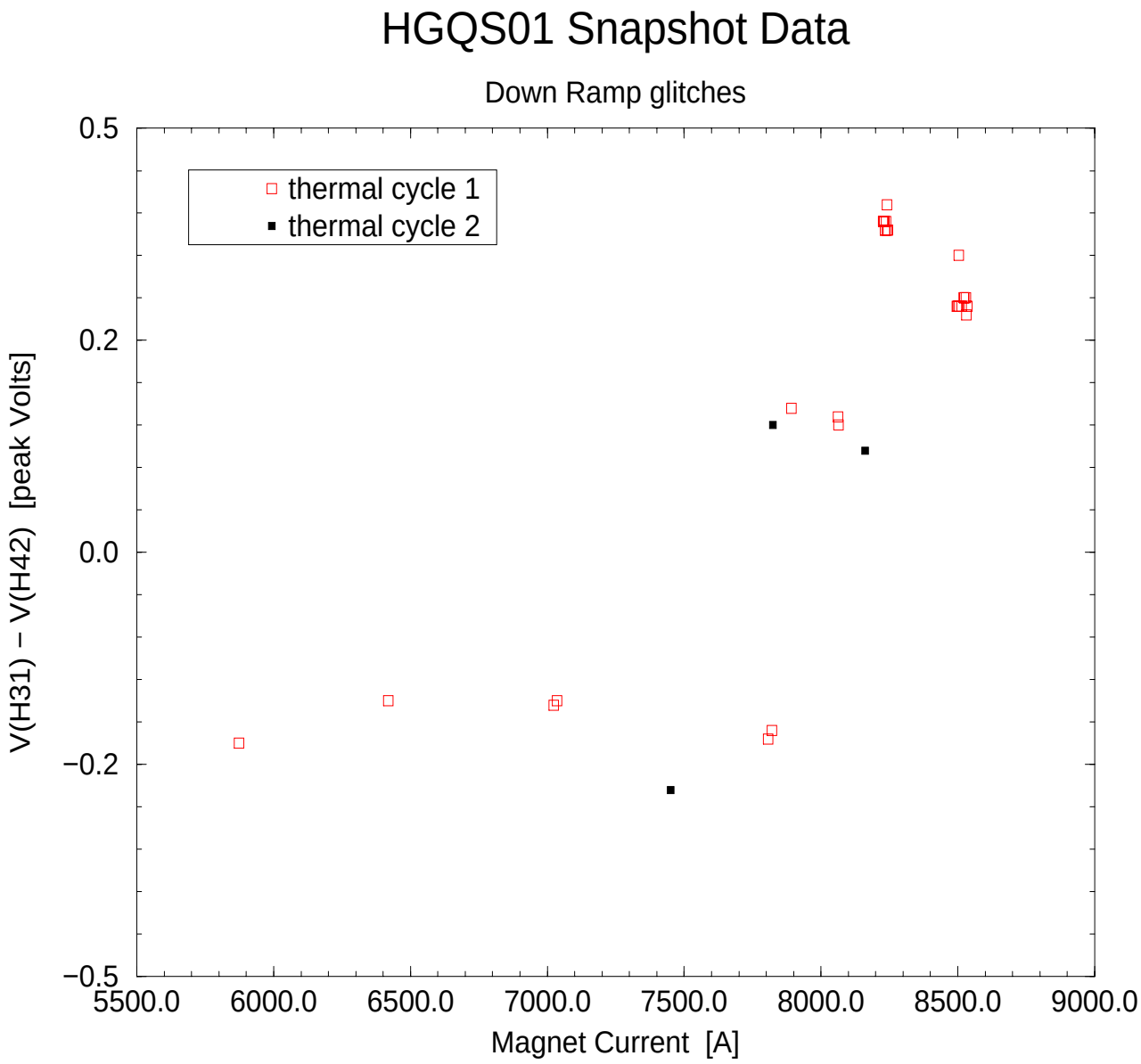

Figure 8.2: Half coil voltage difference versus magnet current for down-ramp snapshots.

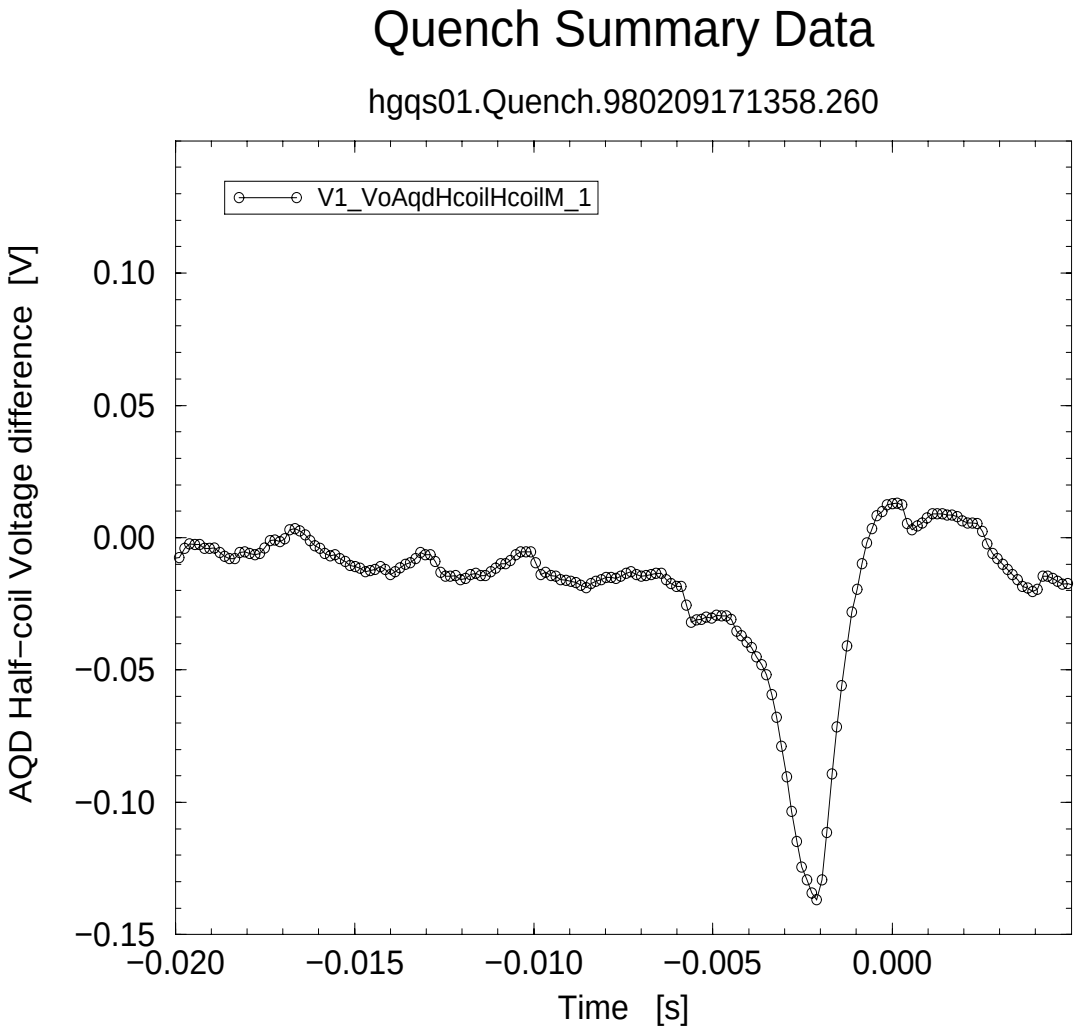

Figure 8.3: Analog quench detection circuit "quench", half coil voltage difference versus time.

Bibliography

[1] G. Sabbi, "HGQ Magnetic Shim Performances", TD-97-054, (1997)

[2] J. DiMarco, M. Lamm, G. Sabbi,P. Schlabach "Conventions for HGQ Field Quality Representation",TD-98-036 , (1998)

[3] G. Sabbi, "omparison of Calculated vs. Measured Harmonics in HGQS01 Lead End", TD-98-036 (1998)

[4] S.S. Kozub et.al."Thermal Conductivity and Electric Resistance of Composite Wires Based on HT-50", Cryogenics, Vol 32 ICEC Supplement (1992) p. 295

Appendix A

HGQS01 TEST PLAN

A.1 Outline

Thermal Cycle I

- Magntic measurements
- Room Temperature Pretest and Cool down
  RRR
- At 4.5K Operation
  Pre-Current excitation Checkout
  2500 amp Heater test
  Magnetic measurements (6-7 kamps)
  Strain gauge runs (including splice resistance measurements)
  Quench Plateau (max. 3-4 quench)
  Ramp Rate Studies
- At 1.9K Operation
  Pre-current excitation Checkout
  3000 amp Heater tests
  Strain gauge runs (including splice resistance measurements)

Quench Plateau

Ramp rate studies

Magnetic measurements

Heater studies

Quench Current vs. temperature

Thermal Cycle II

- Magnetic measurements
- Room Temperature Pretest and Cool down

  RRR
- At 4.5K Operation

  Pre-Current excitation Checkout

  2500 amp Heater test

  Quench the magnet twice
- At 1.9K Operation

  Pre-current excitation Checkout

  3000 amp Heater tests

  Strain gauge runs (including splice resistance measurements)

  Quench Plateau (10-15)

  Magnetic measurements

  Heater studies

  Energy loss measurement

  Quench Current vs. temperature

  Cryogenic tests

A.2 Thermal cycle I

A.2.1 Magnetic measurements

1. Without Yoke
2. With Yoke
3. In the dewar
   (a) Locate magnetic center by scanning ends
   (b) Apply ± 10 A. Take measurements at 8 different z locations. At each z step make 25 rotations. Take these readings with "amplifiers in".

A.2.2 Room Temperature Pretest/Cooldown

1. Follow Present procedures for Strain gauge, voltage taps, thermometer, and heater validation. Procedures include:
   (a) Hi pot the magnet in gaseous He environment. Maximum volts should not exceed V_{max} value (to be determined).
   (b) 4 wire measurement of all strain gages
   (c) 5 amps across magnet, measure voltage across taps Measure magnet resistance and compare it to the value measured at IB3. Verify that there are no shorts in the magnet
   (d) 4 wire heater resistance, system resistance
2. Record at least 10 strain gage readings at room temperature, check values with post assembly readings
3. Set strain gage and thermometer readings to 10 minute intervals
4. Place 5 amps through magnet, measure voltage across magnet (each eigth coils separately), Cool to 4.5 K , 1.1 ATM with unrestricted cooldown following VMTF cool-down procedure and take volage readings for RRR studies (make sure to get data around $\sim$10 K). Take Strain gauge runs as well. Verify that no shorts appeared during cooldown.

A.2.3 At 4.5 K Operation

1. Cold electrical tests prior to magnet testing
   (a) Check magnet resistance to ground
   (b) Hi pot (1.1 ATM helium). Maximum volts should not exceed V_{max} value (to be determined).
   (c) 0 A strain gauge readings
   (d) Protect magnet with a 60 mΩ dump resistor. $I_{max} * R_{dump} \leq 1000V$
   (e) Heater Pretests
      i. Configure QLM to fire heater with 1 sec dump firing delay
      ii. Check inter-layer heater and heater system resistance using 4 wire techniques. System capacitance should be set to approximately 14.4 mF.
      iii. Verify that inter-layer and outer heaters are wired in parallel check system continuity
      iv. Fire inter-layer heaters from VMTF prgram. Verify RC, V heaters, I heaters from data logger plots
   (f) Disable Digital QDC (or set to high tresholds)
   (g) Balance quench detection circuitry for analog QDC
      i. Set dump delay to 0 sec
      ii. sawtooth ramps between 50 A and 200 A at 100 A/sec.
      iii. Establish thresholds based on observed noise versus anticipated signals.
   (h) Set dump delay to 20 msec and the heater delay to 0msec. Manual trip at 1000 A. **Every single analog QDC platform has to be checked separately. Power supply, dump switch, heater and interlock respond should follow the proper quench logic.** Delay heater firing to 1 sec dump delay = 0 sec. Do another manual trip and check L/R, look at all data logger voltage signals; compare V_{max} to $I * R_{dump}$
2. Quench Heater Protection test

(a) Set dump resistor delay to 0 ms, no heater delay, no power supply phase off delay

(b) At 2500A magnet current, determine voltage required to quench heaters with $t_{fn} < 200$ ms

(c) If MIITS o.k dump delay to 20 ms, delay heater firing to 0 ms

(d) Check quench logic signal for proper quench timing sequence

3. Magnetic measurements

(a) Dump resistor set to 60 mΩ, 0 ms delay , delay heater to 0 ms heater value as per 0.2.3 2.b

(b) Since these measurements will be taken prior to first quench of the magnet no cleansing quench will be required prior to any hysteresis loops. (Ampifiers out).

(c) Position the probe at the center of the cold mass. Take loop measurements at 10A/sec ramp rate. The data taking is continuos. The sequence is:

i. 0A - 2000A – 3 repetitions

ii. 800A - 4000A – 3 repetitions

iii. 800A - 6000A – 3 repetitions

(d) DC Loop: Take DC mole measurements at the following currents: 0, 1000, 2000, 3000, 4000, 5000, 6000 A. (up and down)

(e) Z scans: Take measurements at 8 different z location along the length of the cold mass, at each z steps make 25 rotations. Move the probe to the first position and take another measurement.

i. Take Z scans at 2000A

ii. Take Z scans at 6000A

(f) End scan (lead end): Apply 3000A. Move the probe by 2cm increments and at each steps take a measurement. Begin outside of magnet. Make sure to cover $\pm$30 cm of the end region (at least 30 z positions).

4. Strain gauge run

(a) Dump resistor set to 60 mΩ, 20 ms delay , delay heater to 0 ms, heater value as perr 0.2.3 2.b

(b) At Ramp rate = 16 A /sec. :

Measure the inductance of the magnet. Take strain gauge runs, one file per current loop, using the sequences of currents below. Take data at all currents on the way up, and for the currents marked "*" on the way down. S.G. readings taken in 10 intervals of I from 0 to 5400A.

i. Run 1: 0*, 3200, 4500*,5500,6300*, 7100 A

ii. Run 2: 0*, 3200, 4500*,5500,6300*, 7100, 8400 A

iii. Run 3: 0*, 3200, 4500*,5500,6300*, 7100, 8400*, 9000 A

iv. Run 4: 0*, 3200, 4500*,5500,6300*, 7100, 8400*, 9000, 9500 A

v. Run 5: 0*, 3200, 4500*,5500,6300*, 7100, 8400*, 9000, 9500, 10000 A
Note: After Run 1, expect quench during strain gage run

5. Quench plateau.

Before each quench measure the inductance of the magnet. Make sure that the inductance remain unchanged. With ramp rate = 16 A/sec, train the magnet. Do not do more than 4 quenches. The predicted short sample limit currents (inner coil) is 10000 A.

6. Take a strain gauge run to $I_{plateau} - 100A$.

7. RAMP RATE dependence studies.

Ramp to quench at 300 a/s, 150 a/s,

A.2.4 At 1.9K Operation

1. Cold Electrical tests prior to current excitation Repeat section 0.2.3 1.c,d,e

2. Quench Heater Protection Test Repeat Section 0.2.3 2.a,b,c,d with 3000A applied current.

3. Strain gauge run

   (a) Repeat Section 0.2.2 4.a

   (b) At Ramp rate = 16 A /sec. :

   Measure the inductance of the magnet. Make sure that the inductance remain unchanged. Take strain gauge runs, one file per current loop, using the sequences of currents below. Take data at all currents on the way up, and for the currents marked "*" on the way down.

   i. Run 1: 0*, 4500*, 6300, 7800*, 9000, 10000 A
   ii. Run 2: 0*, 4500*, 6300, 7800*, 9000, 10000*, 11000 A
   iii. Run 3: 0*, 4500*, 6300, 7800*, 9000, 10000*, 11000, 11800 A
   iv. Run 4: 0*, 4500*, 6300, 7800*, 9000, 10000*, 11000, 11800*, 12700 A
   v. Run 5: 0*, 4500*, 6300, 7800*, 9000, 10000*, 11000, 11800*, 12700, 13400 A
   vi. Run 6: 0*, 4500*, 6300, 7800*, 9000, 10000*, 11000, 11800*, 12700, 13400, 14200 A

4. Quench plateau.

   With ramp rate = 16 A/sec, train the magnet until 4 plateau quenches have occurred. Do not do more than 10 quenches (only if magnet shows interesting behavior). The predicted short sample limit currents (inner coil) is 14200 A.

5. Take a strain gauge run to $I_{plateau} - 100A$. Scan strain gauges during ramping the magnet up

6. RAMP RATE dependence studies.

   Ramp to quench at 25 a/s, 50 a/s, 75 a/s, 100 a/s, 150, a/s, 200 a/s, 300 a/s

7. Magnetic measurements

   For initial studies, use a default ramp rate of 10 A/sec; all measurement sequences should begin with a "cleansing" quench at $\sim$ 10000A (to be determined):

(a) set the heater delay to 0 sec and dump delay to 20 msec and verify the effect of the cleansing quench (10000A) by checking the remnant magnetic field. If the remnant field is substantial increase the current and quench the magnet again.

(b) Take a "loop measurement". The sequence is:
Three consecutive loops from I_{min} to $I_{quench} - 500A$ with continuous measurements; we define I_{min} as a current near to the injection current; I_{quench} is the quench plateau current reached following training

(c) Take a standardization cycle (see fig A.1). The sequence is:
ramp to flattop current, $I_{plateau}(I_{quench} - 500A)$, dwell at $I_{plateau}$ for t_{dwell} ramp down to 300A, dwell for n sec, ramp to 600A; dwell to $t_{injection}$, then ramp to $I_{quench} - 500A$ at 10A;

(d) repeat standardization cycle with different $I_{plateau}$ other papramеters the same

(e) repeat standardization cycle (see fig A.1) with different $I_{plateau}$ other paprameters the same

(f) pick $I_{plateau}$ from above and repeat standardization cycle with different t_{dwell}

(g) pick $I_{plateau}$ from above and repeat standardization cycle with different t_{dwell}

(h) repeat hysteresis loop in a) with stops at discreet currents - every 100A

(i) repeat hysteresis loop in a) with different ramp rates - 5A/sec, 20A/sec, 40A/sec

(j) repeat hysteresis loop 2 different z position

8. Heater studies at 1.9K

(a) Set dump resistor delay to 20 ms, no heater delay, no power supply phase off delay or delay it within MIITs limit (12 MIITs)

(b) Interlayer Heater study

i. At $I/I_c = 0.2$ magnet current determine Vmin for quench. Fire heaters at additional voltage values:
225, 230, 250, 300, 400. DO NOT EXCEDE MAXIMUM HFU VOLTAGE

ii. $I/I_c = 0.4$ determine Vmin for quench.
200, 220, 250, 300, 400 . DO NOT EXCEDE MAXIMUM HFU VOLTAGE

iii. $I/I_c = 0.7$ determine Vmin for quench.
110, 120, 150, 250, 300, 400. DO NOT EXCEDE MAXIMUM HFU VOLTAGE

iv. $I/I_c = 0.9$ determine Vmin for quench Fire heaters at additional voltage values:
90, 120, 150, 200, 250, 300, 400. DO NOT EXCEDE MAXIMUM HFU VOLTAGE

9. Quench Current vs. temperature

   Ramp magnet to quench at 16 a/s at the following temperatures

   4.2K, 3.7K, 3.2K, 2.7K, 2.2K, 2.1K, 1.8K

   should not be exact value (.2 K)

A.3 Thermal cycle II

A.3.1 Magnetic measurements

1. In the dewar

   (a) Locate magnetic center by scanning ends

   (b) Apply ± 10 A. Take measurements at 8 different z locations. At each z step make 25 rotations. Take these readings with "amplifiers in".

A.3.2 Room Temperature Pretest/Cooldown

1. Follow Present procedures for Strain gauge, voltage taps, thermometer, and heater validation. Procedures include:

(a) Hi pot the magnet in gaseous He environment. Maximum volts should not exceed V_{max}=1000V value.

(b) 4 wire measurement of all strain gages

(c) 5 amps across magnet, measure voltage across taps Measure magnet resistance and compare it to the value measured at IB3 and before the first thermal cycle. Verify that there are no shorts in the magnet.

(d) 4 wire heater resistance, system resistance for all four heaters.

2. Record at least 10 strain gage readings at room temperature, check values with post assembly and frist thermal cycle readings.

3. Set strain gage and thermometer readings to 10 minute intervals

4. Place 5 amps through magnet, measure voltage across magnet (each eigth coils separately).

5. Cool down to 80K, then change strain gage and thermometer readings to 1 minute intervals. Cool to 4.5 K , 1.1 ATM with unrestricted cooldown following VMTF cool-down procedure and take volage readings for RRR studies (make sure to get data around $\sim$10 K). Take Strain gauge runs as well. Verify that no shorts appeared during cooldown.

A.3.3 At 4.5 K Operation

1. Cold electrical tests prior to magnet testing

   (a) Check magnet resistance to ground

   (b) Hi pot (1.1 ATM helium). Maximum volts should not exceed $V_{max} = 1000$.

   (c) 0 A strain gauge readings

   (d) Protect magnet with a 60 mΩ dump resistor.
   $I_{max} * R_{dump} \leq 1000V$

   (e) Heater Pretests

      i. Configure QLM to fire heater with 1 sec dump firing delay

ii. Check inter-layer heater and heater system resistance using 4 wire techniques. System capacitance should be set to approximately 14.4 mF.

iii. Verify that inter-layer heaters are wired in parallel check system continuity

iv. Fire inter-layer heaters from VMTF prgram. Verify RC, V heaters, I heaters from data logger plots

(f) Disable Digital QDC (or set to high tresholds)

(g) Balance quench detection circuitry for analog QDC

i. Set dump delay to 0 sec

ii. sawtooth ramps between 50 A and 200 A at 100 A/sec.

iii. Establish thresholds based on observed noise versus anticipated signals.

(h) Set dump delay to 25 msec and the heater delay to 20 msec. Manual trip at 1000 A. **Every single analog QDC platform has to be checked separately. Power supply, dump switch, heater and interlock respond should follow the proper quench logic.** Delay heater firing to 1 sec dump delay = 0 sec. Do another manual trip and check L/R, look at all data logger voltage signals; compare V_{max} to $I * R_{dump}$

2. Quench Heater Protection test

(a) Set dump resistor delay to 0 ms, no heater delay, no power supply phase off delay

(b) At 2500A magnet current, determine voltage required to quench heaters with $t_{fn} < 200$ ms

(c) If MIITS o.k set dump delay to 25 ms, set heater to protection mode using HFU voltage obtained in and delay heater firing to 0 ms

(d) Before continue with the run check quench logic signal for proper quench timing sequence

3. Quench the magnet twice

(a) set dump delay to 25 ms, set heater to protection mode using HFU voltage obtained in section A.3.3 item 2c and delay heater firing to 0 ms

(b) Before each ramp make sure to start the fast strain gauge run and that the snapshot data taking is running as well.

(c) Before each quench measure the inductance of the magnet. Make sure that the inductance remain unchanged.

(d) Quench the magnet twice with 16A/sec ramp rate. The predicted short sample limit current is 10340 A.

A.3.4 At 1.9K Operation

1. Cold Electrical tests prior to current excitation: Repeat section A.3.3 items 1c,1d,1e.

2. Quench Heater Protection Test Repeat Section A.3.3 iems 2a, 2c, 2c, 2d with 3000A applied current.

3. Strain gauge run

   (a) Repeat Section A.3.3 items 3a, 3b, 3c

   (b) At Ramp rate = 16 A /sec. :

   Take strain gauge runs, one file per current loop, using the sequences of currents below. Take data at all currents on the way up, and for the currents marked "*" on the way down.

   i. Run 1: 0*, 4500*, 6300, 7800*, 9000, 10000 A

   ii. Run 2: 0*, 4500*, 6300, 7800*, 9000, 10000*, 11000 A

   iii. Run 3: 0*, 4500*, 6300, 7800*, 9000, 10000*, 11000, 11800 A

   iv. Run 4: 0*, 4500*, 6300, 7800*, 9000, 10000*, 11000, 11800*, 12700 A

   v. Run 5: 0*, 4500*, 6300, 7800*, 9000, 10000*, 11000, 11800*, 12700, 13400 A

   vi. Run 6: 0*, 4500*, 6300, 7800*, 9000, 10000*, 11000, 11800*, 12700, 13400*, 14200 A

4. Quench plateau.

   Repeat Section A.3.3 items 3a, 3b, 3c

   With ramp rate = 16 A/sec, train the magnet until 4 plateau quenches have occurred. Do not do more than 10 quenches (only if magnet shows interesting behavior). The predicted short sample limit current is 14200 A.

5. Take a strain gauge run to $I_{plateau} - 100A$. Scan strain gauges during ramping the magnet up

6. Magnetic measurements

   For initial studies, use a default ramp rate of 10 A/sec; all measurement sequences should begin with a "cleansing" quench at $\sim$ 10000A (this value was used in thermal cycle I). Before each cleansing quench make sure to set the heater delay to 0 sec and dump delay to 25 msec, repeat Section A.3.3 items 3b, 3c and verify the effect of the cleansing quench (10000A) by checking the remnant magnetic field. If the remnant field is substantial increase the current and quench the magnet again:

   (a) Take a "hysteresis loop measurement" at Z = 1.2 m (for the reference system see Appendix E). The sequence is:

   Three consecutive loops from I_{min} to $I_{quench} - 500A$ with continuous measurements; we define I_{min} as a current near to the injection current; I_{quench} is the quench plateau current reached following training

   (b) Z scans: Take measurements at 8 different z location along the length of the cold mass, at each z steps make 25 rotations. Move the probe to the first position and take another measurement. The reference system is defined in Appendis E.

      i. Take Z scans at 6000A

      ii. Take Z scans at $I_{quench} - 500A$

   (c) Take a standardization cycle (see fig A.1). The sequence is:

   ramp to flattop current, $I_{plateau}(I_{quench} - 500A)$, dwell at $I_{plateau}$ for t_{dwell} ramp down to 50A, dwell for 2 sec, ramp to 800A; dwell to $t_{injection}$ (1/2hour), then ramp to $I_{quench} - 500A$ at 10A;

(d) repeat hysteresis loop in item 6a with stops at discreet currents - every 1000A. (the acceleration d^2I/dt^2 should be $5A/sec^2$)

(e) repeat hysteresis loop in item 6a with a different ramp rate - 80 A/sec

(f) repeat hysteresis loop 2 different z positions. Z = 1.0 m and Z = 1.4 m.

The reference system is defined in Appendix E.

(g) End scan (lead end): Apply 6000A. Move the probe by 2-4cm increments and at each steps take a measurement. Begin outside of magnet. Make sure to cover ± 60 cm of the end region:

$Z \in [0, 40] \sim 9$ data points (5 cm spacing)

$Z \in [40, 50] \sim 4$ data poins (2.5 cm spacing)

$Z \in [50, 75] \sim 5$ data points (5 cm spacing)

The reference system is defined in Appendix E.

7. Heater studies at 1.9K

(a) Set dump resistor delay to 25 ms, no heater delay, no power supply phase off delay or delay it within MIITs limit (12 MIITs) Repeat Section A.3.3 items 3b, 3c.

(b) Interlayer Heater study

i. At $I/I_c = 0.2$ magnet current fire heaters at 400V voltage value.
DO NOT EXCEDE MAXIMUM HFU VOLTAGE

ii. At $I/I_c = 0.4$ magnet current fire heaters at 400V voltage value.
DO NOT EXCEDE MAXIMUM HFU VOLTAGE

iii. $I/I_c = 0.7$ magnet current fire heaters at 400V voltage value.
DO NOT EXCEDE MAXIMUM HFU VOLTAGE

iv. $I/I_c = 0.9$ magnet current fire heaters at 400V voltage value.
DO NOT EXCEDE MAXIMUM HFU VOLTAGE

8. If time permits: Energy loss measurement (at 1.9K)

Repeat Section A.3.3 items 3a, 3b, 3c.

Ramp the magnet up to 10000A from 500A wait 5 sec then ramp down. Repeat this at least three times. Monitor coil voltages.

Change the ramp rate between 30 - 300 A/s (30A/s, 50 A/s, 100 A/s, 150 A/s, 200 A/s, 250 A/s, 300 A/s)

9. Quench Current vs. temperature

   Repeat Section A.3.3 items 3a, 3b, 3c.

   Ramp magnet to quench at 16 a/s at the following temperatures

   1.8K, 2.1K, 2.2K, 2.7K, 3.2K, 3.7K, 4.2K, 4.6K should not be exact value (.2 K)

10. Cryogenic tests These tests will be scheduled in between other tests since these tests have extremely low priority.

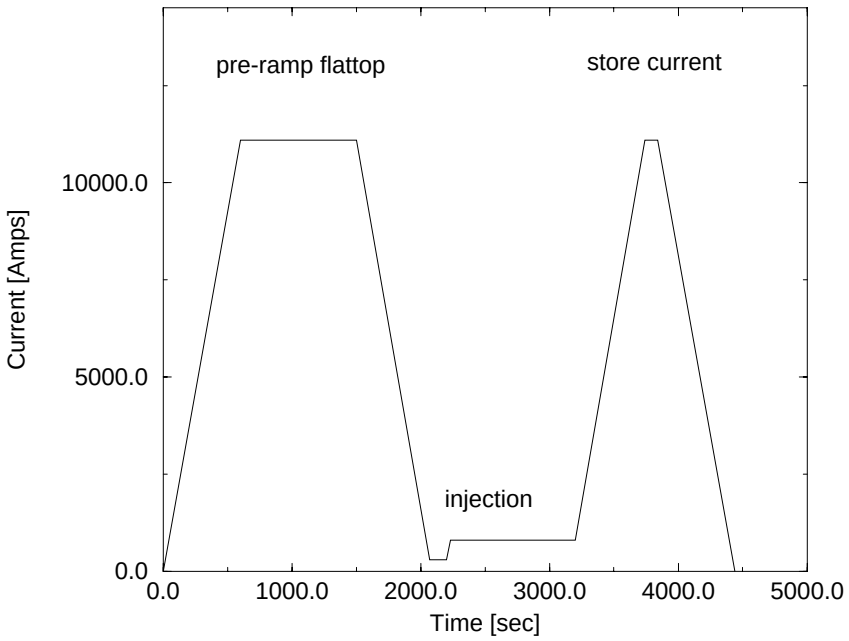

Figure A.1: Standardization cycle sequence

Appendix B

Field Harmonics at a Reference Radius of 17 mm

Selected tables of harmonics are given here at a reference radius of 17 mm. Table B.1 summarizes the field harmonics in the magnet body. Data were measured at $z = 0.818$ m.

	2kA (u) mean	2kA (u) error	2kA (d) mean	2kA (d) error	6kA mean	6kA error	11kA mean	11kA error
b3	0.595	0.0251			0.697	0.0086	0.748	0.023
b4	0.376	0.0116			0.405	0.0053	0.405	0.007
b5	-0.491	0.0119			-0.418	0.0085	-0.359	0.067
b6	-4.009	0.0257	-3.341	0.0208	-3.758	0.0150	-3.675	0.106
a3	0.782	0.0255			0.765	0.0105	0.646	0.228
a4	2.081	0.0100	1.936	0.0106	2.052	0.0093	2.052	0.007
a5	0.108	0.0062			0.123	0.0068	0.098	0.008
a6	-0.001	0.0151			-0.013	0.0073	-0.016	0.049

Table B.1: Field harmonics at 2kA, 6kA, 11kA measured during the first thermal cycle. The reference radius is 17 mm.

Tables B.2 and B.3 summarize the field harmonics measured in axial scans of the magnet.

	TCI mean	10A error	TCI mean	2kA error	TCI mean	6kA error
b3	0.948	0.8462	0.663	0.8904	0.849	0.8549
b4	-0.214	0.2570	0.080	0.1442	0.106	0.1441
b5	-0.297	0.1488	-0.239	0.1103	-0.215	0.1056
b6	-2.432	1.9320	-2.340	1.6962	-2.153	1.7107
b7	0.076	0.0569	-0.002	0.0298	-0.008	0.0378
b8	-0.102	0.0700	-0.007	0.0139	0.026	0.0158
b9	0.179	0.1021	-0.011	0.0128	0.005	0.0331
b10	0.056	0.1572	-0.258	0.0945	-0.291	0.1179
a3	-0.157	0.3936	0.254	0.1861	0.294	0.1837
a4	2.208	0.8101	2.903	0.5677	2.945	0.5623
a5	-0.003	0.1448	0.089	0.1044	0.095	0.1026
a6	0.428	0.3263	-0.102	0.1069	-0.142	0.1025
a7	-0.095	0.1003	-0.032	0.0241	-0.028	0.0163
a8	0.188	0.1888	-0.005	0.0249	0.021	0.0155
a9	-0.078	0.1871	-0.029	0.0202	-0.003	0.0193
a10	0.414	0.2857	0.003	0.0165	-0.005	0.0183

Table B.2: Field harmonics averaged over the length of the magnet from axial scan data at 10A, 2kA, 6kA measured during the first thermal cycle. The reference radius is 17 mm.

	TCII mean	10A error	TCII mean	6kA error	TCII mean	11kA error
b3	1.200	0.7589	0.836	0.7263	0.688	0.7214
b4	0.794	0.2011	0.718	0.2487	0.427	0.1991
b5	-0.325	0.1611	-0.225	0.1348	-0.249	0.1298
b6	-1.112	2.3573	-1.407	2.2940	-1.293	2.3386
b7	-0.152	0.1382	0.009	0.0608	-0.012	0.0346
b8	-0.077	0.3089	0.040	0.0489	0.005	0.0163
b9	-0.093	0.2297	0.004	0.0158	-0.015	0.0220
b10	-0.364	0.1823	-0.264	0.1033	-0.234	0.0713
a3	1.826	1.1881	2.940	0.8828	1.811	0.6807
a4	2.145	0.6249	3.047	0.4521	2.993	0.4885
a5	-0.310	0.2792	0.054	0.1852	0.074	0.1641
a6	-0.260	0.6372	-0.051	0.0700	-0.095	0.0538
a7	-0.110	0.1383	-0.014	0.0193	-0.030	0.0226
a8	-0.091	0.1892	0.024	0.0379	0.045	0.0459
a9	-0.356	0.2903	0.025	0.0173	-0.014	0.0367
a10	-0.004	0.1061	-0.023	0.0280	-0.015	0.0197

Table B.3: Field harmonics averaged over the length of the magnet from axial scan data at 10A, 6kA, 11kA measured during the second thermal cycle. The reference radius is 17 mm.

Appendix C

List of Magnetic Measurements During the First Thermal Cycle

ZSC-CC-10A-W-FE1	Axial scan of collared coil (10 A, warm, FE1 probe)
ZSC-CM-10A-W-FE1	Axial scan of cold mass (10 A, warm, FE1 probe)
ZSC-BFTC1-10A-W	Axial scan before thermal cycle 1 (10 A, warm, VMTF)
ZSC-AFTC1-10A-W	Axial scan after thermal cycle 1 (10 A, warm, VMTF)
CLP-Z0-2kA-T45	Loop to 2 kA (z=0, 4.5 K)
CLP-Z0-4kA-T45	Loop to 4 kA (z=0, 4.5 K)
CLP-Z0-6kA-T45	Loop to 6 kA (z=0, 4.5 K)
SSL-Z0-6kA-T45	Stair-step loop to 6 kA (z=0, 4.5 K)
ZSC-2kA-T45	Axial scan at 2 kA, 4.5 K
ZSC-6kA-T45	Axial scan at 6 kA, 4.5 K
LES-6kA-T45	Lead end axial scan at 6 kA, 4.5 K

CLP-Z0-11kA-10As-T19	Loop to 11 kA with 10 A/s ramp rate at 1.9 K
CLP-Z0-11kA-20As-T19	Loop to 11 kA with 20 A/s ramp rate at 1.9 K
CLP-Z0-11kA-40As-T19	Loop to 11 kA with 40 A/s ramp rate at 1.9 K
SSL-Z0-11kA-T19	Stair-step loop to 11 kA (z=0, 1.9 K)
CLP-P228-11kA-T19	Loop to 11 kA (z=+22.8", 1.9K)
CLP-M228-11kA-T19	Loop to 11 kA (z=-22.8", 1.9K)
ACL-9kA-T19	Accelerator cycle with 9 kA precycle current (1.9 K)
ACL-11kA-T19	Accelerator cycle with 11 kA precycle current (1.9 K)
ACL-2min-T19	Accelerator cycle with 2 min wait at 10.5 kA (1.9 K)
ACL-5min-T19	Accelerator cycle with 5 min wait at 10.5 kA (1.9 K)
ACL-10min-T19	Accelerator cycle with 10 min wait at 10.5 kA (1.9 K)
LDC-T19	Measurements at low DC currents

Appendix D

List of Magnetic Measurements During the Second Thermal Cycle

ZSC-BFTC2-10A-W	Axial scan before thermal cycle 2 (10 A, warm, VMTF)
ZSC-6kA-T19-TC2	Axial scan at 6kA thermal cycle 2, 1.9K
ZSC-11kA-T19-TC2	Axial scan at 11kA thermal cycle 2, 1.9K
LES-6kA-T19-TC2	Lead end axial scan at 6 kA, 1.9K, TC2
SSL-Z0-11kA-T19-TC2	Stair-step loop to 11 kA, TC2 (z=0, 1.9 K)
CLP-Z0-11kA-10As-T19-TC2	Loop to 11 kA with 10 A/s, 1.9 K TC2
CLP-Z0-11kA-80As-T19-TC2	Loop to 11 kA with 80 A/s, 1.9 K TC2
ACL-11kA-T19-30m-TC2	Accel. cycle with 11 kA precycle, 30 min porch (1.9 K)
CLP-Zn0.2-11kA-10As-T19-TC2	Loop to 11 kA, 10 A/s, 1.9 K, -0.2m from center
CLP-Zp0.2-11kA-10As-T19-TC2	Loop to 11 kA, 10 A/s, 1.9 K, +0.2m from center

Appendix E

Reference frame and powering conventions

The HGQ magnet axis is chosen as the z axis of a cylindrical coordinate system. The z axes is oriented from the magnet lead end towards the return end. The origin of the z axis is chosen at the outer surface of the lead end plate. In the transverse plane, the azimuthal coordinate increases counter-clockwise looking from the positive z axis. The reference azimuth $\theta = 0$ is at the boundary between quadrant 1 and 4, as labelled during magnet production. With this definition, quadrant 1 occupies the sector $0 < \theta < \pi/2$, quadrant 2 is in the sector $\pi/2 < \theta < \pi$, etc. On top of the cylindrical coordinate system, a cartesian system is defined with same z axis, x axis at θ=0, y axis at $\theta = \pi/2$. The magnet is powered to provide a current flow in the negative z direction in the octants which are next to the horizontal (x) mid-plane, in the positive z direction in the octants which are next to the vertical (y) mid-plane. With the present (HGQS01) quadrant splice configuration, the main leads are connected to the inner coils of quadrant 1 and 2. This convention corresponds to powering the magnet with the quadrant 2 lead at the positive terminal of the power supply, and with the quadrant 1 lead at the negative terminal. These definitions are illustrated in Figure E.1.

More detailed description of coil orientation in x,y plane is shown in Figure E.2. Each quadrant houses an inner coil and an outer coil. In the magnet straight section, each coil is symmetric with respect to the pole plane. The two sides of each coil are labelled as A and B using the following convention:

side A is the one which contains the pole lead, side B is the one which contains the midplane lead. With this definition, in each quadrant the A and B sides of the outer layer coil are switched with respect to those of the inner layer coil. The octants are labelled according to the quadrant in which they are located and the direction of the current flow: octant 1N for quadrant 1, negative current flow ($0 < \theta < \pi/4$); octant 1P for quadrant 1, positive current flow ($\pi/4 < \theta < \pi/2$); and so forth.

The magnetic field in the bore is described in terms of multipole coefficients defined according to the following expression:

$$\begin{aligned} B_\theta(r,\theta) &= \sum_{n=1}^{\infty} \left(\frac{r}{r_0}\right)^{n-1} (B_n \cos n\theta + A_n \sin n\theta) \\ B_r(r,\theta) &= \sum_{n=1}^{\infty} \left(\frac{r}{r_0}\right)^{n-1} (-A_n \cos n\theta + B_n \sin n\theta) \end{aligned}$$

The same multipole coefficients appear in the equivalent expansion in complex notation:

$$B_y(x,y) + iB_x(x,y) = \sum_{n=1}^{\infty} (B_n + iA_n) \left(\frac{x+iy}{r_0}\right)^{n-1}$$

With the present conventions, the main field component B_2 is positive, and the quadrupole magnet will horizontally focus and vertically defocus a positive charged beam travelling in the positive z direction. A reference radius r_0 of 1 cm is adopted.

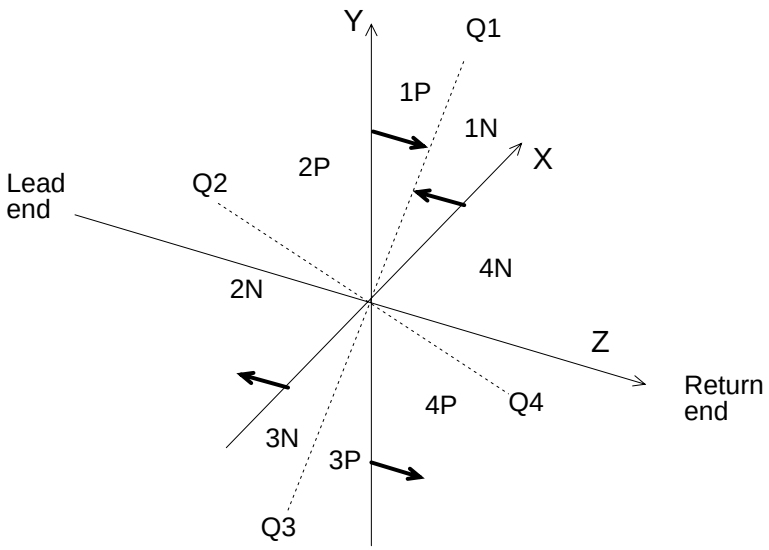

Figure E.1: Reference frame and magnet powering.

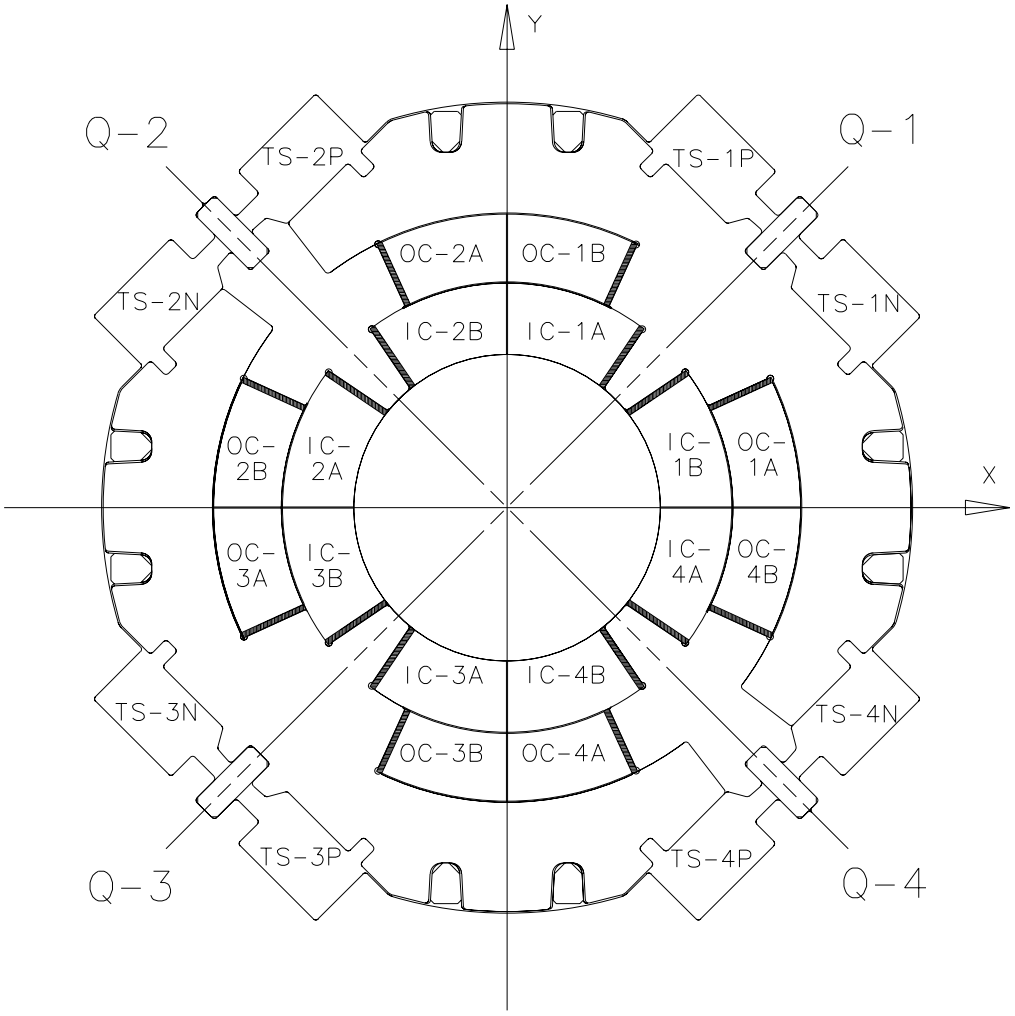

Figure E.2: HGQ collared coil cross-section detail (view from return end).